Photoreflectance and photoluminescence investigations of nitrogen diluted III-V alloys and their low dimensional structures

Robert Kudrawiec

Supervisor: Prof. Jan Misiewicz

Institute of Physics, Wrocław University of Technology

Wybrzeże Wyspiańskiego 27, 50-370 Wrocław, Poland

Wrocław, Maj 2004

Version 1.1

Abstract

In this thesis photoreflectance (PR) and photoluminescence (PL) spectroscopies have been applied to determine the optical properties of nitrogen diluted III-V compounds and their low dimensional structures. The thesis is organized as follows. In the Chapter 1 entitled *Introduction* the motivation of this investigation is explained. Experimental techniques and samples used in this study are presented in the Chapter 2 entitled *Experiment and samples*. In the Chapter 3 entitled *Fundamentals of Ga(In)NAs* a short overview of the knowledge on Ga(In)NAs is presented. In this overview the author has focused on PR and PL investigations of Ga(In)NAs system performed during last years. In addition, the author has presented theoretical approaches, which have been applied to explain the unusual properties of Ga(In)NAs. The Chapter 4 entitled *Results and discussion* is the original part of this thesis. In the two first Sections of this chapter the author has focused on the issue of post-growth annealing of (Ga,In)(As,Sb,N) layers and its influence on optical properties. It has been shown that the annealing process improves the optical properties of (Ga,In)(As,Sb,N) layers and shifts to blue the band gap energy. In order to explain the improvement of optical properties and the origin of the band gap blueshift a simple band gap diagram has been proposed. Within assumed band gap diagram the character of PL bands has been explained and the origin of the blueshift has been attributed to the two phenomena: (i) the reduction of the tail of density of states and (ii) the change in nitrogen nearest-neighbour environment. In the Section 4.3 energy level structure of GaInNAs/GaAs quantum wells (QWs) has been analysed. The number of confined states for the electron and hole wells has been determined, and electron effective mass and the conduction band offset for this system have been determined. In addition, the influence of step-like barrier on energy level structure has been considered. In the Section 4.4 the issue of the post-growth annealing of GaInNAs/GaAs QW structures has been investigated. In this case it has been shown that the main origin of the blueshift of QW transitions is the change in the nitrogen nearest-neighbour environment, while the effect associated with the atom interdiffusion across QW interfaces is very small in comparison to InGaAsP/InP systems. Moreover, an unusual phenomenon associated with decrease in PR signal with the temperature decrease has been observed for investigated samples. This phenomenon has been connected with the effect of carrier localisation at low temperatures and has been explained in the last section.

Preface

The work presented in this thesis has been carried out at the Laboratory of Semiconductor Spectroscopy at the Institute of Physics Wrocław University of Technology during 2001-2004.

I would like to express my gratitude to Professor Jan Misiewicz, the supervisor of this thesis, for an opportunity to work in interesting field of semiconductor spectroscopy, and for his support during these years.

I would like to thank my friends from the laboratory, especially Dr. G. Sek, Dr. K. Ryczko for the cooperation. I am grateful to the people of the collaborating research groups at other universities: D. Gollub and Prof. A. Forchel from Wurzburg University in Germany; Dr. J.C. Harmand from Laboratoire de Photonique et de Nanostructures (LPN) CNRS in France; Prof. M. Hammar from Royal Institute of Technology (KTH) in Sweden; E.-M. Pavelescu and Prof. M Pessa from Optoelectronics Research Center in Finland; Dr. J. Derluyn and Prof. I. Moerman from INTEC University Gent in Belgium; H. Yuen and Prof. J.S. Harris from Stanford University in USA.

This work was partly supported by EC/EU IST project GIFT No. IST-1999-12700 and by the Committee for Scientific Research in Poland under Grant No. 4 T11B 008 23 and Grant No. 2P03B 108 25. In addition, this work was supported by Grant of Rector of Wrocław University and Technology.

List of publications

This thesis consists of an overview and the following publications:

[1] **R. Kudrawiec**, J. Misiewicz, L.H. Li, and J.C. Harmand, *'The exciton binding energy in a strained $GaN_{0.02}As_{0.98}$ layer'*, '27th International Conference on Semiconductor Physics', Flagstaff, USA

[2] **R. Kudrawiec**, J. Misiewicz, E.-M. Pavelescu, J. Konttinen, and M. Pessa, *'Photoreflectance investigations of temperature dependence of the 'different' energy gaps in GaInNAs compound'*, '27th International Conference on Semiconductor Physics', Flagstaff, USA

[3] **R. Kudrawiec**, J. Misiewicz, E.-M. Pavelescu, J. Konttinen, and M. Pessa, 'Metastability of band gap energy in GaInNAs compound investigated by photoreflectance', Acta Physica Polonica in press (2004).

[4] **R. Kudrawiec**, J. Misiewicz, E.-M. Pavelescu, J. Konttinen, and M. Pessa, *'Post-grown annealing of GaInNAs layers and GaInNAs/GaAs multiple quantum wells studied in photoreflectance spectroscopy'*, IEE Proceedings Optoelectronics in press (2004).

[5] **R. Kudrawiec**, M. Motyka, J. Andrzejewski, J. Misiewicz, D. Gollub, and A. Forchel, *'Photoreflectance and photoluminescence study of step-like GaInNAs/GaInNAs/GaAs quantum wells'*, IEE Proceedings Optoelectronics in press (2004).

[6] **R. Kudrawiec**, E.-M. Pavelescu, J. Andrzejewski, J. Misiewicz, A. Gheorghiu, T. Jouhti, and M. Pessa, *'The energy-fine structure of GaInNAs/GaAs multiple quantum wells grown at different temperatures and post-grown annealed'*, J. Appl. Phys. in press (2004).

[7] **R. Kudrawiec**, E.-M. Pavelescu, J. Wagner, G. Sęk, J. Misiewicz, J. Konttinen, and M. Pessa, *'The photoreflectance evidence of multiple band gaps in dilute GaInNAs layers lattice–matched to GaAs'*, J. Appl. Phys. in press (2004).

[8] J. Misiewicz, **R. Kudrawiec**, K. Ryczko, G. Sęk, A. Forchel, J.C. Harmand, and M. Hammar, *'Photoreflectance investigations of the energy level structure in GaInNAs-based quantum wells'*, J. Phys. Cond. Mat. in press (2004).

[9] **R. Kudrawiec**, G. Sek, J. Misiewicz, L.H. Li, and J.C. Harmand, *'Investigation of recombination processes involving defect-related states in (Ga,In)(As,Sb,N) compounds'*, Eur. Phys. J. B, in press (2004).

[10] W. Rudno-Rudzinski, **R. Kudrawiec**, J. Misiewicz, and J. Derluyn, *'Influence of TBAs flow in MOCVD growth on nitrogen incorporation in GaAsN alloy and its optical quality detected by photoreflectance'*, phys. stat. solidi (c) 1, 329 (2004).

[11] **R. Kudrawiec**, J. Misiewicz, M. Fischer, and A. Forchel, *'Optical properties of GaInNAs/GaAs quantum wells: character of optical transitions and carrier localisation effect'*, phys. stat. solidi (a) 201, 364 (2004).

[12] **R. Kudrawiec**, G. Sęk, J. Misiewicz, L.H. Li, and J.C. Harmand, *'Influence of carrier localization on modulation mechanism in photoreflectance of GaAsN and GaInAsN'*, Appl. Phys. Lett. 83, 1379 (2003).

[13] **R. Kudrawiec**, G. Sek, J. Misiewicz, D. Gollub, and A. Forchel, *'Explanation of annealing-induced blueshift of the optical transitions in GaInAsN/GaAs quantum wells'*, Appl. Phys. Lett. 83, 2772 (2003).

[14] **R. Kudrawiec**, G. Sek, K. Ryczko, J. Misiewicz, P. Sundgren, C. Asplund, and M. Hammar, *'The nature of optical transitions in $Ga_{0.64}In_{0.36}As_{1-x}N_x$/GaAs single quantum wells with low nitrogen content ($x \leq 0.008$)'*, Solid State Commun. 127, 613 (2003).

[15] **R. Kudrawiec**, J. Misiewicz, L.H. Li, and J.C. Harmand, *'Experimental investigation of the C_{MN} matrix element in the band anticrossing model for GaAsN and GaInAsN layers'*, Solid State Commun. 129, 353 (2004).

[16] J. Derluyn, I. Moerman, M.R. Leys, G. Patriarche, G. Sek, **R. Kudrawiec**, W. Rudno-Rudzinski, K. Ryczko, and J. Misiewicz, *'Control of nitrogen incorporation in Ga(In)NAs grown by metalorganic vapor phase epitaxy'*, J. Appl. Phys. 94, 2752 (2003).

[17] J. Misiewicz, P. Sitarek, K. Ryczko, **R. Kudrawiec**, M. Fischer, M. Reinhardt, and A. Forchel, *'Influence of nitrogen on carrier localization in InGaAsN/GaAs single quantum wells'*, Microelectronics Journal 34, 737 (2003).

Author's contribution

All photoreflectance and photoluminescence spectra presented in the papers and this thesis were measured by the author. Samples were grown by the co-authors of the publications. XRD and Raman measurements were preformed by the co-authors of publications. Therefore, the author would like to thank E.-M. Pavelescu and Prof. J. Wagner for the use of XRD and Raman data in this thesis. The calculations of QW structures were performed by Dr. K. Ryczko. The manuscripts of papers 1 to 15 were written by the author.

Contents

1. Introduction

Semiconductor lasers operating at 1.3 and 1.55 μm wavelength are very important light sources in optical communications since the quartz fibre used as a transport media of light has dispersion and attenuation minima, respectively, at these wavelengths see Fig.1.1 [1]. These long-wavelength lasers have been traditionally fabricated on InP substrates using InGaAsP bulk layers and quantum wells (QW) as an active material. However, this material system has relatively poor high-temperature characteristics and the power output is limited due to the poor electron confinement in the QWs. Therefore, there has been considerable effort for many years to fabricate long-wavelength laser structures on other substrates, especially on GaAs. The manufacturing cost of GaAs-based components is lower and the processing techniques are well developed.

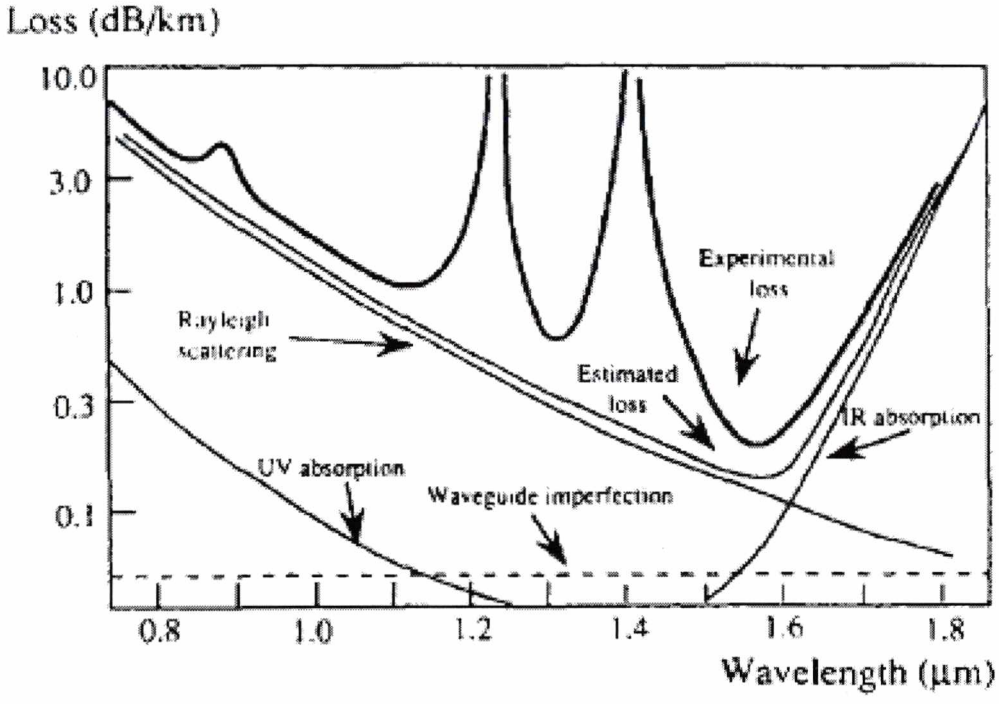

Figure 1.1. Fiber loss vs. wavelength of a silica based fiber with the transmission windows at 1.3 and 1.5 μm [1].

GaAs is already successfully used in 850 nm vertically cavity surface-emitting lasers (VCSELs) which have become common in short-range optical communications. The incredible growth of the internet and data transmission has pushed the bit-rate requirements for local area networks (LANs) and metro area networks (MANs) from 100 Mbps to 10 Gbps. Therefore, there is a great demand for low-cost, 1.3 or 1.55 μm VCSELs that will operate uncooled under

ambient conditions. The requirement for such longer wavelength lasers is illustrated in Fig.1.2 [2]. For 850 nm VCSELs at 100 Mbps, the transmission distance is 7-8 km, while at 10 Gbps, the transmission distance is only about 50 m, not even useful for a small, intra-building LAN. While InGaAsP/InP-based Bragg grating and distributed feedback (DFB) lasers have been the sources for long-haul, 1.55 μm optical fibre backbone networks for the past three decades, their cost is simply far too high to meet the demands of tens of million lasers that might be utilized in each MAN and LAN in modern datacom network architecture. There has been intense effort to realize such low cost, long wavelength VCSELs over the past decade, however, the physical properties of the previously utilized semiconductor systems made this nearly impossible. Therefore, in order to realize low cost and high efficient VCSELs lasers emitting at 1.3 or 1.55 μm a new material concept is necessary.

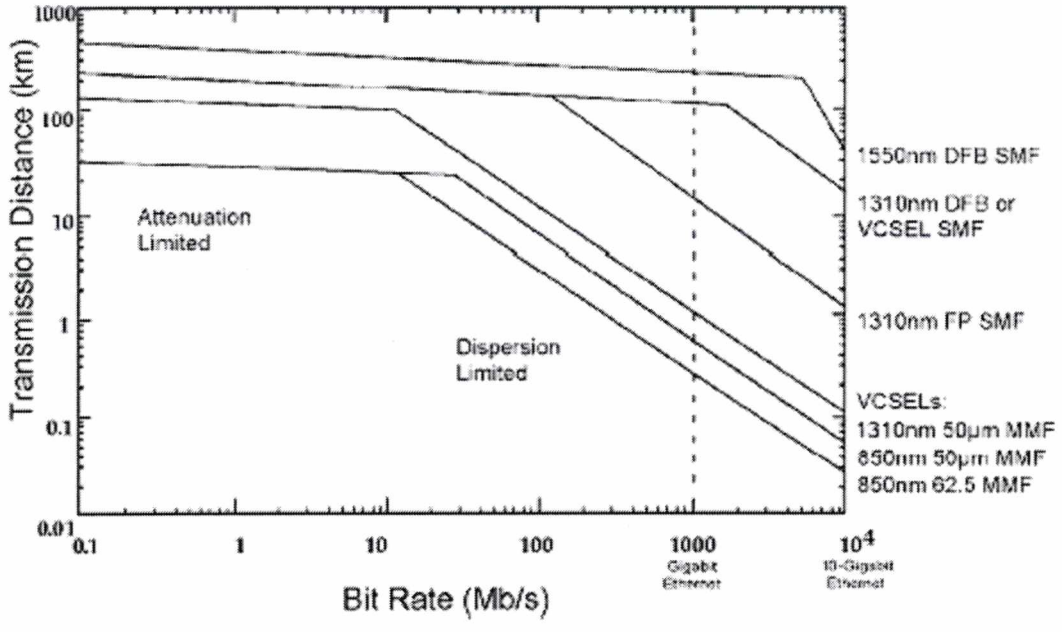

Figure 1.2. Transmission distance versus laser modulation frequency for a variety of optical-fibre/laser-diode sources utilized in optical networks [2].

Different III-V alloys are shown in Fig.1.3. Semiconductor lasers operating in 1.3-1.6 μm region require materials with band gaps between 0.95 and 0.78 eV. Moreover, one of the requirements for alloy semiconductor is that they must be reasonably close lattice matched to readily available binary substrate (GaAs, InP or GaSb). For many years it was believed that there was no suitable alloy lattice matched to GaAs that would emit at >1.1 μm, so InGaAsP on InP was the only materials system that meet the perceived criteria. Therefore, almost all the long-wavelength communication lasers presently in use are fabricated from this system. While InGaAsP met the needs of edge-emitting lasers, it is almost impossible to meet the requirements

for growth of distributed Bragg reflector (DBR) quarter-wave VCSEL mirrors, particularly at 1.3 μm. This is because the refractive index contrast of InP/InGaAsP is insufficient, and both thermal and electrical conductivities are to low to realize the required combination of high reflectivity and low thermal and electrical resistance. Thermal issues are particularly a problem for InGaAsP-based VCSELs because of their low T_0, which results from the relatively small conduction band offset InGaAsP and InP: $\Delta E_C = 0.4 \cdot \Delta E_g$. This allows electrons to escape from the quantum well when they have enough thermal energy. Because of the thermal performance and limited gain of the active regions in VCSELs, it is of utmost importance to minimize the DBR electrical and thermal resistance, as well as avoid free carrier absorption from high doping. These almost impossibly conflicting requirements have pushed the investigation of alternative approaches for long-wavelength lasers.

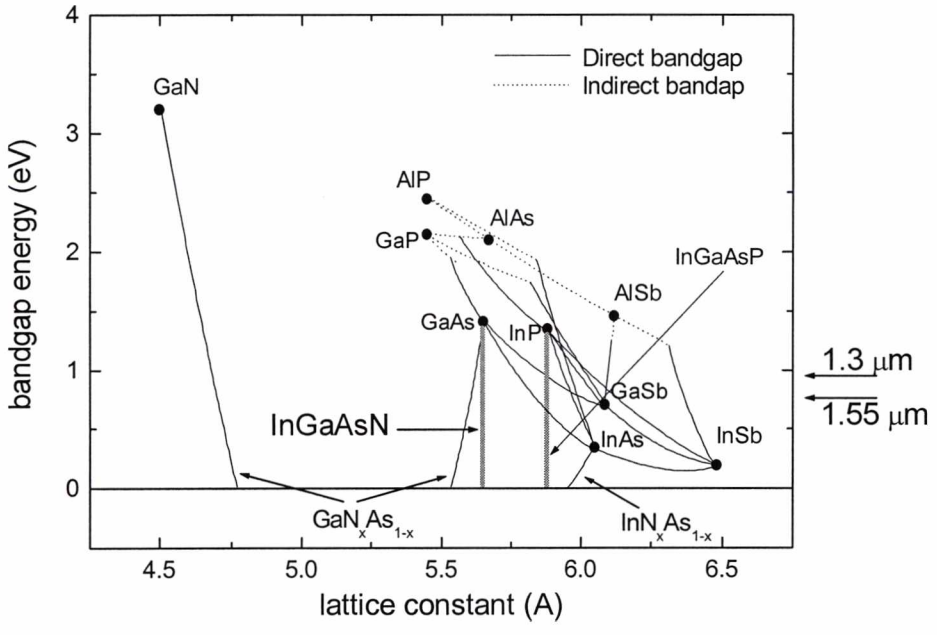

Figure 1.3. Lattice constant and band gap energy of III-V semiconductors. The vertical grey areas illustrate application area of GaAs and InP substrates.

A lot of work is concentrating on structures grown on GaAs substrate [3]. One approach to achieve 1.3 μm emission on GaAs is to use self-assembled In(Ga)As quantum dots (QDs) in the active region [4]. The QDs are three-dimensional self-organized In(Ga)As islands formed on GaAs when a critical thickness for island formation is extended. Although QW lasers have been predicted to have better characteristics than QW lasers, such as lower threshold current density and negligible temperature dependency, the commercial breakthrough has not yet occurred. Another approach was introduced in 1996 by Kondow *et al.* [5] who proposed a novel

quaternary material GaInNAs, which could be grown lattice matched on GaAs and used to fabricate long-wavelength lasers with better temperature characteristic compared to InP-based lasers. Ga(In)NAs is unusual candidate for small band gap semiconductor. Contrary to general rules of III-V alloy semiconductors where a smaller lattice constant increases the band gap, the electronegativity of N and its small covalent radius cause a very strong negative bowing parameter and the addition of N to GaAs or GaInAs dramatically decreases the band gap, as shown in Fig.1.3. The large band gap bowing with nitrogen incorporation has been observed for the first time for the ternary alloy GaNAs by Weyers *et al.* [6] back in 1992. The study of these and other III-V-N alloys has been increasing ever since. The development of a GaInNAs/GaAs VCEL operating at 1.3 μm wavelength has been rapid, and the first commercial products of Infinion have appeared in 2004 year. GaInNAs can also be used to improve the characteristics of multijunction solar cells [7] and heterojunction bipolar transistors [8]. The aim of this thesis is the application of photoreflectance and photoluminescence spectroscopies to investigate the optical properties of III-V-N alloys and their low dimensional structures grown on GaAs substrate.

2 Experimental techniques and samples

In this chapter experimental techniques applied to investigate the optical properties of III-V-N semiconductor alloys and their low dimensional structures are presented. The author has introduced Sections devoted principles of PR spectroscopy and methods of the analysis of PR spectra. In the case of PL technique, which is more popular, the author presents only a brief description of this method. Moreover, the experimental setup for PR and PL measurements are described.

2.1 Photoreflectance

Photoreflectance spectroscopy is one of the classes of modulation spectroscopy (MS). Each class of optical MS utilizes a general principle of experimental physics, in which a periodically applied perturbation either to probe or the sample leads to derivate-like features in the optical response of the sample. Therefore, the objective of modulation spectroscopy is to change some parameter of the sample (internal modulation) or of the measuring system (external modulation) so as to produce a change in the optical reflectance or transmittance spectrum of the sample. In either case the changes are usually small so the difference spectra are closely related to the derivate of the absolute spectrum with respect to the modified parameters. The derivate nature of modulation spectroscopy emphasizes features localized in the photon energy region of interband transitions of semiconductor structures and suppresses uninteresting background effects. Also weak features that may not have been detected in the absolute spectra are often enhanced and a large number of sharp spectral features can be observed even at room temperature [9-12]. Mentioned advantages of MS spectroscopy are illustrated qualitatively in Fig.2.1, which compares three types of spectra obtained at room temperature (RT) for a typical GaInNAs/GaAs single quantum well (SQW).

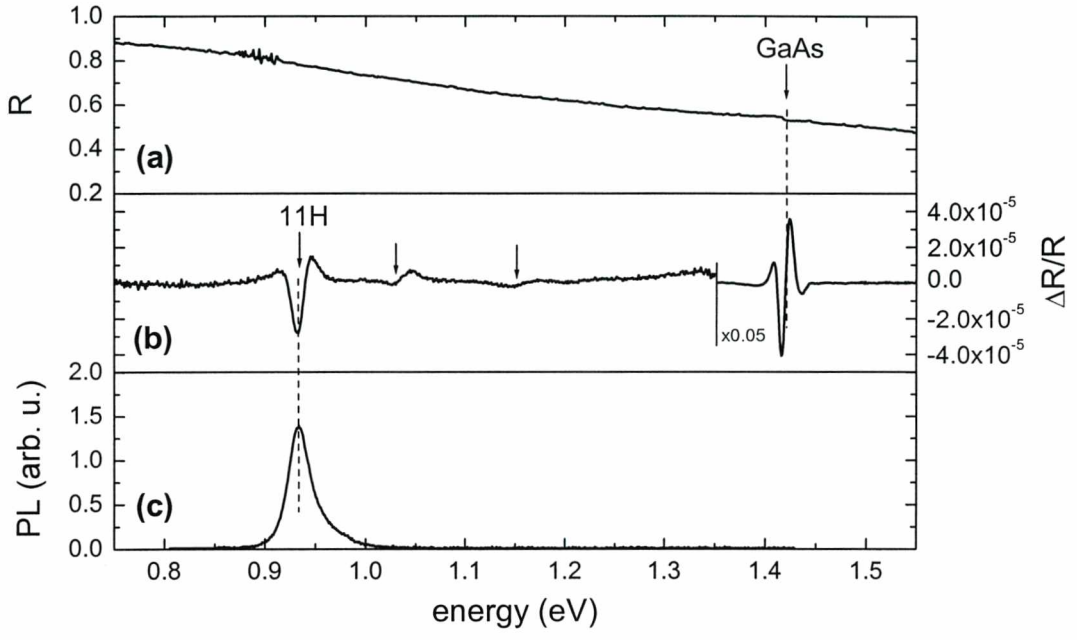

Figure 2.1. Comparison of room temperature reflectance (a), photoreflectance (b) and photoluminescence spectra (c) of a GaInNAs/GaAs single quantum well structure.

While the reflectance spectrum (R) is characterized by broad features, the photoreflectance (PR) spectrum is dominated by a series of very sharp lines with zero signal as a baseline. In PR spectrum we observe transitions related to absorption in both the GaInNAs/GaAs QW and GaAs barriers. In the case of QW, both the ground (11H) and excited state transitions are observed. In contrast, photoluminescence (PL) probes only the ground state transition. Combination of PR (absorption-type experiment) and PL (emission-type experiment) is a powerful tool to investigate the nature of recombination processes.

2.1.1 Principles of electromodulation in electro- and photo-reflectance spectroscopy

The condition to obtain electro- or photo-reflectance spectra is the existence of a built-in electric field in the structure being under investigation [8-12]. This condition is usually fulfilled in majority structures, because every good quality structure posses a surface electric field. In electroreflectance, an applied electric field is modulated so as to produce a periodic variation in the dielectric function. The electric field can be applied to the sample in a variety ways. By electric contacts or without such contacts. In the last mode, 'so called' contactless electrorefletance (CER), sample is put in a light transparent capacitor. The other mode of ER

which is also contactless technique is the PR. In the case of PR, the modulation of the electric field in the sample is caused by photoexcited electron-hole pairs created by the pump source (usually laser) which is chopped with a given frequency. The photon energy of the pump source is generally above band-gap of the semiconductor being under study. There is a possibility to use a below band-gap modulation through the excitation of impurity or surface states [13]. The mechanism of the photo-induced modulation of the built-in electric field F_{DC} is explained in Fig.2.2 for the case of an n-type semiconductor. Because of the pinning of the Fermi energy E_F at the surface, there exists a space-charge layer. The occupied surface states contain electrons from the bulk (Fig.2.2(a)). Photoexcited electron hole pairs are separated by the built in electric field, with the minority carrier (holes in this case) being swept toward the surface. At the surface, the holes neutralize the trapped charge, reducing the built-in field from F_{DC} to F_{DC}-F_{AC}, where F_{AC} is a change in the built in electric field (Fig.2.2(b)). As it is seen, a built in electric field in the sample is necessary for photomodulation of the dielectric function.

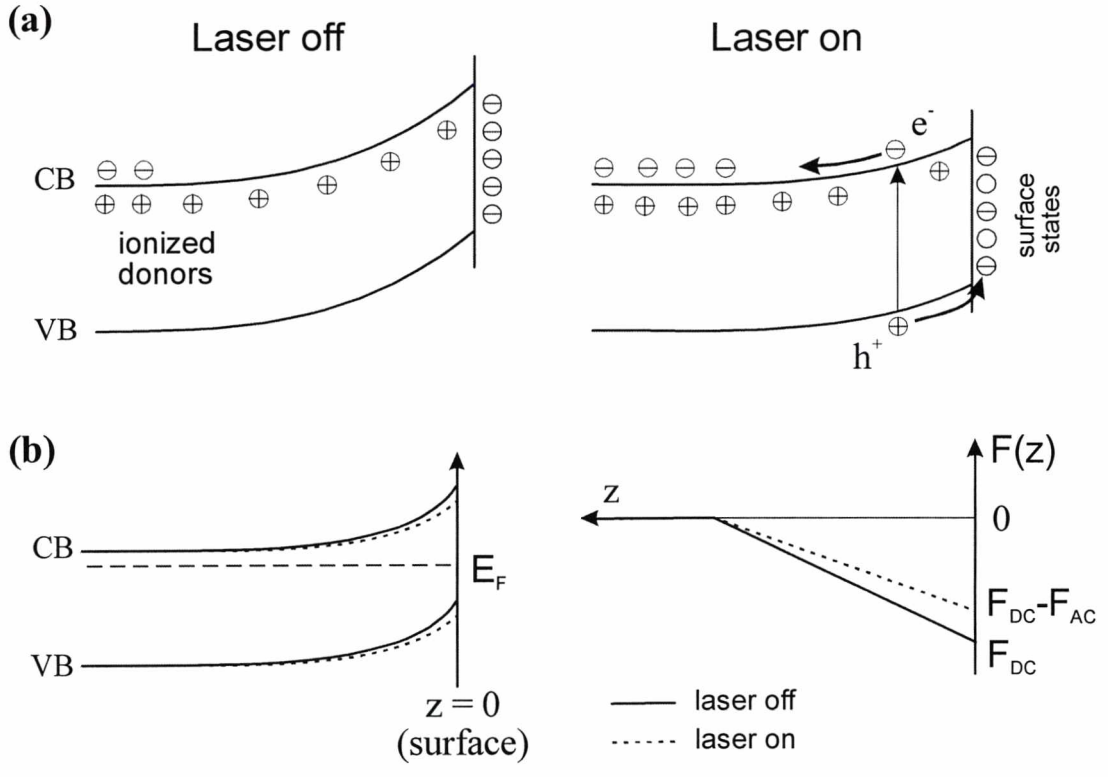

Figure 2.2. Schematic representation of the photoreflectance effect (a), and the photoinduced changes in electronic bands at the surface built-in electric field (b), for an n-type semiconductor.

In PR spectroscopy, relative changes in the reflectivity coefficient are measured. The changes we can define as

$$\frac{\Delta R}{R} = \frac{R_{off} - R_{on}}{R_{off}}. \tag{1}$$

In the above expression R_{off} and R_{on} are the reflectivity coefficients, when the pump beam (laser) is 'off' and 'on', respectively. These normalized changes can be related to the perturbation of the dielectric function ($\varepsilon = \varepsilon_1 + i\varepsilon_2$) expressed as [9, 10]

$$\frac{\Delta R}{R} = \alpha(\varepsilon_1, \varepsilon_2)\Delta\varepsilon_1 + \beta(\varepsilon_1, \varepsilon_2)\Delta\varepsilon_2, \tag{2}$$

where α and β are the Seraphin coefficients, related to the dielectric function, and $\Delta\varepsilon_1$ and $\Delta\varepsilon_2$ are related by Kramers-Kronig relations.

The line shapes of the PR response can be discussed in terms of electromodulation mechanisms. Electromodulation can be classified into three categories depending on the relative strengths of characteristic energies [9-14]. In the low-field regime $|\hbar\Omega| \leq \Gamma$, where $\hbar\Omega$ is the electro-optic energy given by Eq.(3)

$$(\hbar\Omega)^3 = \frac{q^2\hbar^2F^2}{2\mu}. \tag{3}$$

In above equation, F is the electric field; μ is the reduced interband mass in the direction of the field. In the intermediate-field case, when $|\hbar\Omega| \geq \Gamma$ and $qFa_0 << E_g$ (a_0 is the lattice constant), the Franz-Keldysh oscillations (FKO) appear in the spectrum. In the high-field regime the electro-optic energy is much greater than the broadening but $qFa_0 \approx E_g$ so that Stark shifts are produced. Recently, Pollak [10] and Glembocki and Shanabrook [11] provided a most detailed theoretical background of the electro- and photo-reflectance techniques.

2.1.2 Methods of the analysis of PR spectra

Electro- and photo-reflectance spectra of simple, lightly-doped systems, measured under low field conditions, can often be modelling using Aspnes third derivate functional form (TDFF) [14], so-called Lorentzian line shape Eq.(4)

$$\frac{\Delta R}{R} = \mathrm{Re}\left[C e^{i\theta}\left(E - E_g + i\Gamma\right)^{-m}\right], \tag{4}$$

where E_g is the critical point (CP) energy, Γ is the broadening parameter ($\Gamma \sim \hbar/\tau$), A and θ are the amplitude and the phase factor, respectively. The term m refers to the type of CPs, i.e. the nature of optical transitions, namely: $m=2$, 2.5 and 3 for an excitonic transition, a three-dimensional one-electron transition and a two-dimensional one-electron transition, respectively. This formula is appropriate at low temperatures for a high quality structures. At room temperatures the Lorentzian dielectric function is inappropriate and Eq.(4) must be replaced by more general formula Eq.(5) [15]

$$\frac{\Delta R}{R} = \mathrm{Re}\left[\frac{C \cdot e^{i\theta}\left[G(z) + i \cdot F(z)\right]}{E^2}\right], \tag{5}$$

where $G(z)$ and $F(z)$ are the electro-optic functions and broadening is included via the normalized energy $z = \dfrac{E_0 - E + i \cdot \Gamma}{\hbar\theta}$. The Eq.(5) becomes complex for the Gaussian-like form of the dielectric function. Such form of Eq.(5) is called as the first derivate Gaussian line shape (FDGL), and this form is the most appropriate at room temperature and/or for a sample with high inhomogeneities. Notice that in the some range of temperature the line shape is an intermediate form between Lorentzian and Gaussian line shape [10, 11].

An alternative method for determining of E_g, Γ and C (but not θ) has been developed based on a Kramers-Kronig transformation of the PR (or ER) spectrum [16-18]. In this case, the complex PR function is defined as below:

$$\Delta\tilde{\rho}(E) = \Delta\rho_R(E) + i\Delta\rho_I(E) = \Delta\rho(E)e^{i\Theta(E)}, \tag{5}$$

where the measured value of the ER or PR signal is equal to

$$\frac{\Delta R}{R}(E) = \Delta\rho_R(E) = \Delta\rho(E) \cdot \cos\Theta(E). \tag{6}$$

After mathematical considerations similar to that carried out for other optical constants functions, the Kramers-Kronig relation for the complex PR function Eq.(5) can be written:

$$\Delta\rho_I(E_0) = \frac{2E_0}{\pi} P\int_{E_a}^{E_b} \frac{\Delta R}{R} \frac{1}{E_0^2 - E^2} dE, \tag{7}$$

where $P\int$ means the principal value of the integral and (E_a, E_b) is the energy range in which $\frac{\Delta R}{R}$ is measured. The values of E_a and E_b should be chosen in a way that $\frac{\Delta R}{R}(E_a) = \frac{\Delta R}{R}(E_b) = 0$ having all the oscillations interesting for us inside this range. Knowing the values of $\Delta\rho_I$ the modulus $\Delta\rho$ can be determined by means of the simple formula:

$$\Delta\rho(E) = \sqrt{\left(\frac{\Delta R}{R}(E)\right)^2 + (\Delta\rho_I(E))^2}, \tag{8}$$

which can be treated as the modulus of PR resonance.

In the framework of standard fitting procedure, e.g. Eq.(4), the modulus of PR resonance is defined by Eq.(9)

$$|\Delta\rho(E)| = \frac{|A|}{\left[(E - E_0)^2 - \Gamma^2\right]^{\frac{m}{2}}}, \tag{9}$$

In order to plot the modulus C, E_0, θ, and Γ parameters have to be determined by using the fitting procedure. The advantage of the Kramers-Kronig analysis (KKA) is to avoid the fitting procedure. Such approach is very useful if the line-shape of PR data changes between Lorentzian- and Gaussian-like. Notice that the integrated modulus of PR resonance is interpreted as the oscillator strength of the optical transition while E_0 and Γ are the transition energy and the transition broadening, respectively. The broadening is related to the sample quality and is temperature dependent parameter. A comparison of the analysis of PR data using standard fitting procedure and KKA is shown in Fig.2.3.

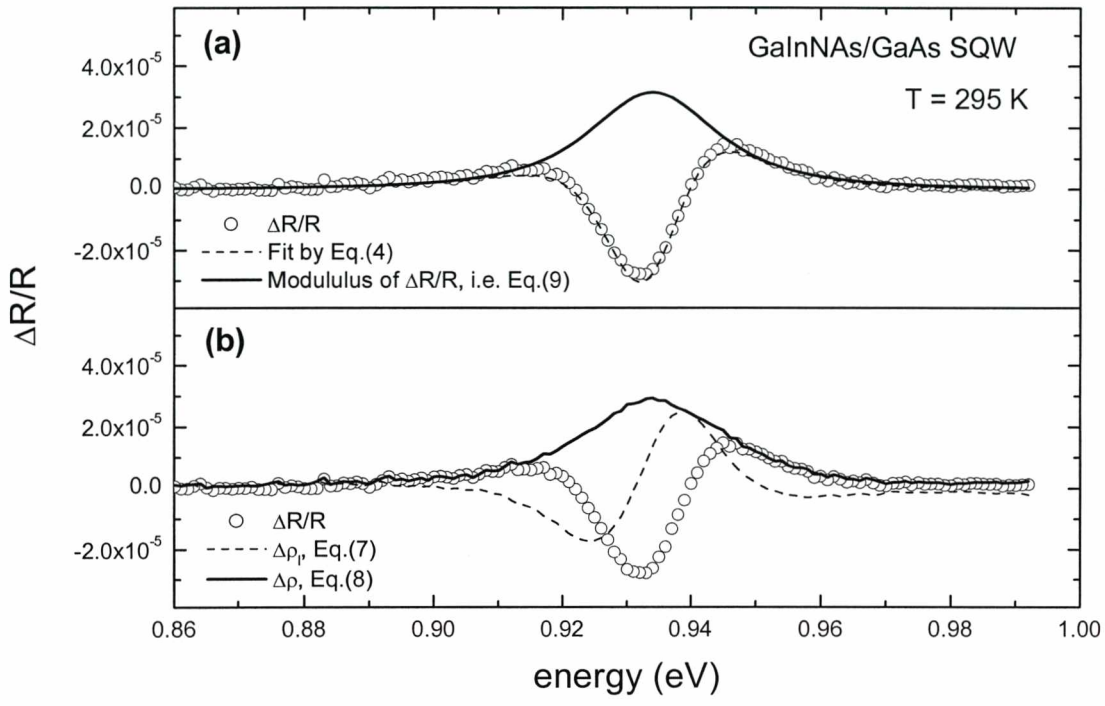

Figure 2.3. Photoreflectance spectrum (open points) of GaInNAs/GaAs SQW (the same as in Fig.2.1) in the vicinity of ground state transition, and its analysis by standard fitting procedure (a) and the Kramers-Kronig analysis (b). Note the same dependencies of modulus of ΔR/R determined by the two approaches.

The panel (a) of Fig.2.3 shows experimental data (open points) which are fitted by Eq.(4) with $m = 3$ (dashed line), together with the modulus of the resonance Eq.(9) (solid line). The panel (b) of Fig.2.3 shows the same experimental data (open points) with the modulus of PR resonance obtained using KKA Eq.(8) (solid line). The dashed line in Fig.2.3(b) shows the $\Delta\rho_I$ obtained from the Eq.(7). As it is seen in Fig.2.3 the same transition energies, broadenings Γ, and intensities have been obtained using the two different approaches.

2.2 Photoluminescence

PL spectroscopy is a widely-used, non-destructive characterization method which gives information about energy states and different radiative recombination channels in semiconductors. The photons from the excitation beam are absorbed by the sample and electron-hole pairs are created. The carriers thermalize quickly to the band edge though phonon emission, diffuse in the structure and recombine radiatively or non-radiatively. A typical PL spectrum is

composed of several types of transitions. Common radiative transitions are a band-to-band transition, a transition from the conduction band to an acceptor state (from the donor state to the valence band), a donor-acceptor pair transition, and bound- and free-exciton transitions.

Measurements as a function of temperature and excitation laser power are two frequently used methods for identification of the different transitions. From temperature-resolved PL measurements the thermal activation energies of the transitions can be extracted and thus information about energy states can be gained. The temperature dependence of the integrated PL intensity can be formulated as

$$I(T) = \frac{I_0}{1 + \sum_{i=1}^{n} c_i \cdot e^{\frac{-E_i}{kT}}}, \tag{10}$$

where c_i is a temperature-dependent parameter for each transition mechanism I, E_i is the corresponding thermal activation energy and I_0 is the intensity at $T=0$ K [19].

From PL measurement as a function of excitation laser power a shift of PL band can be detected. Usually, the presence of the shift is typical of defect-related recombination and the absence of the shift is typical of recombination between extended states [19].

In the case of QW structures the emission peak related to the ground state transition in the QW is a superposition of excitonic and free carrier recombinations [20]. Excitonic recombination is described using a Gaussian line-shape multiplied by the Bolzmann distribution:

$$I_x(\hbar\omega) = A_x \cdot \exp\left(-\frac{[\hbar\omega - E_x]^2}{2 \cdot \sigma_x^2}\right) \cdot \exp\left(-\frac{(\hbar\omega - E_x)}{k_B T}\right), \tag{11}$$

where A_x, E_x, and σ_x denote the amplitude, energy and broadening parameter of the heavy-hole exciton peak, respectively. The free carrier recombination terms include a broadened step-like two-dimensional density of states, multiplied by the free carrier statistical distribution in Bolzmann approximation and the two-dimensional Sommerfield factor:

$$I_c(\hbar\omega) = A_c \cdot \frac{1}{1 + \exp\left(-\frac{[\hbar\omega - E_c]}{\sigma_c}\right)} \cdot \frac{2}{1 + \exp\left(-2\pi \cdot \sqrt{\frac{R^*}{[\hbar\omega - E_c]}}\right)} \cdot \exp\left(-\frac{\hbar\omega}{k_B T}\right). \tag{12}$$

Here A_c, E_c, and σ_c are the amplitude, energy and broadening parameter of the free carrier recombination, respectively.

The distribution of partial contributions of the two recombination channels depends on the temperature. The excitonic recombination is dominant at low temperatures while the band-to-band recombination is dominant at room temperature [20-23].

Moreover, the character of the recombination process in QW structures can be concluded from Eq.(13)

$$I_{PL}(P) = \beta \cdot P_{ex}^{\alpha}, \tag{13}$$

where I_{PL} is the integrated intensity, P_{ex} is excitation power, β and α are fitting parameters. The exponent α has the following values: $\alpha = 1$ for excitonic recombination (whether radiative or non-radiative recombination dominates); $\alpha = 2$ for free carrier recombination (assuming that non-radiative recombination dominates); $1 < \alpha < 2$ for the intermediate case where both free exciton and free carrier recombinations take place [24].

2.3 Experimental setups

A schematic diagram of the photoreflectance apparatus used in this thesis is shown in Fig.2.4. The probe light is a monochromatic beam obtained from a quartz halogen lamp dispersed through a monochromator. This beam of intensity I_0 is focused on the sample. The laser (pumping) beam illuminates the same spot of the sample. The laser beam is chopped with frequency of a few hundreds Hz. The photon energy of the pump source should be generally above the band gap of the semiconductor being investigated. Lasers with different wavelengths are used as typical pump sources. The intensity of the laser light can be adjusted by a variable, neutral density filter. The light reflected from the sample is detected by a photodiode or a photomultiplier. In order to prevent the detection of laser light, an appropriate longpass glass filter is used in front of the photodetector. The signal separator, connected to the detector, separates the signal into two components. The DC component is proportional to I_0R, and AC component is proportional to $I_0\Delta R$. The AC component is measured with a lock-in amplifier. A

computer divides the AC signal by the DC component giving the photoreflectance spectrum, $\frac{\Delta R}{R}(E)$, where E is the photon energy of the incident beam.

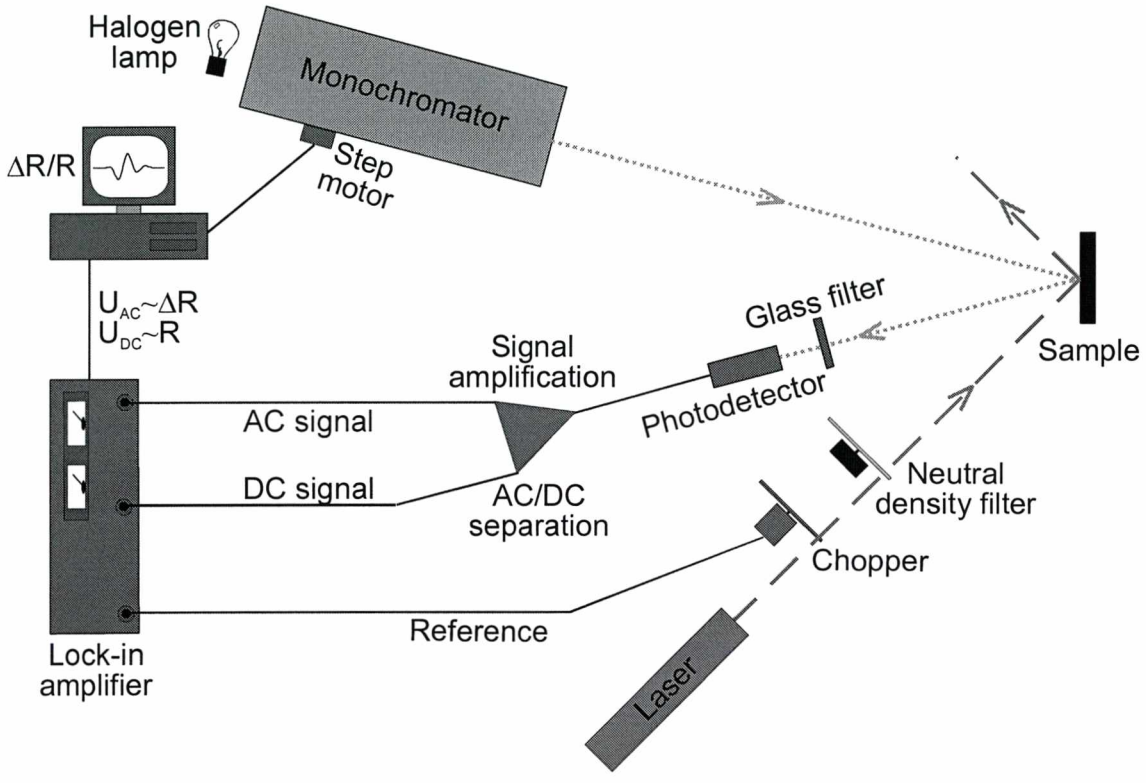

Figure 2.4. A scheme of apparatus for photoreflectance measurements.

In the case of photoreflectance, it is important for the apparatus to have good filtering of the stray laser light, because it has the same frequency (chopped) as the signal of interest and can easily be detected. The scattered pump light can be reduced by means of an appropriate longpass filter in front of the detector. Furthermore, the laser illumination can produce a band gap photoluminescence, which under certain conditions is more in intense than the signal of interest it can be eliminated by using long-focal-length optics. In one of PR setups used to measurements a double detector system is used for photoluminescence background and residual stray light compensation [25, 26].

PL setup used in this thesis is presented in Fig. 2.5. The laser light from a laser was guided with mirrors through a chopper and focused (or not focused) onto a sample The photoluminescence emitted from the sample was focused by lenses to the input slit of the monochromator and dispersed with a grating of the monochromator and detected by photodiode or photomultiplier.

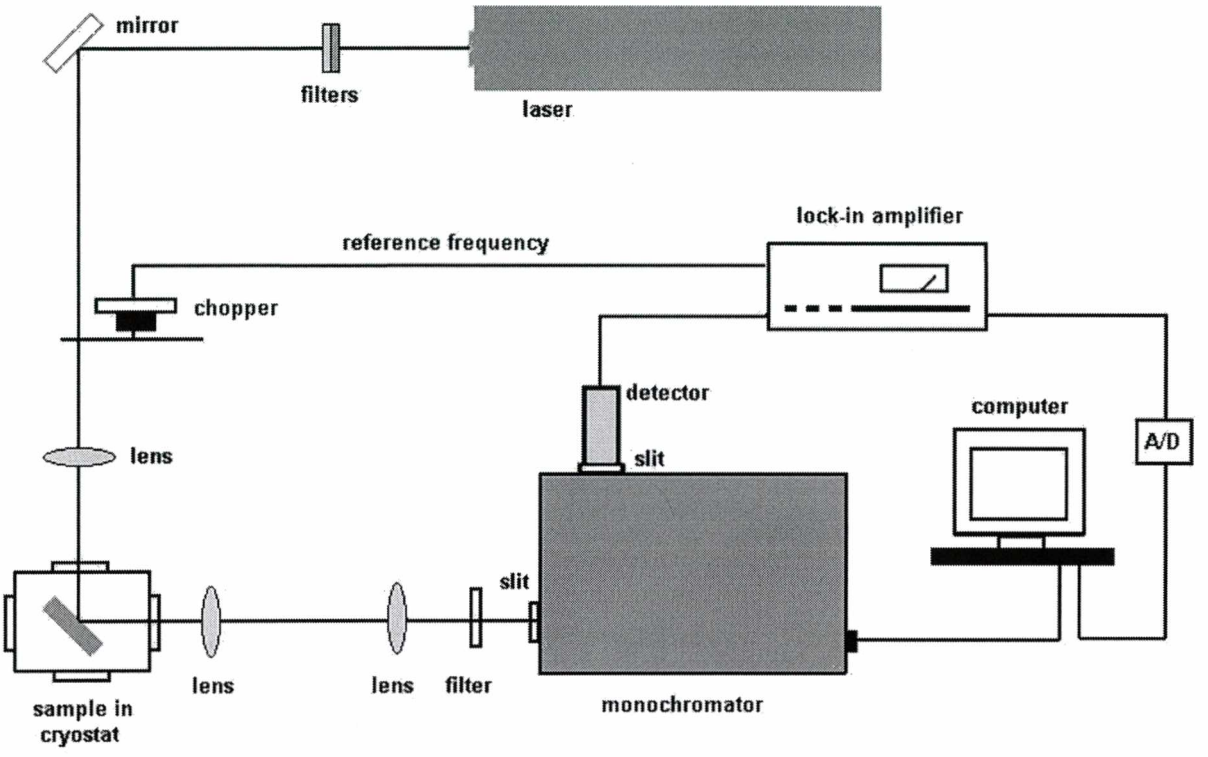

Figure 2.5. A scheme of apparatus for photoluminescence measurements.

All measurements presented in this thesis were preformed on two setups. One based on a double grating GDM 1000 monochromator and second based on a single grating Yobin-Yvon TRIAX 550 monochromator. The first setup is dedicated only for PR measurements, but possesses high sensitivity ($\Delta\left(\frac{\Delta R}{R}\right) < 10^{-6}$). The second setup has possibility to measure both PR and PL, therefore, most of measurements were preformed on this setup. For low temperature PR and PL measurements samples were attached to a cold finger of a closed-cycle helium cryostat, as in Fig.2.5. The cryostat can be cooled down to 9 K and heated up to 320 K. Different laser lines obtained from a He-Ne laser, semiconductor lasers, Ar-ion lasers were used as the pump beam in PR and excitation beam in PL. A thermoelectrically cooled GaInAs photodiode or a germanium photodiode cooled with liquid nitrogen were used to detect the light intensity at selected wavelength. PL and PR signals were detected in the 'so-called' Lock-in technique by using SR830 or SR510 Stanford Lock-in amplifiers.

2.4 Samples

Both molecular beam epitaxy (MBE) and metal-organic vapour-phase epitaxy (MOVPE) grown samples were used in this study. MBE samples were grown at the Wurzburg University (WU) in Germany, at the Laboratoire de Photonique et de Nanostructures (LPN) CNRS in France, at the Stanford University (SU) in USA, and at the Tampere University of Technology (TUT) in Finland. MOVPE samples were grown at the Royal Institute of Technology (KTH) in Sweden and at INTEC University Gent (UG) in Belgium. More details about MOVPE and MBE machines and growth process can be found elsewhere [27-31]. A description of samples used for this thesis (i.e. the content of GaInNAs layers, the width of QWs ect.) is introduced in subsections which report results obtained for appropriate samples.

3. Fundamentals of Ga(In)NAs

So far, it has been possible to grown Ga(In)NAs on GaAs substrate with the content of a few percent of N atoms [2]. However, the basic parameters, like conduction band and valence band energies, Ga(In)NAs/GaAs band offsets, or effective masses are not well known and the results of different research groups are inconsistent [2]. This is due to the difficult growth conditions and the very exceptional physical properties of the alloy. The first step in understanding physical properties of low dimensional semiconductor structures and advanced devices, e.g. laser structures, is to determine the band structure of bulk materials. An intensive progress in this field was possible due to the applications of the optical modulation spectroscopy, i.e. photo- or electro-reflectance [32-65]. The aim of this thesis is the application of PR spectroscopy to investigate III-V-N semiconductor alloys and their low dimensional structures. Therefore, a brief 'state of the art' of the photomodulation spectroscopy preformed on Ga(In)NAs semiconductors is presented in this section. PL spectroscopy is the second experimental technique used for this thesis. This technique is treated as a complementary experiment to PR one, therefore, only a brief summary for PL properties is presented in this chapter. Moreover, the author has introduced theoretical approaches, which have been proposed to describe the band structure of III-V-N semiconductors.

3.1 Anomalous properties of III-V-N compounds

In a typical isovalent AB_xC_{1-x} alloy semiconductor, the properties of AB_xC_{1-x} change gradually from the properties of the material AC to the properties of the material AB as the composition x is increases from 0 to 1. Most of the material parameters change linearly with composition. The linear behavior of lattice constant is known as the Vegard's law. The band gap energy usually exhibits nonlinear bowing (see Fig.1.3 in Chapter 1), and the change in the band gap energy is expressed as

$$E_{g,ABC}(x) = x \cdot E_{g,AB} + (1-x) \cdot E_{g,AC} - b \cdot x \cdot (1-x), \tag{13}$$

where b is a bowing coefficient. The value of c is usually less than 2 eV and it is composition-independent. In contrast, alloying GaAs with nitrogen leads to a giant band gap bowing with

increasing nitrogen mole fraction, see in Fig.3.1 [66]. Similar effects have been observed for other III-V-N semiconductor alloy with a few percent of nitrogen mole fraction [66].

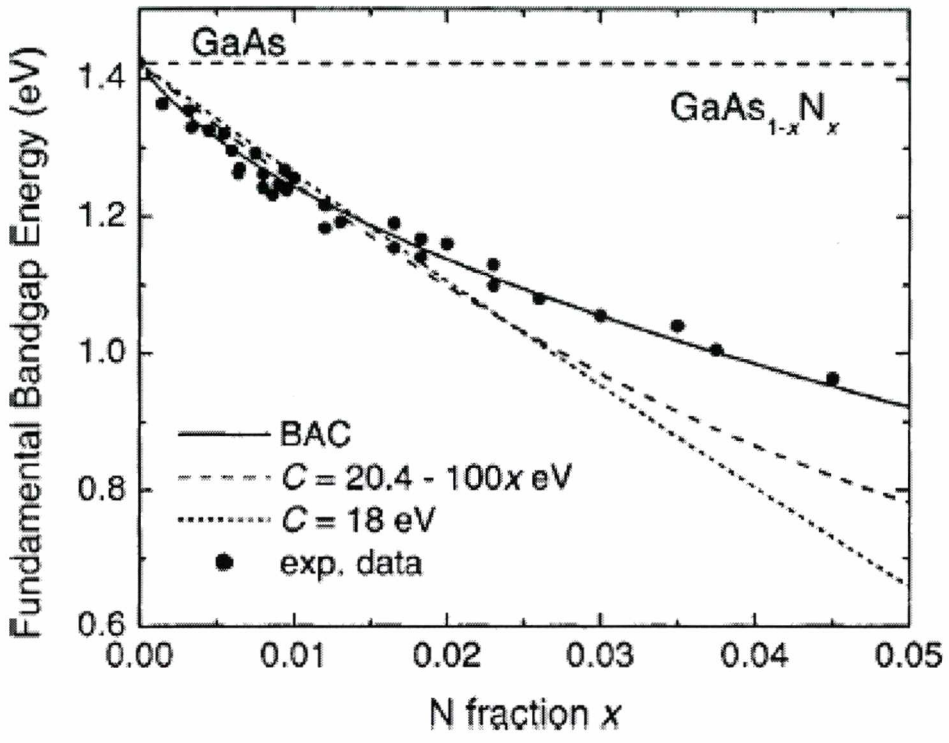

Figure 3.1. Energy of the fundamental band gap transition in GaAsN as a function of nitrogen fraction x (a) from BAC model (solid curve), (b) using the variable bowing parameter (dashed curve), and (c) using a constant bowing parameter (dotted curve). For comparison, the available experimental data is also ploted (circles) [66].

The anomalous properties of GaAsN arise from the large size difference between the N and As atoms. The covalent radii of N is 0.068 nm compared to that of 0.121 nm for As. The large electronegativity (Pauling scale) of N (3.04) compared to Ga (1.81) and As (2.18) makes the Ga-N bond more polar that the Ga-As bond and favours the electron localisation around the N atom. The large difference between the As and N atoms creates anomalous electrical and optical properties. However, the lattice constant and elastic properties have a linear behaviour with increasing substitutional N content of GaAsN [67]. This enables the determination of N composition with a conventional x-ray diffraction method.

The other anomalous properties of III-V-N alloys which are usually attributed to the presence of the few percent of N atoms are an increase in the electron effective mass [68], a strong carrier localisation at low temperatures [69-71], a strong line width broadening of all optical transitions [45], and a blueshift of band gap energy after annealing at no-change in the compound composition [72-75]. All these properties are investigated in this thesis.

3.2 Photo- and electro-reflectance of Ga(In)NAs layers and quantum wells

Ga(In)NAs compounds have been investigated using modulation spectroscopy at the first time in the end of the nineties [31-38]. Significant progress in describing the effect of N on the electronic structure of III-V-N alloys has been made due to investigations of the pressure dependent PR spectra of GaInNAs alloys [32]. Shan et al. [32] have investigated (0.5-5 μm) thick GaInNAs layers grown by MOVPE. In this paper the authors have observed an extra feature (E_+) on a higher energy side in the PR features related to the fundamental band gap transition (E_- transition) and the transition from the top of the spin-orbit split-off valence band to the bottom of the conduction band ($E_-+\Delta_0$), see in Fig.3.2.

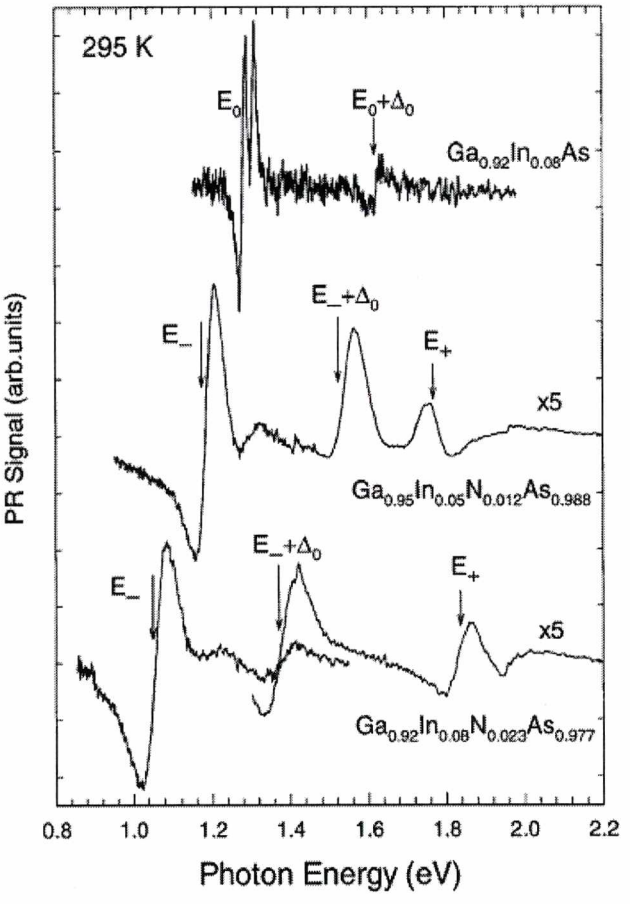

Figure 3.2. PR spectra of $Ga_{1-x}In_xN_yAs_{1-y}$ samples: (top) $Ga_{0.92}In_{0.08}As$ (y = 0), the E_0 and $E_0+\Delta_0$ transitions are observed; (middle) $Ga_{0.95}In_{0.05}N_{0.012}As_{0.988}$, the E_- and $E_-+\Delta_0$ transitions shift to lower energy, and a new feature E_+ appears; (bottom) $Ga_{0.92}In_{0.08}N_{0.023}As_{0.977}$ (this sample has the same In content as the top sample), the addition of more N pushes the E_- and $E_-+\Delta_0$ to lower energy and E_+ to higher energy. The arrows indicate the transition energy positions [32].

While the E_- and $E_-+\Delta_0$ transitions shift to lower energy with the increasing In and N concentrations, the E_+ transition moves in the opposite direction. This demonstrates that the splitting between E_- and E_+ increases with N content. In order to explain the experimental data and their pressure dependencies Shan et al. has proposed a simple band anticrossing (BAC) model, which is presented briefly in next part of this section. Very similar experimental results were simultaneously obtained by Perkins et al.[33]. These researchers were measured ER spectra for a series of GaN_xAs_{1-x} (1-7 μm) thick layers with $x<0.03$ as well as two quaternary $Ga_{0.95}In_{0.05}N_{0.013}As_{0.987}$ and $Ga_{0.92}In_{0.08}N_{0.022}As_{0.978}$ layers. The authors have observed the fundamental band gap transitions (E_0), the transition from the spin-orbit split-off valence band ($E_0+\Delta_0$) and an additional transition (denoted E_+) for $x>0.008$ (see ER spectra in Fig.3.3).

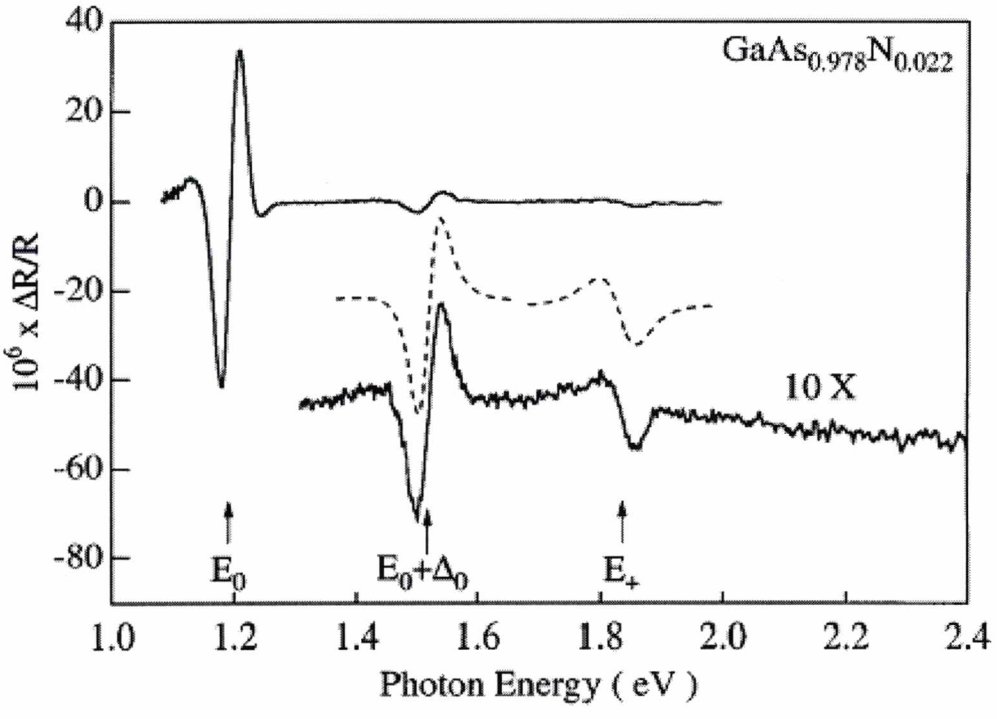

Figure 3.3. Electroreflectance spectra for a 2 μm thick $GaAs_{0.978}N_{0.022}$ film on a GaAs substrate. The band gap transitions (E_0) at 1.19 eV as well as the transition from the spin-orbit spin-off valence band ($E_0+\Delta_0$) at 1.52 eV are easily seen. An additional weak feature (E_+) at 1.83 eV is more clearly seen in the second spectra shown at 10× and offset for clarity. The fitted line shape for the $E_0+\Delta_0$ and E_+ transitions are shown with dashed lines and offset for clarity [33].

It is seen in Fig.3.4, that E_0 decreases monotonically with increasing nitrogen content and the $E_0+\Delta_0$ transition shifts with the band gap energy at constant offset of ~0.3 eV. Unlike E_0 and $E_0+\Delta_0$, E_+ feature increases with increasing nitrogen content. The lack of interaction between

$E_0+\Delta_0$ and E_+ indicates that E_+ transition corresponds to an electronic transition between the valence band maximum and a level above conduction band minimum [33].

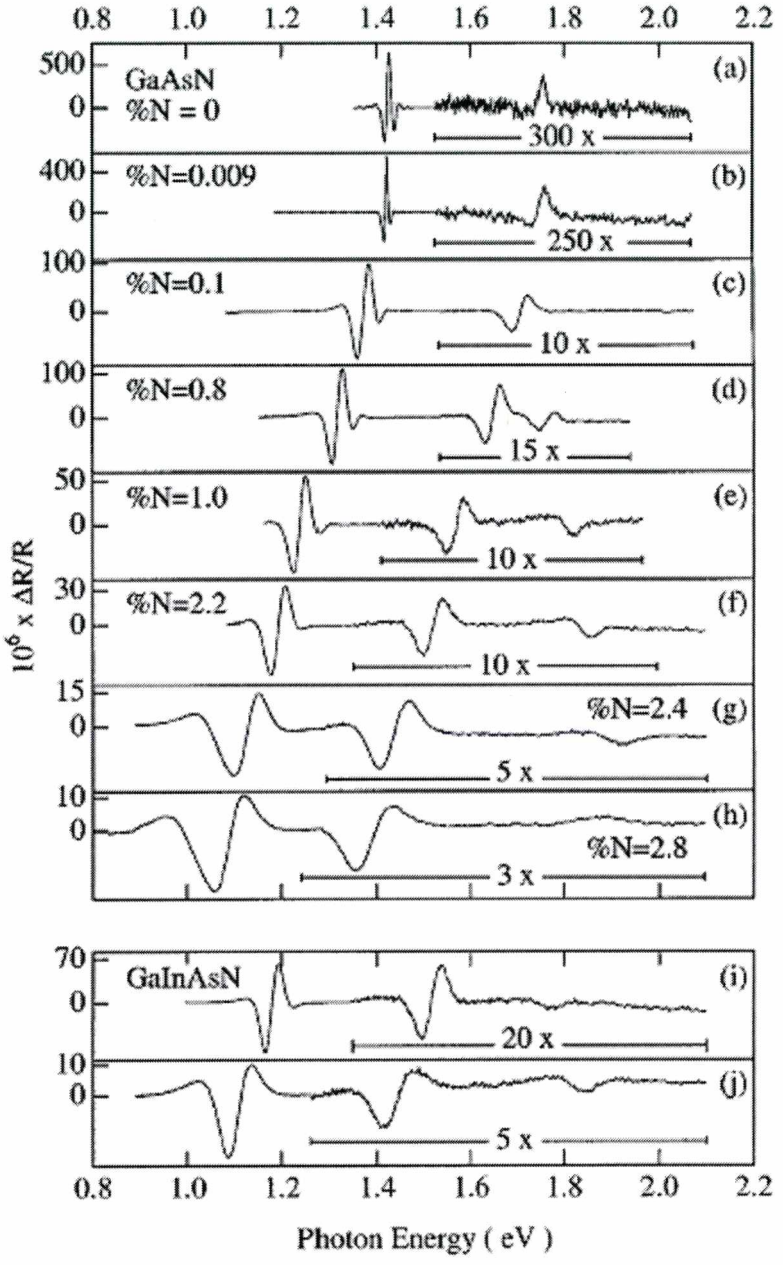

Figure 3.4. Electroreflectance spectra for $GaAs_{1-x}N_x$ [(a)-(h)] and GaInAsN [(i) and (k)]. Note the different scale used for each panel as well as the expanded scale within each panels used to more clarity display the above band gap transitions. For the $GaAs_{1-x}N_x$ samples, the nitrogen content ranges from x = 0 (a) to x = 0.028 (h). For the GaInAsN samples, the compositions are $Ga_{0.95}In_{0.05}As_{0.987}N_{0.013}$ (i) and $Ga_{0.92}In_{0.08}As_{0.978}N_{0.022}$ (j) [33].

Optical transitions above E_+ transition were investigated by using modulation spectroscopy by Perkins et al. in [38]. Fig.3.5 shows ER spectra for GaAs and $GaN_{0.01}As_{0.99}$ layer obtained by the authors. Besides E_0, $E_0+\Delta_0$, and E_+ transitions, a PR feature related to $E_++\Delta$

transition is observed in this figure. The two remaining resonances, E_1 and $E_1+\Delta_1$ which includes the VB splitting Δ_1, correspond to Λ-line related transitions occurring along the k-space (111) direction near to and including the zone-edge L-point. The E_1 and $E_1+\Delta_1$ transitions in GaNAs are not sensitive to N mole fraction and strongly broadened compared to GaAs. The weak feature labeled by * seems to be nitrogen-induced transitions because it evidently appear after incorporation of nitrogen [38]. Perkins et al. have assumed that the E^* transition originates from the VB L-point where there is a large density of states due to the flat VB dispersion.

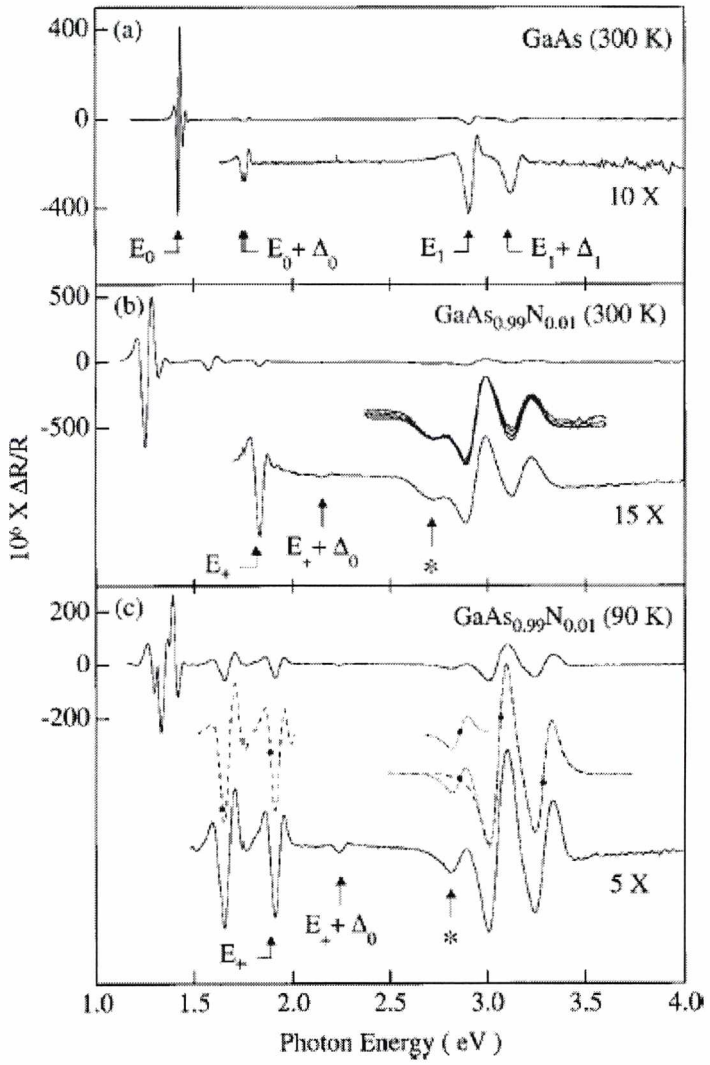

Figure 3.5.. Electroreflectance spectra for a GaAs film at T=300 K (panel a) as well as for a $GaAs_{0.99}N_{0.01}$ film at T=300 K (panel b) and T=90 K (panel c). In panel c, the dashed or dotted lines show the fitted line shape with the solid circles (●) showing the fit determined critical point [38].

All the experimental results demonstrate that incorporation of N into GaAs or GaInAs affects mostly the conduction band and has a negligible effect on the electronic structure of the valence band. As it was mentioned earlier, the significant progress in the description of the

conduction band was possible due to the measurement of the pressure dependencies of E_- and E_+ transitions in PR spectroscopy. Shan et al.[32] have determined the energy positions of the E_- and E_+ transitions in the $Ga_{0.95}In_{0.05}N_{0.012}As_{0.988}$ layer as a function of applied hydrostatic pressure. A classical anticrossing behavior of the two branches has been observed (see Fig.3.6). In order to explain the experimental data Shan et al. have introduced a band anticrossing model (BAC), which is presented in a separate subsection of this thesis.

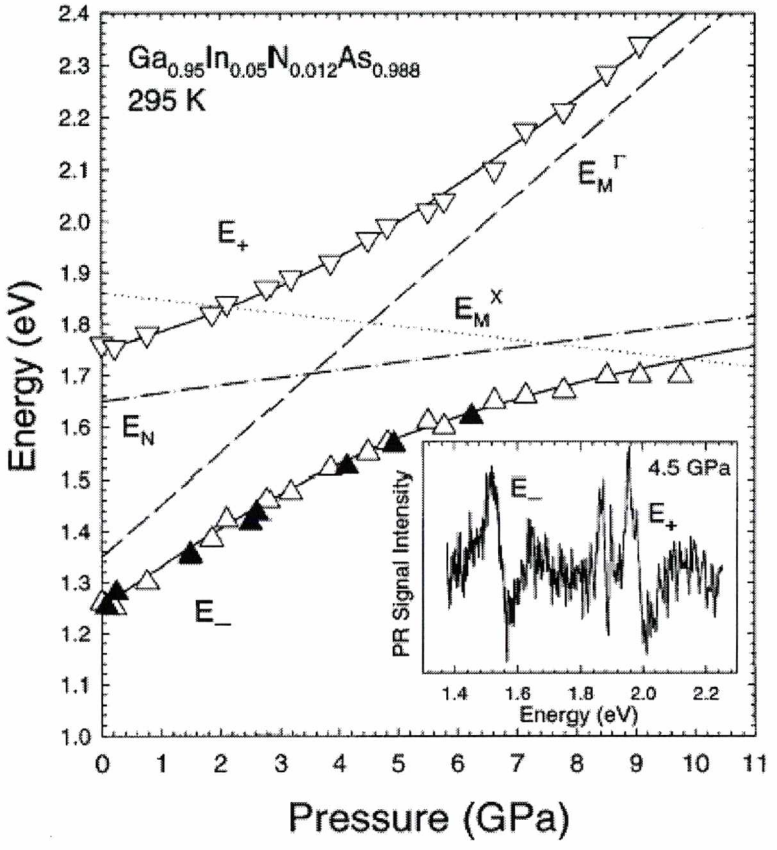

Figure 3.6. Change of the E_- and E_+ transition energies in $Ga_{0.95}In_{0.05}N_{0.012}As_{0.988}$ as a function of applied pressure. The open triangles are PR data and the filled triangles are photomodulated transmission data. The solid lines are model calculation results for the band anticrossing. The dashed, dotted, and dot-dashed lines are the pressure dependence of the Γ and X conduction band edges of the $Ga_{0.95}In_{0.05}As$ matrix and the N level relative to the top of the valence band, respectively. The inset shows a PR spectrum taken at 4.5 GPa. The narrow PR spectra feature at energy below E_+ originates from the GaAs substrate [32].

So far, the E_+ transition was also reported in other papers [39-42]. However, the character of this transition is still unclear. Especially, that the relative intensity between E_- and E_+ changes from sample to sample. It can indicate that the character of E_+ transition changes between direct and indirect. Already, Shan at al. [32] have observed that the increase in hydrostatic pressure causes a change in the ratio of the PR signals associated with the E_- and E_+ transitions. Within

BAC model such behaviour may suggest that with the increase of the hydrostatic pressure the character of the E_- branch changes from extended E_M-like to localised E_N-like and the character of the E_+ branch from localised-like to extended-like (see Fig.3.6).

The exact nature of the N-induced perturbation of the electronic band structure and the origin of E_+ transition is still controversial. Calculations in the framework of an empirical pseudopotential method have shown that the band structure of Ga(In)NAs compounds is more complicated [76-80]. The band structure includes two types of electronic states. First, nitrogen pairs or other atomic cluster states which are created randomly in the bulk during growth. The localized energy states due to nitrogen related clusters are formed around the conduction band either in the gap or in the continuum of the band. Second, the perturbed host states represent mixing of the Γ-X-L and other conduction states by the N-induced perturbation. Hence, there is expected a coupling and anticrossing of Γ, X, L edges instead of the two-level BAC approach where only the interaction of the conduction band with the localized nitrogen level is taken into account.

Moreover, in the case of GaInNAs compounds, theoretical calculations and experimental investigations have shown that the band gap energy in this compound is not well defined. During the epitaxial growth of GaInNAs compound the chemical dynamical processes occurring at the surface favour Ga-N bonds instead of In-N ones [81]. The surface state is quasi-frozen during the nonequilibrium growth process; hence, after growth a N atom is surrounded by four Ga atoms. However, such atom configurations lead to a crystal structure with 'small atom - small atom' and 'large atom - large atom' arrangements which is less preferable in terms of strain than 'small atom - large atom' environment. Consequently, the annealing process leads to formation of different nitrogen-nearest neighbour environments i.e. N-centred $N–Ga_{4-m}In_m$ ($0 \leq m \leq 4$) short-range-order clusters. The change of N bonds after annealing is one the most interesting features of GaInNAs compound. Kim and Zunger have studied theoretically the distribution of bonds using Monte Carlo simulation and found that the number of In-N and Ga-As bonds increases relative to random alloys [78]. So far, the Fourier transform infrared (FTIR) absorption confirms that Ga-N bonds are most frequent after growth [82, 83]. The formations of In-N bonds after annealing have been observed in Raman spectroscopy [84, 85] and infrared transmission [86, 87]. There is a general consensus that post-grown annealing increases the number of In-N bonds instead Ga-N ones. The change in N bonds has important consequences for the band gap energy. With the change in N environment from Ga-rich to In-rich due to annealing a blue shift of band gap energy appears. This phenomenon was many times observed in PL spectroscopy. However,

due to the sensitivity of PL to defect state and the probing only the ground state transition the fine structure of the band gap energy was not observed in PL spectra. Klar et al. [43] have investigated QW structures grown by MOVPE and have shown that the appearance/increase of In-N bonds leads to a change in the band gap energy (E_g), and that for the same composition (x and y) different band gaps can occur by rearranging of the N environments from Ga-rich to In-rich. The particular gaps can be usually probed by modulation spectroscopy.

Most optoelectronic devices adopt QW structures. Hence, the knowledge of the band gap energy, the number of confined electron and hole states, the electron effective mass and the band gap alignment is necessary. The GaInNAs/GaAs QW structures have been investigated for the first time by PR spectroscopy in 2000 by Sek et al. [45]. The authors have observed a red shift of QW transitions with the increase in the concentration of N atoms in the GaInNAs/GaAs SQW like in bulk-like GaInNAs layers. Since 2001 year a rapid progress in understanding of the energy level structure of Ga(In)NAs has been done and a lot of papers devoted PR spectroscopy of Ga(In)NAs-based QW structures have appeared [46-65]. On the basis of PR data, the band gap alignment and/or the electron effective mass have been determined by Heroux et al. [50] Choulis et al. [53]. However, the knowledge about the energy level structure in this system is still poor and not consistent. Therefore, thesis of this work is to find the number of confined states in Ga(In)NAs-based QW structures, the band gap alignments and electron effective mass for Ga(In)NAs-based structures with different composition and thickness of Ga(In)NAs layer.

3.3 Photoluminescence of Ga(In)NAs layers and quantum wells

Photoluminescence studies have unambiguously established [39, 88-90] that with incorporation of N in GaAs PL spectra transform from a series of sharp lines related to bound exciton recombination at the pairs of N atoms (for N compositions x within the doping limit, i.e. $x<0.003$ %), to some broader overlapping emissions (within the transition range of x=0.01-(0.2-0.7)%), and eventually to a structureless PL band (in the alloy region with higer N compositions). The energy positions of the N-related PL features observed within the transition region were found [89, 90] to be insensitive to N incorporation (see Fig.3.7). This finding suggests the PL origin as being due to excitonic transitions within deep defects tentatively attributed to the N-related clusters [39]. With increasing N content the defect-related PL lines gradually disappear starting from the ones at the highest energy due to the reduction of the band gap energy. They can no longer be detected in the PL spectra when then compositions exceed

some critical value (between 0.2% and 0.7% in different experiments). Instead, the broad, structureless PL band emerges and exhibits a strong red shift with increasing N content (see Fig.3.8). This new PL band is believed to represent a true near-band edge emission of the alloy. The emission exhibits the following characteristic properties which allowed the identification of PL mechanism as being due to the recombination of the localized excitons (LE) [89, 90], traped within band tail states.

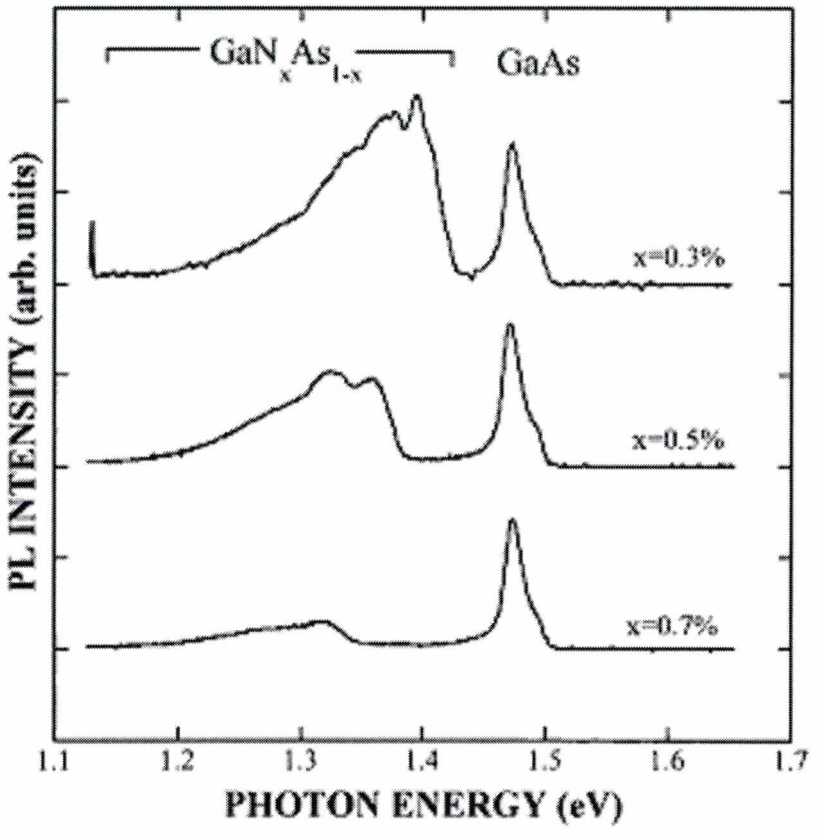

Figure 3.7. Compositional dependence of the PL spectra measured from the GaNAs alloys with low N composition [89].

(i) Asymmetric lineshape. The near band gap emission in Ga(In)NAs typically exhibits a very asymmetric lineshape (Fig.3.7), and has a tail at low energies that shift to a higher energy with increasing excitation power. The exponential dependence of the low energy tail states with an expotential density distribution, typical for random fluctuations of alloy composition.

(ii) Large Stokes shift between PL emission and absorption PLE or PR spectra. Since absorption spectra are mainly determined by optical transitions between extended states whereas the radiative transitions occur within the localized states, a large Stokes shift is typically observed in Ga(In)NAs (Fig.3.8) The energy of Stokes shift can be used to characterize the fluctuation potential.

(iii) *S-shape thermal depedence of the PL maximum*. The depedence of the PL maximum position on measurements temperature has an apparent S-shape [89, 90] (Fig.3.9). At low temperatures, a strong redshift of the PL maximum with increasing T is observed and reflects thermal depopulation of the localized states which starts from the shallowest localization potential. At the elevated temperatures, the apperance of free exciton (FE) recombination (see Fig.3.9) causes a blue shift of the PL maximum position.

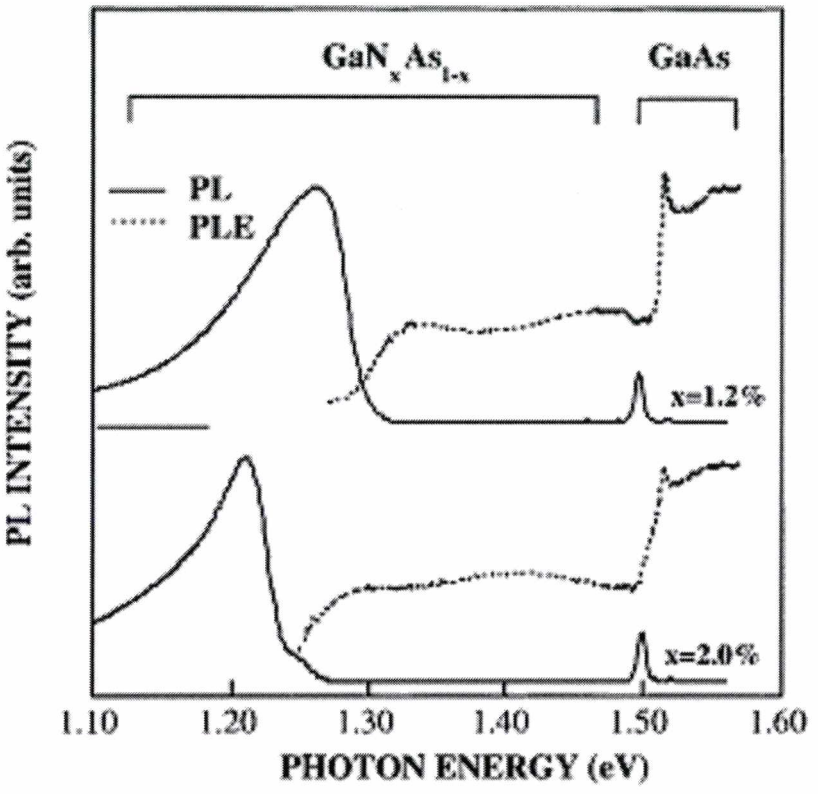

Figure 3.8. Typical PL spectra (solid lines) of near-band edge emission in GaNAs alloys measures from the GaNAs/GaAS multiple QW structures with two nitrogen compositions. The corresponding PLE spectra are shown by the dashed lines and demonstrate a clear red shift of the GaNAs band gap with increasing N content. The spectra are offset in the vertical direction, for clarity [89].

Moreover, despite the reasonably good structural properties of Ga(In)NAs, the intensity PL decreases rapidly with increasing N composition. This has been attributed to the increasing concentration of nonradiative point defects in the material [89, 90]. Similar behavior of PL band has been observed for Ga(In)NAs-based QW structures [90-95].

The N-induced weakness of PL is the main difficulty in obtaining high efficient lasers. Thus, a lot of works have been devoted to increase optical quality of this system. Rao et al. [96] used large excitation intensity in the PL studies of GaNAs and found that the PL intensity is greatly enhanced after laser treatment of thermal annealing. With growth optimization and

thermal annealing the optical quality of Ga(In)NAs system has developed to be comparable to that of conventional GaInAs [97]. Therefore, very important issue for Ga(In)NAs-based structures is to find optimal conditions for the growth process and the post-grown treatment, and to understand physical mechanisms responsible for changes in the optical properties due to post-growth treatment. Therefore, one of the thesis of this work is to investigate the influence of the growth conditions and the post-grown annealing on the optical properties the Ga(In)NAs-based structures.

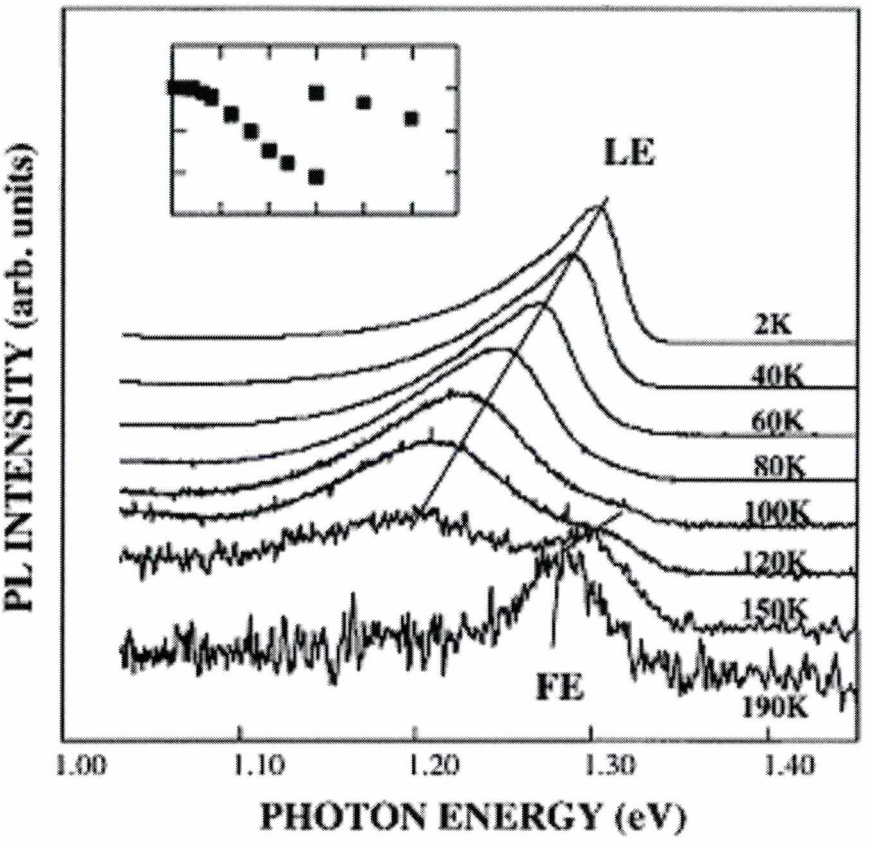

Figure 3.9. Temperature dependence of the PL spectra measured from the $GaN_{0.011}As_{0.989}$/GaAs multiple QW structure. All spectra are normalized to their peak intensity and also shifted in vertical direction, for clarity. The inset shows the PL maximum position as a function of measured temperature [89].

3.4 Theoretical approaches

The mechanism by which the addition of nitrogen changes the band gap in III-V materials appears to be fundamentally different from that in other III-V alloy systems such as AlGaAs or InGaAs. So far, different approaches such as the band anticrossing model [32], empirical pseudopotential supercell method, first principles pseudopotential method [98, 99] and thigh

binding method [43] have been applied to study the anomalous effects seen in III-V nitrides, yielding sometimes conflicting results. Many of the approaches consider a single structural motif throughout the alloy volume (isomorphous models). Experimental verifications show a significant scatter in results depending on the sample preparation. It indicates that GaInNAs is very metastable compound and an isomorphous model can be valid in some cases because more than one structural motif could be important for a sample. In exhaustive theoretical treatment the following structural motives should be taken into consideration: (i) different nitrogen nearest-neighbour environments, (ii) N-related defect states inside the band gap and above the conduction band, and (iii) alloy content fluctuations. Due to the immense complexity of GaInNAs system such extended model seems to be very complicated. Therefore, the simplest model, which is the BAC model, is very often used to predict the band gap energy or the electron effective mass in Ga(In)NAs system.

3.4.1 Band anticrossing model

As was mentioned the band anticrossing model was introduced by Shan et al [32] to describe the observed two-level repulsion in the GaInNAs alloy. In this model, the incorporation of nitrogen atoms into a host matrix compound (GaAs or GaInAs) leads to a strong interaction between the conduction band and a narrow resonant band formed by the nitrogen states (see Fig.3.10(a)). The interaction between the extended conduction states of the matrix semiconductor and the localised nitrogen states is treated as a perturbation which leads to the following eigenvalue problem

$$\begin{vmatrix} E-E_M & V_{MN} \\ V_{MN} & E-E_N \end{vmatrix}, \tag{10}$$

where E_M are the conduction states of the matrix semiconductor, E_N are the localized states, related to nitrogen atoms, and V_{MN} is the matrix element describing the interaction between E_M and E_N. Solving of the eigenvalue problem gives the following subbands energies

$$E_{\pm} = \frac{1}{2}\left[E_N + E_M \pm \sqrt{[E_N - E_M]^2 + 4V_{MN}^2}\right]. \tag{11}$$

V_{MN} and E_N have to be extracted experimentally. Lindsay and O'Reilly [100] have found that for nitrogen diluted GaAs the V_{MN} element varies with the nitrogen content as $V_{MN} = C_{MN}\sqrt{x}$, where C_{MN} is a constant and x is the nitrogen content. The authors have also obtained that E_M and E_N vary with the nitrogen content according to $E_N = E_N^0 - \gamma \cdot x$ and $E_M = E_0 - \alpha \cdot x$, respectively, where $E_N^0 = 1.675\ eV$, $\gamma = 2.52\ eV$, $\alpha = 1.55\ eV$, and E_0 is the energy of Ga(In)NAs compound in the absence of nitrogen atoms. In this way, the new bands, E_- and E_+, can be expressed as

$$E_{\pm}(k) = \frac{1}{2}\left[E_N + E_M(k) \pm \sqrt{[E_N - E_M(k)]^2 + 4C_{MN}^2 \cdot x}\right], \tag{12}$$

where C_{MN} is a constant describing the strength of the anticrossing interaction and x is the N composition. This constant has been determines to be 2.7 eV for GaNAs [32]. In the case of GaInNAs alloys, it is expected that this constant decreases with the increase in the concentration of In atoms. The BAC model also gives a simple analytic expression for the electron effective mass. Using Eq.(12) the effective mass is derived as [68, 101]

$$\frac{1}{m^*} = \frac{1}{\hbar^2 k}\left|\frac{\partial E_-(k)}{\partial k}\right|_{k=0} = \frac{1}{2m_M}\left[1 - \frac{E_M(0) - E_N}{\sqrt{(E_M(0) - E_N)^2 + 4C_{MN}^2}}\right], \tag{13}$$

where m_M is the electron effective mass in the host crystal. Equation (13) can be simplified to the form

$$m^* = m_M\left(1 + \frac{x \cdot C_{MN}^2}{(E_N - E_-)^2}\right). \tag{14}$$

Figure 3.10(b) shows the electron effective mass of GaN_xAs_{1-x} calculated with Eq.(14). The model predicts that the effective mass will increase rapidly to about $0.1\ m_0$ when $x=0.01$ and then saturates to the value of about $0.11\ m_0$ with larger x. It is not obvious that the prediction for the effective mass is correct, even if the prediction for the band gap is very good. Despite the oversimplified physical picture, the model has been shown to describe the material properties of Ga(In)NAs very well. The advantage of the BAC model is that it provides simple analytical

expression for the conduction band dispersion and for the electron effective mass as a function of N composition x.

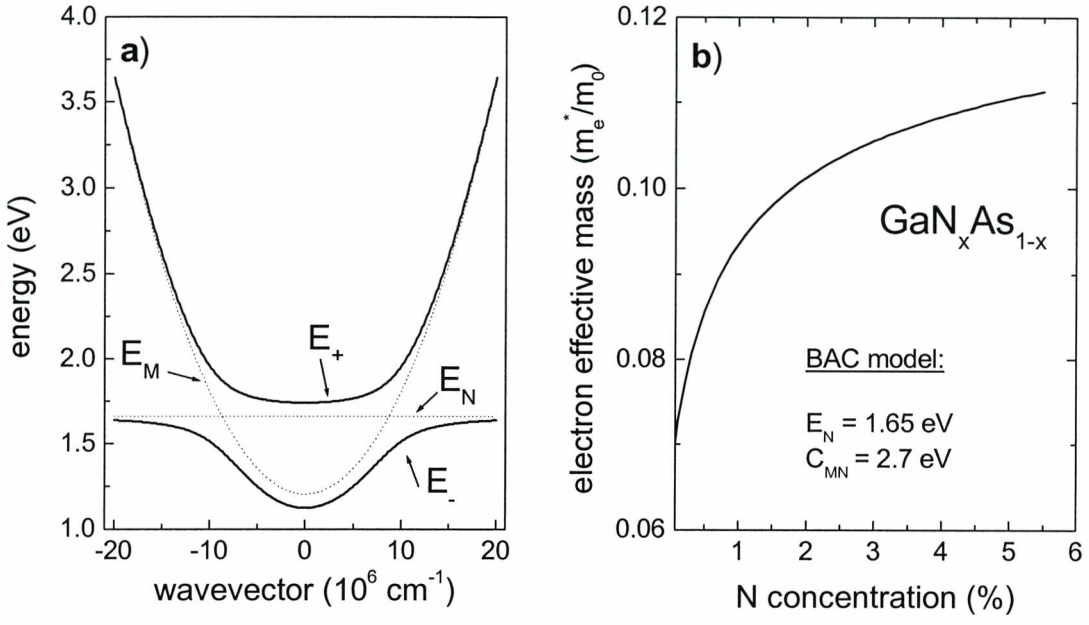

Figure 3.10. Schematic illustration of BAC model for Ga(In)NAs compounds (a). Electron effective mass in GaN_xAs_{1-x} calculated with band anticrossing model (b).

3.4.2 Empirical pseudopotential approach to nitrogen diluted III-V

In the framework the empirical pseudopotential method (EPM) in such alloy systems as GaAs:N the 'cluster states' (CS) appear within the fundamental band gap, as a progression of narrow energy levels associated with single impurities, impurity pairs, triplets, ect., whereas the 'perturbed host states' (PHS) appear as sharp resonances ('virtual bound states') within the continua. Such alloy systems lack 'majority representation' wave vectors, as Bloch symmetry is lost [77]. Since such strong perturbing impurities introduce fundamentally new levels (rather than modified host levels), the alloy properties do not manifest a gradual and smooth evolution with composition. Figure 3.11 depicts the spectral dependence of average nitrogen localisation for nitrogen-localised CS and quasilocalised PHS of GaAsN for a few nitrogen concentrations obtained by Kent and Zunger [77]. The authors concluded, that EPM calculations lead to following physical picture for the evolution of alloys states in III-V nitrides: The alloys are distinguished from other isovalent hierarchical distribution of different CS inside the band gap

and PHS, resulting from strong multiband ($\Gamma - L - X$) coupling in the continuum of conduction states. As the alloy composition increases, the energies of the highly localised CS stay fixed, but the PHS move down in energy CS one by one into the conduction band. This leads, at x_c, to an amalgamation of states at the band edge composed of localised low-energy states developed from the CS, and delocalised states developed from the PHS. The localised-delocalised duality of the band edge is responsible for the poor PL of this system.

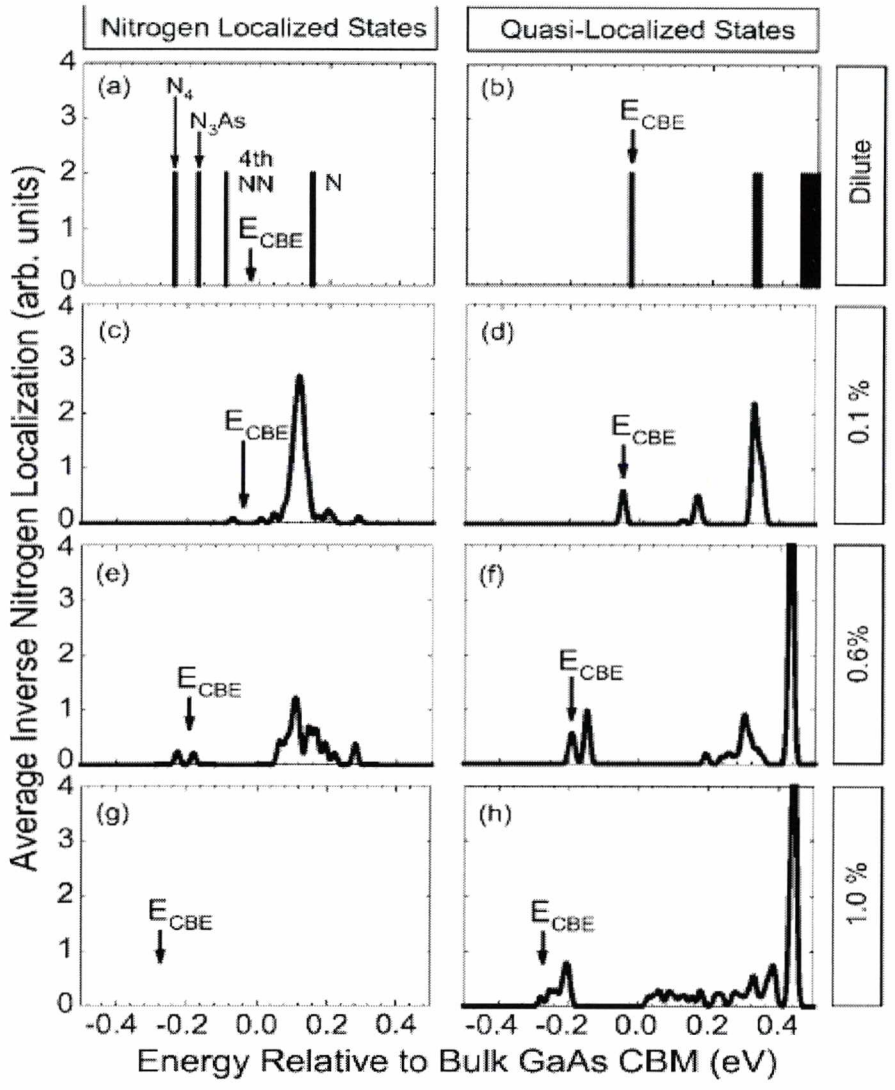

Figure 3.11. Spectral depedence of average nitrogen localisation for (left) nitrogen-localised 'cluster states' and (right) quasi-localised 'perturbed host states' of GaNAs for a few nitrogen concentrations. States with at least 20% of total change within 4.1 Å radius of any nitrogen atom are classified as nitrogen localised. The verdical arrows show the position of the alloy conduction band edge E_{CBE}. For the dilute limit we show the energies of several illustrative cluster states: a quadruplet (N_4), triplet (AsN_3), 4th neighbour pair (4th NN), and the isolated impurity level (N) [77].

The main difference between the BAC model and the EPM is the origin of the E_+ band. In the BAC model the E_+ band is formed due to the anticrossing of the GaAs conduction band and the localised N state, while in EPM the E_- and E_+ bands originate from mixing of $a_1(\Gamma)$, $a_1(L)$ and $a_1(X)$ states with a negligible contribution of the N state. Therefore, using the BAC model actually means that we replace the complex interaction with higher-energy states by the coupling to only one 'effective' nitrogen level to get a simple empirical description of the Ga(In)NAs band structure. In general, the 'effective' nitrogen level may not correspond to a real state. However in order to find the band gap energy of GaInNAs compound the BAC model is rather sufficient. The best advantage of the BAC model is its simplicity and quite good agreement with experimental data. Therefore, many authors use the BAC model as the sufficient theoretical approach.

4. Results and discussion

Results obtained in this thesis are shown and discussed in this chapter. They are presented in six sections focused on the individual sets of samples. In the first section the issue of the post-growth annealing of bulk-like III-V-N layers is discussed. The second section is devoted the energy level structure of GaInNAs/GaAs SQWs. In next two sections, Section 4.3 and Section 4.4, the influence of step-like barrier and Sb atoms on the QW energy level structures and the optical quality of the QWs is analysed. The issue of post-growth annealing of GaInNAs/GaAs QW structures is investigated in Section 4.5. In the last section the phenomenon of the carrier localisation at low temperature is discussed in the context of its influence on the mechanism of band bending photomodulation in photoreflectance spectroscopy.

4.1 Post-growth annealing of N containing III-V layers

The N-containing structures are usually annealed in order to reduce N-related defects. It significantly increases the efficiency of PL but it simultaneously shifts band gap energy to blue [47, 96, 102, 103]. The origin of the blueshift is still controversial. In the case of GaInNAs compounds it is rather established that the increase in band gap energy after annealing is due to the change in nitrogen nearest-neighbour environment from Ga-rich to In-rich [43, 44, 63]. However, it is not excluded that other phenomena affect the band gap energy. Especially, that a blueshift of the band gap energy has been observed for post-grown annealed GaNAs compounds [104, 105]. In this case, the absence of indium atoms supports the other phenomena. Another phenomenon which could be responsible for the blue shift of band gap energy is a reduction of DOS tail by post-grown annealing [104]. Moreover, it is expected that the semiconductor matrix should influence the magnitude of the band gap blueshift besides the parameters of post grown annealing, i.e. the temperature and the time of annealing. This issue is considered in this subsection.

4.1.1 Post-growth annealing of (Ga,In)(N,As,Sb) layers

In order to compare the effect of post-grown annealing for different semiconductor matrix containing N atoms three samples with the same nitrogen content have been selected to this study. The samples were grown by molecular beam epitaxy on semi insulating GaAs substrates. They consist of a 120 nm thick GaAs buffer layer followed by 100 nm thick $GaAs_{0.98}N_{0.02}$, $Ga_{0.95}In_{0.05}As_{0.98}N_{0.02}$ and $GaAs_{0.90}Sb_{0.08}N_{0.02}$ layers and capped by 20 nm of GaAs. Further details of the growth process are described elsewhere [106]. A piece of every sample has been annealed at the same conditions, i.e. at 750 °C for 10 minutes. The structural properties of the samples have been carefully analysed, comparing their characteristics before and after annealing. High resolution X-ray diffraction (HRXRD) did not reveal any changes in the average composition of these two samples. In addition, transmission electron microscopy (TEM) did not show any significant alloy fluctuations, suggesting that composition uniformity was not affected by annealing. Therefore, it is concluded that the compound content is the same before and after annealing.

Figure 4.1 (a), (b), and (c) show PL and PR spectra for as-grown and annealed $GaN_{0.02}As_{0.98}$, $Ga_{0.95}In_{0.05}N_{0.2}As_{0.98}$, and $GaN_{0.02}As_{0.9}Sb_{0.08}$ layers, respectively. It is noted that the three layers possess different strains. The GaNAs ternary layer is tensily strained ($\varepsilon = -7.9\times10^{-3}$) and its PL and PR spectra, shown in Fig.4.1(a), clearly exhibit two structures which are related to the heavy- and light-hole splitting. The splitting is *~20 meV* for the as-grown and annealed layers. The GaInNAs layer is almost lattice-matched to GaAs substrate ($\varepsilon = -0.7\times10^{-3}$), and thereby unstrained. In consequence, we do not evidence any splitting of the valence band in this sample, and a single structure is observed on the PR spectra (see Fig.4.1(b)). In the case of GaNAsSb layers it has been found that the layer is compressively strained ($\varepsilon = 4.5\times10^{-3}$). Such strain leads to an essential splitting of the valence bands. The line-shape of PR spectrum confirms the splitting.

In the case of PR measurements, which are not sensitive to defect related states, the absorption between extended states is observed. At room temperature these resonances are associated with the band-to-band absorption. The negligible Stokes shift between emission and absorption (i.e. the energy of transitions observed in PL and PR spectra) indicates that the band-to-band recombination of free carriers is dominant in PL at room temperature.

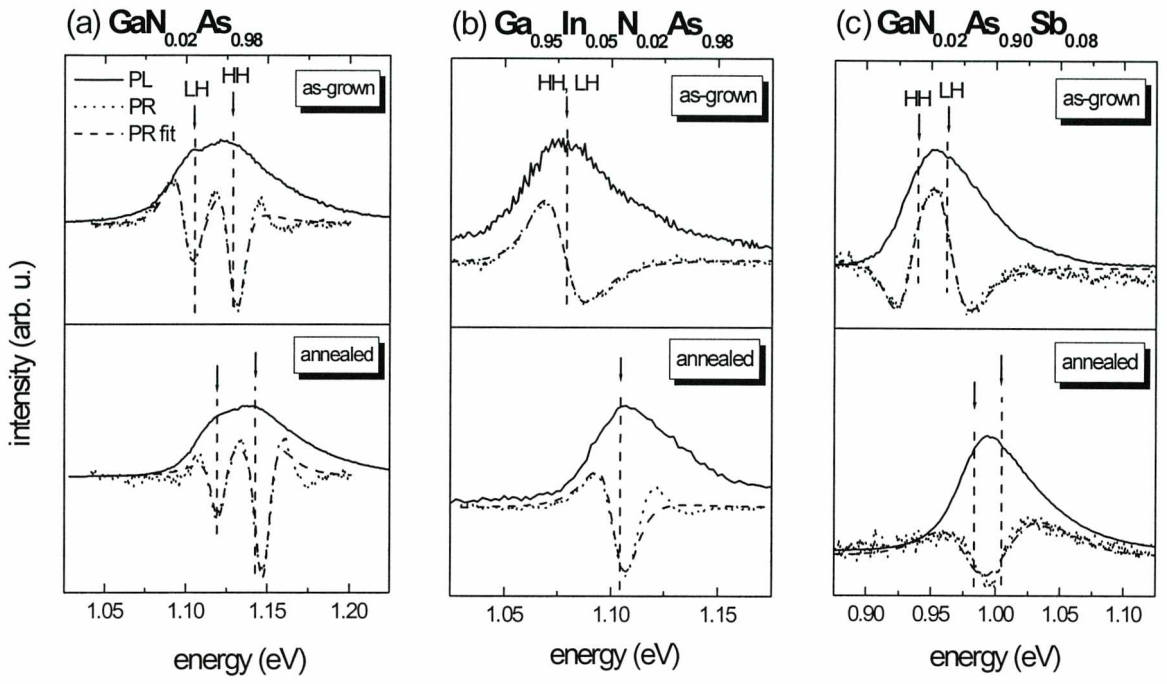

Figure 4.1. Room temperature PL and PR spectra of as-grown and annealed $GaN_{0.02}As_{0.98}$ (a), $Ga_{0.95}In_{0.05}N_{0.2}As_{0.98}$ (b), and $GaN_{0.02}As_{0.9}Sb_{0.08}$ (c) layers. PR spectra are fitted by FDGL curves. In the case of $GaN_{0.02}As_{0.98}$ and $GaN_{0.02}As_{0.9}Sb_{0.08}$ layers PR spectrum has been fitted by two resonances while in the case of $Ga_{0.95}In_{0.05}N_{0.02}As_{0.98}$ layer PR spectrum has been fitted by one resonance. Samples were grown at LPN in France.

The room temperature PL and PR spectra for annealed layers are presented in the bottom part of Fig.4.1. It has been found that the blueshift of band gap energy equals 20, 27, and 54 meV for GaNAs, GaInNAs, and GaNAsSb layers, respectively. These shifts cannot be attributed to an atom outdiffusion, because it has been excluded by structural investigations. Moreover, it has to be noted that the transition energies are not sensitive to possible interdiffusion at the interfaces, since the layer is thick enough to cause negligible quantum confinement (bulk like case). Hence, this phenomenon has been attributed to the effect of the change in nitrogen nearest-neighbour environment and the effect of the reduction of DOS tail [104]. Both effects appear as the result of the annealing and their magnitude depends on the conditions of the annealing. The effect of the nitrogen nearest-neighbour environment is important only for GaInNAs compound while for GaNAs compound this effect is absent. Hence, the blueshift for this compound is smaller than for GaInNAs one. In the case of GaNAsSb layer the effect of nitrogen environment also can be important. In this case the second nitrogen nearest-neighbours can influence the band gap energy. However, no theoretical predictions have been done so far. The effect of the reduction of DOS tail due to annealing can be different for every sample because the DOS tail

usually changes from sample to sample. Such a tail is the origin of the effect of band gap shrinkage. The post-growth annealing reduces shrinkage effect due to the reduction of the DOS tail. The presence of a DOS tail was strongly manifested at low temperature in PL spectra [104].

Figure 4.2 (a), (b) and (c) show a comparison of the absorption-like (reflectance and photoreflectance) and emission-like (photoluminescence) spectra for GaNAs, GaInNAs and GaNAsSb layers, respectively, measured at 10 K. Each figure shows spectra for as-grown (top panel) and annealed samples (bottom panel).

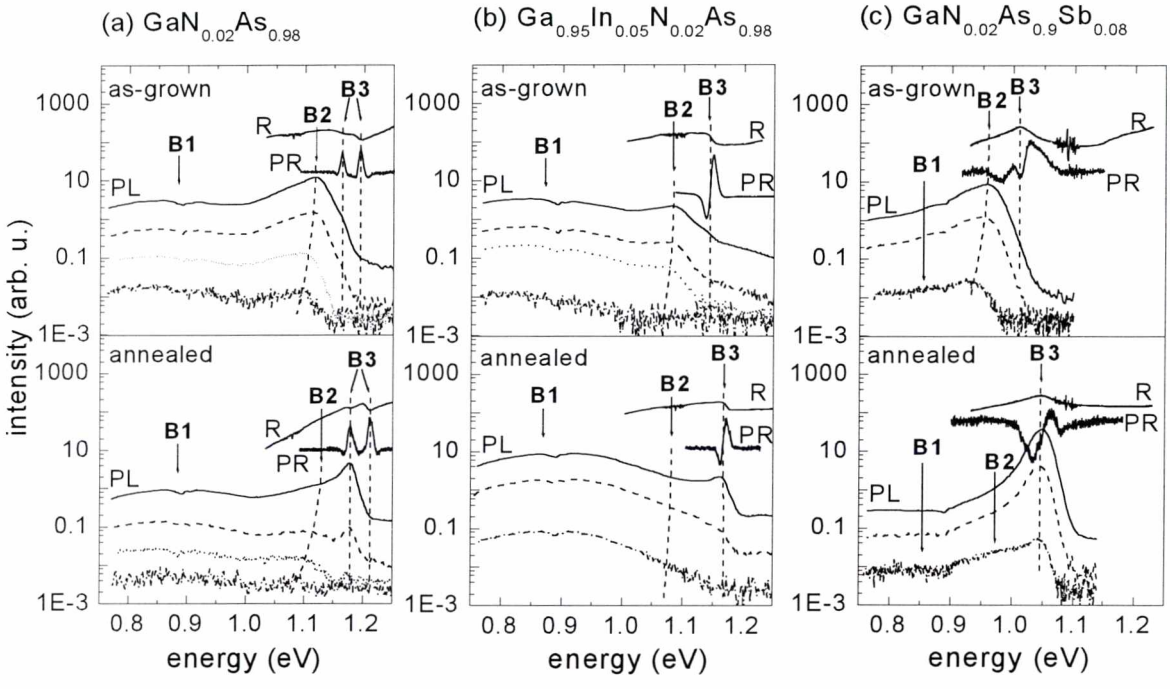

Figure 4.2. PL, R, and PR spectra of $GaN_{0.02}As_{0.98}$ (a), $Ga_{0.95}In_{0.05}N_{0.02}As_{0.98}$ (b), and $GaN_{0.02}As_{0.9}Sb_{0.08}$ layers (c) recorded at 10 K. In the case of PL spectra the density of excitation power is 0.08, 0.24, 0.54, and 7.5 W/cm^2 for solid, dashed, dotted, and dash dot lines, respectively. Samples were grown at LPN in France.

For GaAsN and GaInAsN layers the character of the R and PR lines is probably excitonic at 10 K. In the case of GaAsSbN layer the line shape of R spectrum suggests a band-to-band transition. The strain in this layer leads to quite significant splitting of the valence band (~15 meV). The complex character of the line shape of PR spectrum confirms the splitting. However, a detailed analysis of the PR spectrum is difficult in this case. Results obtained from absorption-like experiments determine the energy band gap in the compound and they enable an identification of the nature of PL bands. In order to determine the nature of PL bands the temperature dependent measurements have been preformed. Figure 4.3 (a), (b), and (c) show

temperature dependencies of PL spectra for GaNAs and GaInNAs, and GaNAsSb layers, respectively.

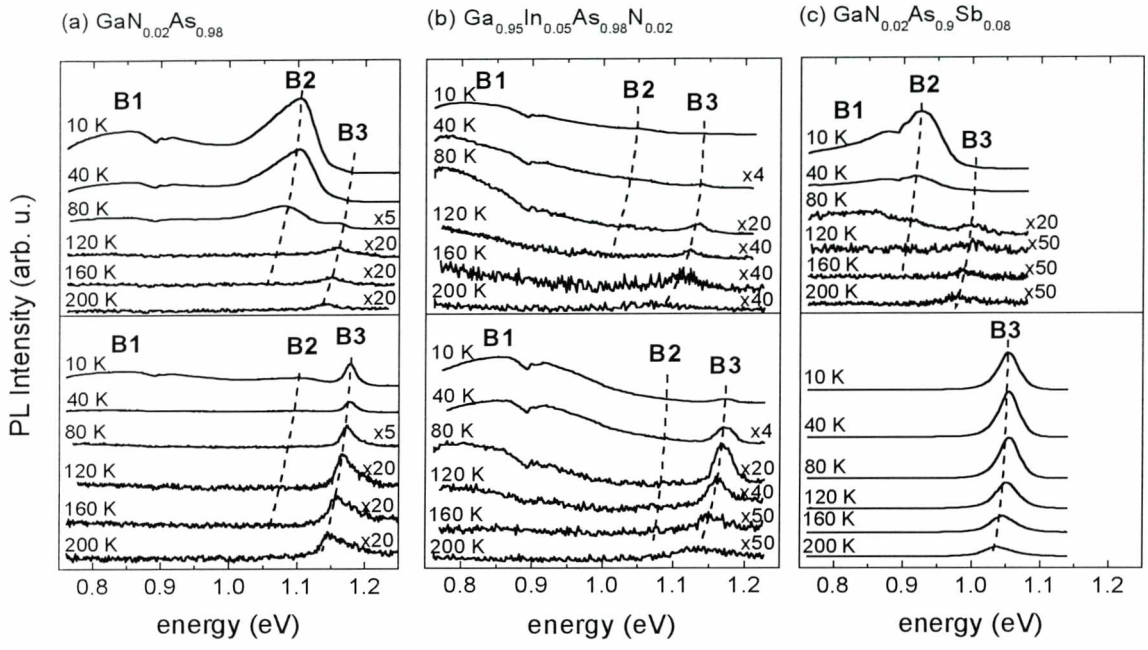

Figure 4.3. Temperature dependence of PL from $GaN_{0.02}As_{0.98}$ (a), $Ga_{0.95}In_{0.05}N_{0.02}As_{0.98}$ (b), and $GaN_{0.02}As_{0.9}Sb_{0.08}$ layers (c). The density of excitation power is 10 W/cm^2. Samples were grown at LPN in France.

The photoluminescence of the three compounds exhibits similar features:

i) *Very broad emission band at ~0.85 eV (B1 in Fig.4.2 and 4.3):* It exhibits a strong dependence on temperature (see Fig.4.3 (a), (b), and (c)) and rather weak dependence on the excitation power. This band is the least intensive for GaAsSbN layer and it disappears for this layer after annealing.

ii) *A band ~80 meV below band gap energy (B2 in Fig.4.2 and 4.3):* This band shifts to blue with an increase of the excitation power and it depends strongly on temperature. It has been observed that this band disappears above 80 K and the post-growth annealing evidently reduces its intensity.

iii) *Not well resolved band gap-related emission (B3 in Fig.22 and 23):* This band is not observed for as-grown layers and it appears after annealing. The intensity of B3 band depends strongly on the excitation power and at low excitation conditions this band is almost not observable. With an increase in the excitation power the B3 band becomes dominant in PL spectrum. In the case of GaAsSbN layer, this band is already dominant for low excitation powers.

iv) *A blue shift of the optical transitions after annealing.* The shift is observed in absorption-like experiments and is directly associated with an increase of band gap energy. In the case of photoluminescence, the blue shift is seen mainly for the band gap-related emission (B3 band) whereas it is rather not observed for B1 and B2 bands.

The similar emission and absorption features of the three compounds suggest that the optical properties could be explained within the same band gap diagram in a first approximation. In order to explain the optical properties, a band gap diagram as in Fig.4.4 has been proposed. This diagram assumes that some defect states exist within the band gap, and the conduction band possesses some fluctuations in the minimum energy. The existence of defect state within energy band gap has been suggested many times and it has been also confirmed by deep level transition spectroscopy (DLTS) [107-109]. However, the nature of the defect states is unclear and is still being investigated. In this model, it is assumed, after Kent and Zunger calculations [77], that N pairs and triplets lead to a defect states which are close to the conduction band edge. It is expected that these defect states are crucial in the III-V-N compounds. In addition, we introduce some defect levels which are close to valence band and they are probably not associated with N-atoms. The existence of such defect levels has been confirmed by DLTS investigations [107], but their origin has not been identified yet.

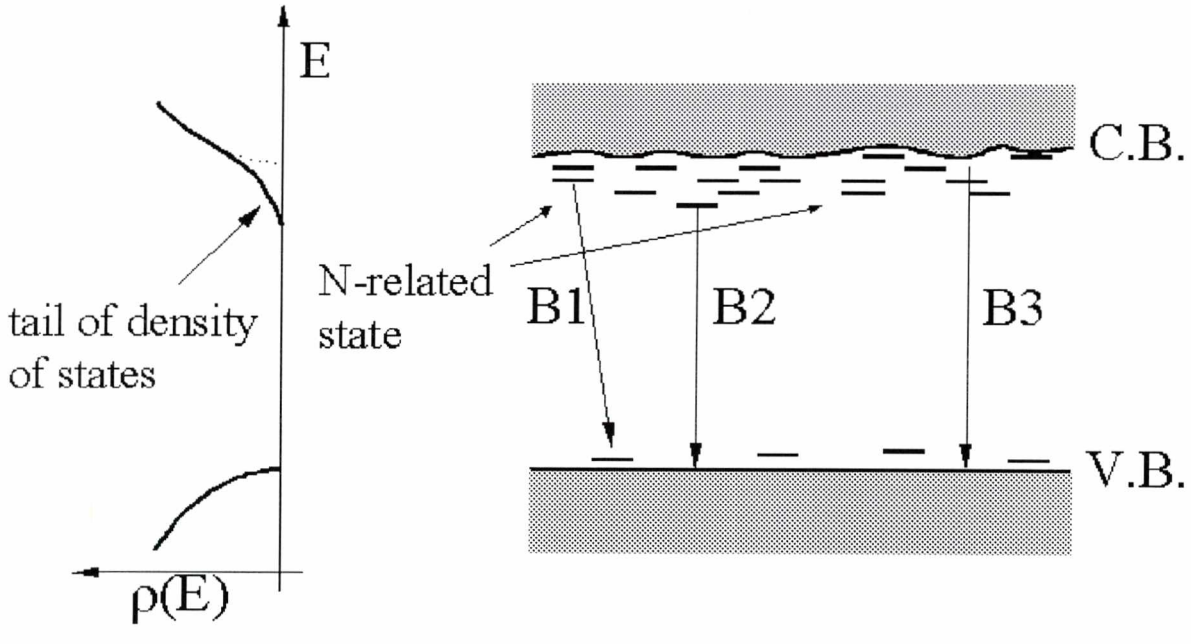

Figure 4.4. Band gap diagram of the III-V-N compound.

The fluctuations of conduction band minimum result from both alloy content fluctuations and a non-homogenous distribution of the N-related defects. Usually, alloy content fluctuations lead to band gap fluctuations where both conduction and valence bands have their extrema. Nitrogen content fluctuations in III-V-N compounds, like GaAsN, GaInAsN, and GaAsSbN, lead to a specific variation of the band gap energy. In this case, the variation of band gap is mainly due to the changes of conduction band energy while the change of valence band can be neglected [56]. Such behaviour is simple to explain within the BAC model [32] which assumes that the resonant nitrogen level interacts only with the conduction band of host matrix (i.e. compound without nitrogen atoms). The magnitude of the interaction strongly depends on the nitrogen content and a small fluctuation in N content leads to significant fluctuation in energy of the conduction band. In our case, the alloy fluctuations are rather small because they were not detected by TEM measurement.

The non-homogenous distribution of the N-related defects is another phenomenon, which takes place in these compounds and leads to a local conduction band edge minima in the real space. In this case, energy levels related to N-defects are close to conduction band, and lead to a tail of DOS in the conduction band and a shrinkage of the band gap.

The structural investigations have shown that the post growth annealing causes a homogenisation of the compound content and a reduction of point defect density. Within this model, it is expected that after annealing the magnitude of conduction band fluctuations decreases and energy levels within the energy band gap disappear, hence the tail of DOS reduces. All these facts should influence optical properties of a compound described by such band gap diagram.

The band at 0.85 eV is attributed to radiative recombination between the N-related levels and 'acceptor like' states at the valence band. A spatial distribution of the states causes that this band is very broad. The second band, (B2), ~80 meV below the band gap energy has been attributed to the recombination between N-related defect levels and the valence band. This band strongly depends on the temperature, the excitation power, and the post-growth treatment. The blue shift of this band observed with the increase of excitation power is attributed to a saturation of N-related energy levels. It has been observed that this band disappears above 80 K. The low temperature quenching suggests that the character of this recombination is excitonic, and the excitons have a localised character. The post-growth annealing evidently reduces the intensity of this band. It can mean that the number of N-related defects and/or the localisation energy decreases after annealing. In this case, the localisation potential is attributed to some non-homogeneities in N-defect distribution and N-content fluctuations.

The third band, (B3), related to energy band gap strongly depends on post-growth treatment. This band is almost not observed for non-annealed layers at 10 K, and it appears after annealing. In contrast to the B1 and B2 bands, the intensity of B3 band exhibits much weaker temperature dependence. With the temperature increase the B3 band starts to dominate in PL and the character of the recombination changes from excitonic to band-to-band. It has been found that the B3 band shifts to blue after annealing according to the observation obtained at room temperature (see in Fig.4.1). Within assumed model, see in Fig.4.4 a reduction of potential fluctuations and tail band states is responsible for an increase of the effective band-gap. Experimental data show that the blue shift is correlated with the intensity of the B2 band (N-defect related band). The highest reduction of the intensity of this band is observed for GaAsSbN layer and also for this layer the blue shift has the highest value. Therefore, the blue shift has been attributed to the reduction of the tail of DOS. In the case of GaInAsN compound, a change in nitrogen nearest-neighbour environment is the additional phenomenon which, besides the phenomenon of the reduction of tail band states, leads to the blueshift of band gap energy. Note the fact that the time of annealing was relatively long while the temperature of annealing could not be high enough for essential changes in nitrogen nearest-neighbour environment, i.e. to obtain In-rich environment. In general, an interplay between the two effects is expected for GaInNAs system. It is expected that the interplay depends on both sample quality and annealing conditions. For example, the change in nitrogen nearest-neighbour environment is the dominant effect for GaInNAs layers annealed at temperatures higher than 750°C. This issue is investigated in next subsection of this thesis.

4.1.2 Post-growth annealing of GaInNAs layers

As has been shown in the previous section the post-grown annealing of (Ga,In)(As,Sb,N) layers leads a blueshift of band gap energy due to reduction of point defects, i.e. the tail of DOS. However, in the case of GaInNAs the change in the nitrogen nearest-neighbour environment influences the band gap energy besides the tail of DOS. It has been shown that that change in the nitrogen nearest-neighbour environment from four Ga atoms to four In atoms shifts the band gap energy to blue more than 100 meV [43]. In general, the magnitude of the shift depends on the content of GaInNAs compound [43]. Due to the finite number of the possible nearest-neighbour environments of N atom (five N centred $N–Ga_{4-m}In_m$ $(0 \leq m \leq 4)$ short-range-order clusters) a fine structure of the band gap energy is expected for GaInNAs.

The samples discussed in this section were grown by MBE on *n*-type GaAs:Si (100) substrates at a growth temperature of 470 °C. Each sample consisted of a GaAs buffer layer, a 300-nm thick $Ga_{0.947}In_{0.053}N_{0.026}As_{0.974}$ layer, and a 10-nm GaAs cap layer, all nominally undoped. The samples were annealed *ex situ* at 800 and 900 °C for 60 seconds. Crystallographic properties were monitored before and after annealing by measuring double-crystal X-ray diffraction (XRD) rocking curves. Figure 4.5 shows (004)-reflection XRD rocking curves for as-grown and annealed $Ga_{0.947}In_{0.053}N_{0.026}As_{0.974}$ layers. The GaInNAs diffraction peak appears at slightly larger diffraction angles than that of the GaAs substrate, indicating a slight residual lattice mismatch of $\Delta a/a = 0.144$ %. However, such a small residual biaxial tensile strain is expected to have a negligible effect on the PR spectrum, because the strain-induced light-hole – heavy-hole splitting at the Γ point of the Brilloiun zone is less than 6 meV, much smaller than the peak splitting in PR, as shown below. Distinct Pendellösung fringes are resolved in the diffraction profiles, which is indicative of a good crystalline quality. The rocking curves are almost unaffected by annealing at 800 or 900 °C. Thus one may conclude that the composition remains constant.

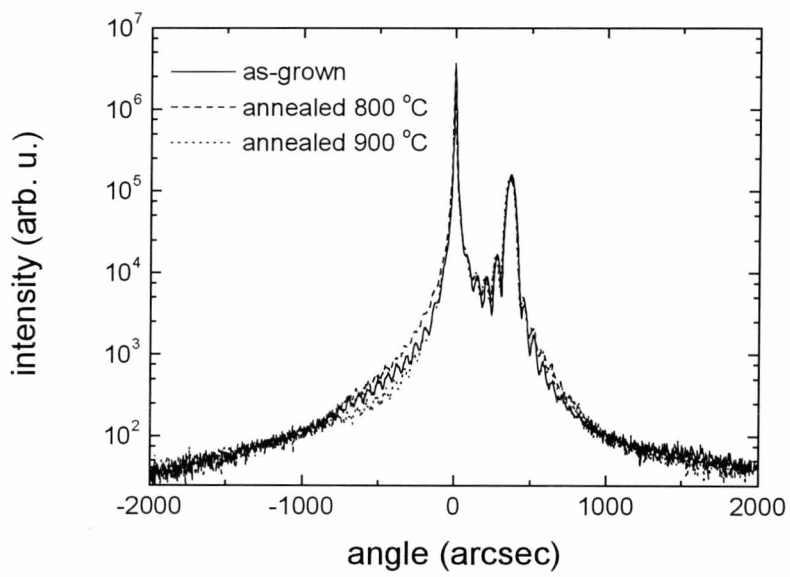

Figure 4.5. X-ray diffraction rocking curves taken for an MBE-grown $Ga_{0.947}In_{0.053}N_{0.026}As_{0.974}$ sample closely lattice-matched to GaAs (no post-growth annealing, solid line) and for two other samples of the same composition annealed at 800 °C (dashed line) and 900 °C (dotted line). Reminiscent lattice-mismatch $\Delta a/a \approx 0.144$ %. Samples were grown at ORC in Finland.

Raman spectra were recorded at 77 K in backscattering from the (100) growth surface, using the 568.2 nm line of a Kr^+ laser. The incident and scattered light were both polarized parallel to the same (110) crystallographic direction. Figure 4.6 shows Raman spectra of the as-grown (solid line), annealed at 800 (dashed line), and 900 °C (dotted line) GaInNAs layers. A peak associated with Ga-N bonds at 473.6 cm^{-1} dominates the spectrum of the as-grown sample. Two additional peaks associated with In-N bonds, 462.0 and 492.2 cm^{-1}, appear after annealing and their amplitudes increase with annealing temperature. In contrast, the strength of the Ga-N related peak decreases, suggesting a considerable re-distribution in nitrogen nearest-neighbour bonds towards In-N bonding [84, 85].

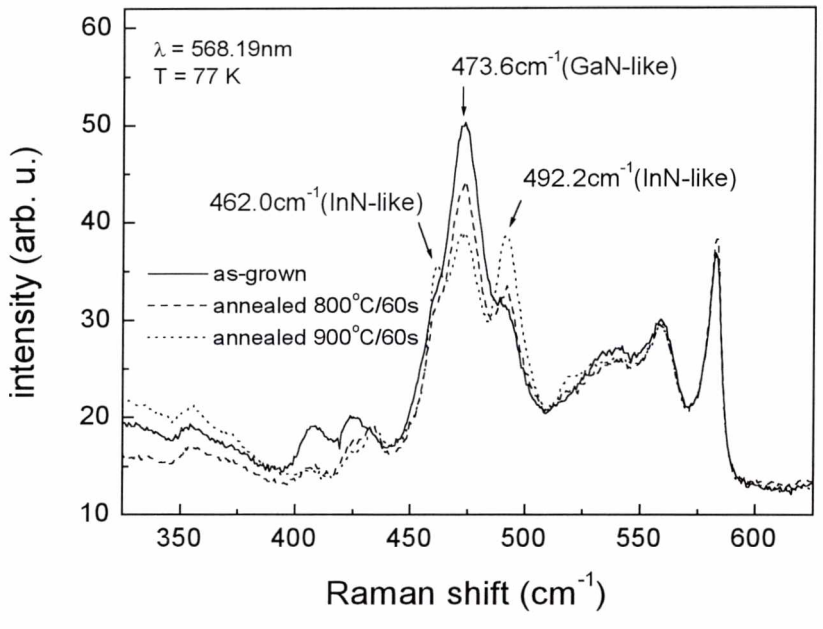

Figure 4.6. Raman spectra for as-grown and annealed GaInNAs layers measured at 77 K. Signals assigned to In – N bonds and Ga – N bonds are clearly resolved; their relative intensities depend on the post-growth annealing procedure. Samples were grown at ORC in Finland.

The XRD and Raman data confirm that samples selected to this study are GaInNAs layers with the same content and different nitrogen nearest-neighbour environments. The environment changes from Ga-rich for the as-grown layer to In-rich for annealed layers. The band gap energy of GaInNAs layers was investigated by PR spectroscopy. Due to the doping in GaAs substrate PL signal from the GaInNAs layer interfere with the signal from the substrate. Therefore, these samples were not investigated in PL.

Figure 4.7 illustrates room-temperature PR spectra recorded for the present set of samples. A long-period oscillatory behaviour of the signal is seen for all samples throughout the energy

range studied, onto which the actual GaInNAs and GaAs band gap features are superimposed. These long-period oscillations are due to interference effects and it does not influence the line shapes associated with critical points of the band structure [10]. For a detailed analysis of the spectra, these oscillations have been removed by subtracting calculating oscillating-like curves, computed from the equation $\Delta R/R = \alpha \cdot sin(\beta \cdot E + \varphi)$, where α, β, and φ are fitting parameters. These calculated curves were fitted to replicate the experimentally observed long-period oscillations in the energy range of interest, i.e. 0.9 – 1.15 eV. In the resulting difference spectra the enhanced critical point features are clearly resolved, as can be seen in Fig.4.8(a). The critical point, or resonance energies were extracted from the difference spectra shown in Fig.4.8(a) by a standard PR line shape fitting procedure assuming Lorenzian oscillators (Eq.(4)), followed by a Kramers-Kronig analysis [16-18] which produces well-resolved moduli of the PR (Fig.4.8(b)).

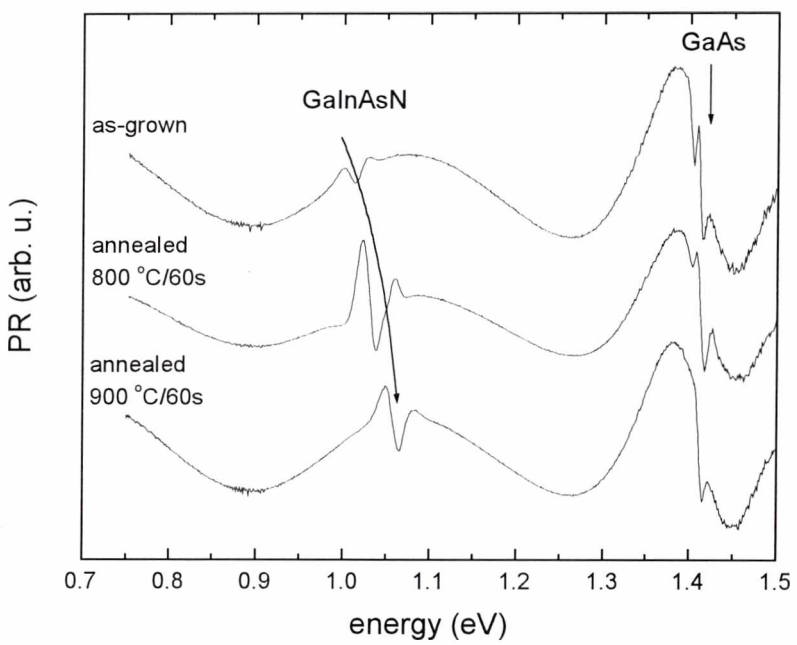

Figure 4.7. Room temperature PR spectra of as-grown and annealed $Ga_{0.947}In_{0.053}N_{0.026}As_{0.974}$ layers. Samples were grown at ORC in Finland.

The PR spectra change significantly upon annealing. A set of at least three discrete transitions at well defined, sample independent energies is resolved with the maximum in oscillator strength shifting to higher energies upon annealing. For the as-grown sample, the main PR feature can be interpreted as being due to band-to-band transitions related to the N – Ga_4 configuration ('4Ga' for short). A second feature, located at a by 25 meV higher energy (Fig.4.8(b)), can be assigned to the presence of a second nitrogen configuration, such as

'3Ga1In', both co-existing in that particular sample. Upon annealing at 800 °C, the signal arising from the '4Ga' configuration decreases, while that from the '3Ga1In' configuration is significantly increased, and a new feature assigned to the '2Ga2In' configuration appears at the high-energy side. Upon annealing at 900 °C, the '3Ga1In' signal disappears and the '2Ga2In' is enhanced. All these observations are consistent with theoretical predictions [43, 77]. It has been reported that for the annealed strained high In-content GaInNAs quantum wells the most preferred configuration is '1Ga3In' [43]. Corresponding features, as well as features due to the extreme '4In' configuration are not detected in the present PR spectra. A reason for this could be the relatively small amount of indium incorporated in our samples (x = 0.053), preventing the formation of indium-rich '1Ga3In' and '4In' atom configurations, or formation of these indium-rich environments is hindered by the low growth temperature as compared to MOVPE growth, not compensated by the present annealing.

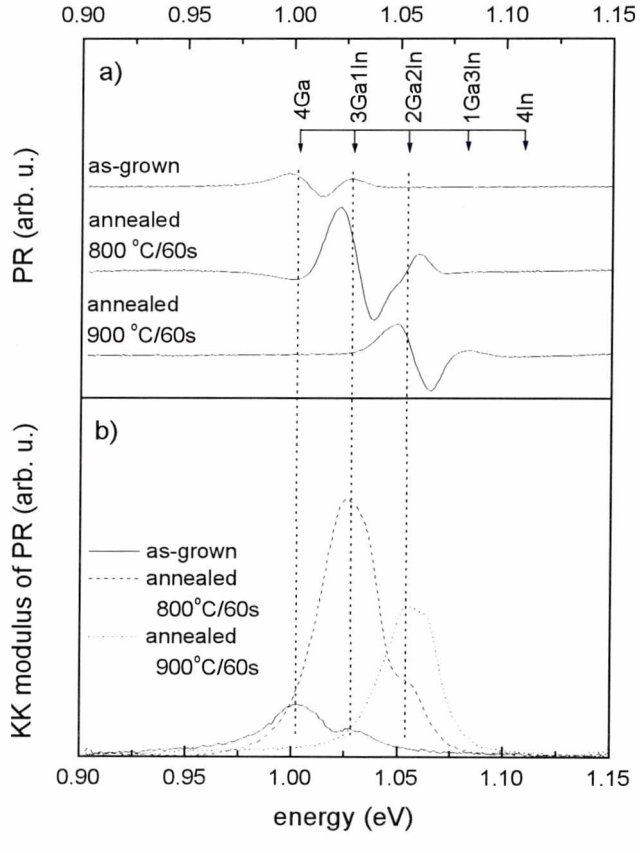

Figure 4.8. PR spectra after subtracting an oscillating background (a); Kramers-Kroning modulus of PR signals (b). Three different nitrogen nearest-neighbour environments are suggested to be found, two of which co-exist in the same sample giving rise to two different band gaps with an energy splitting of 25 meV. Samples were grown at ORC in Finland.

Summarizing the above findings, it has been concluded that three different band gaps ($0 \leq m \leq 2$) out of five predicted ones ($0 \leq m \leq 4$) can be discerned for low In-content lattice-matched GaInNAs. Further, at least two different bonding configurations, with a 25 meV difference in band gap energy, are found to co-exist in the as-grown and annealed (800 °C) samples. The coexistence of two well-resolved band gaps confirms a cluster-like character of GaInNAs material.

The mechanism for the re-distribution of nitrogen environment upon thermal annealing is not understood at present. One can speculate that atomic migration, for example hopping of N from a Ga-rich nearest-neighbour environment to an In-rich environment at elevated temperatures, or vacancy-assisted migration of In and Ga atoms, is responsible for a reconfiguration of the group III-nitrogen bonding, and thus the observed variations in PR oscillator strength of the various transitions. Lordi et al. [110] and Albrecht et al. [111] reported on the segregation of In towards nitrogen and the homogenisation of the In distribution, respectively, upon post-growth annealing of GaInNAs. Thus, both reports give support to the view that group III migration is causing the rearrangement of the group III-nitrogen bonding.

As was shown in previous section, N-related defects can influence the GaInNAs band gap energy due to formation of a tail of density of states (DOS). The post-growth annealing leads to a reduction of the DOS and thereby to blueshift of band gap energy. Hence, the total bueshift of band gap energy is a sum of the two components: (i) change in nitrogen nearest-neighbour environment from Ga-rich to In-rich, and (ii) reduction of DOS tail. The first component has discrete character due to finite number of N-centred $N–Ga_{4-m}In_m$ ($0 \leq m \leq 4$) short-range-order clusters, while the second component has continuous character. Results presented in this Section evidently demonstrate that for these samples the first component is dominated because the multiple band gap structure is observed.

4.2 Energy level structure of GaInNAs/GaAs single quantum wells

Most optoelectronic devices adopt QW structures. Hence, the knowledge of the band gap energy, the number of confined electron and hole states, the electron effective mass and the band gap alignment is necessary. In this section the photoreflectance approach to investigate these issues is presented. Within this approach the theoretically predicted QW transition energies are compared with those obtained by using modulation spectroscopy. Unknown parameters of

GaInNAs/GaAs QW structure, like e.g. the band gap alignment or the electron effective mass, are deduced from this comparison. Such approach has been many times applied to InGaAs/GaAs [112], InGaAs/InAlAs [113], or InGaAs/InGaAsP [114] QW structures. In the case of Ga(In)NAs-based QW structures PR spectroscopy has been applied in [43, 46-65]. The band gap alignment and/or electron effective mass have been determined from the PR data by Heroux et al.[50] Choulis et al.[53] and Misiewicz et al.[54].

4.2.1 Theoretical approach

PR spectroscopy, besides the energy of ground state transition, yields energies of barrier and higher-order QW transitions. For square-like QWs, allowed transitions between hole subbands (index *n*) and electron subbands (index *m*) obey the selection rule *n - m = even*. In circumstances wave-function mixing can occur and this rule may be violated, causing 'parity-forbidden' transitions, *n- m = odd*, to be observed [10-12]. Therefore, forbidden as well as allowed transitions can be observed in modulation spectroscopy. A comparison such experimental data with theoretical models enables to verify information about the QW thickness, strain, QW and barrier compositions, effective masse of carriers, and band gap alignments. In addition, some unknown material parameters can be determined on the basis of comparing theoretical calculations with experimental data. For example, the band gap alignment has to be determined in this way because this parameter cannot be measured directly. The heterojunction band gap alignment is defined here as

$$Q_C = \frac{\Delta E_C}{\Delta E_C + \Delta E_V^{HH}}, \tag{12}$$

where ΔE_C is the discontinuity in the conduction band (CB) between the two materials and ΔE_V^{HH} is the discontinuity in the heavy-hole valence band (VB).

The calculations of QW energy levels were performed within the framework of the usual envelope function approximation [115]. The excitonic effect was neglected. In order to find the band gap energy of GaInNAs compound, the BAC model with typical parameters: E_N=*1.65 eV*, E_M=E_g*(GaInAs)*, and C_{NM}=*2.7 eV* has been adopted. BAC parameters were not varied with the increase in nitrogen and indium contents. According to the BAC model, the influence of nitrogen

on the valence band structure is neglected. Hence, it was assumed that the effective mass of light- and heavy-hole does not change after adding of nitrogen atoms. In the calculations, the strain effects were included. The biaxial strain was calculated based on the Pikus-Bir Hamiltonian as in Ref.[46]. The energy shifts due to hydrostatic δE_H and shear δE_S strain components equal

$$\delta E_H = 2a\left(1-\frac{C_{12}}{C_{11}}\right)\varepsilon, \tag{3}$$

$$\delta E_S = 2b\left(1-2\frac{C_{12}}{C_{11}}\right)\varepsilon, \tag{4}$$

where ε is the strain tensor in the plane of the interfaces, C_{11} and C_{12} are elastic stiffness constants, and a and b are the hydrostatic and shear deformation potentials, respectively. All the parameters have been obtained by linear interpolation between the parameters of a relevant binary semiconductor [66].

The procedure for matching experiment with theory is as following. The QW transitions energies are calculated as a function of m_e^* using the hole effective masses taken from the literature and the nominal QW parameters, i.e. compositions, thickness. These energies are then compared with those found from the PR spectra using a plot similar to that shown in Fig.4.8. Here, the experimental transition energies are shown as full points while those calculated from the model are shown as lines. To obtain a match, the Q_C is varied until the intersection of each experimental and theoretical line in Fig.4.8 occurred close to a single value of m_e^*, indicated in Fig.4.8 by a vertical dotted line. Using this method, the optimum match between theory and experiment could be judged by eye, the greatest weight being given to the most dominant, ground state and excited allowed QW transitions in the PR spectrum. Very similar procedure for matching experiment with theory is reported in [112-114].

Figure 4.8 shows the matching procedure for a $Ga_{0.72}In_{0.28}As$/GaAs SQW, which the PR spectrum is shown in Fig.4.9. A good agreement between experimental data and theoretical calculations is obtained for the nominal QW thickness and content, and the effective masses and the conduction band offset taken from the literature [66].

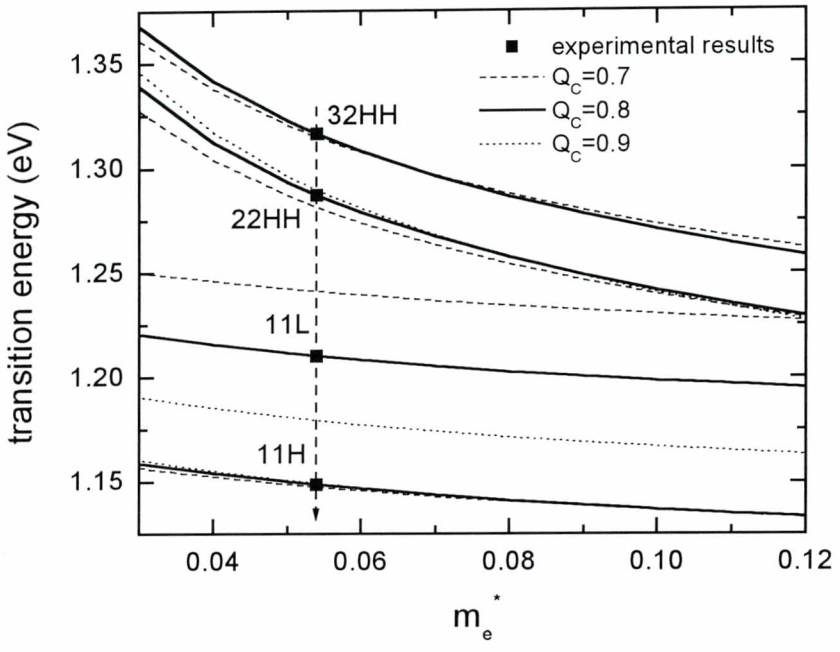

Figure 4.8. The illustration of the method used to achieve a match of theoretical QW transition energies (lines) with those found from fitting the PR spectra (points). The vertical dashed line show the deduced electron effective mass. The sample selected to this illustration is a 9 nm thick $Ga_{0.72}In_{0.28}As/GaAs$ SQW which PR spectrum is shown in next section. Obtained mass and conduction band offset well agree with values reported in the literature for such SQWs.

In the case of $Ga_{1-x}In_xN_yAs_{1-y}/GaAs$ SQW the nominal QW thickness and content are assumed, and the most optimal value for the m_e^* and Q_C is investigated. In addition it is assumed that the light- and heavy-hole effective mass is the same as for reference $Ga_{1-x}In_xAs/GaAs$ SQW. During the identification of QW transitions we take into consideration the intensity of PR resonance and we compare PR resonances to well defined QW transitions in the reference sample. Hence, the reference QW is very useful. Moreover, the observation of nominally forbidden QW transitions is very helpful during the determination of Q_C parameter.

4.2.2 Photoreflectance of GaInNAs/GaAs single quantum wells

Four subsets of GaInNAs/GaAs SQWs with different indium and nitrogen contents have been selected to present the evolution of energy level structure after the incorporation of nitrogen atoms into GaInAs well. The first subset consists of three samples with In content of 28 %, QW with 9 nm and nitrogen concentration of: AR-0 % (reference sample), A1-0.35 %, and A2-0.5 %.

In the second subset there are three samples with In content of 36 %, QW width of 7.2 nm and nitrogen concentration of: BR-0% (reference sample), B1-0.7%, and B2-1%. The third subset consists of four samples with In content of 41 %, QW width 9 nm and nitrogen concentration of: CR-0% (reference sample), C1-2%, C2-3.7%, and C3-5.2 %. The fourth subset was grown by MOVPE in opposition to the three above grown by MBE. This subset consists of three samples with In content of 34 %, QW width of 6.5 nm and nitrogen concentration of: DR-0 % (reference sample), D1-0.5 %, and D2-0.8 %. All samples have a ~100 nm thick GaAs capping layer. The last subset was selected in order to compare the quality of MOVPE and MBE GaInNAs/GaAs QWs.

Figure 4.9 and 4.10 show room temperature PR spectra of the three subsets of SQWs grown by MBE and one subset of SQWs grown by MOVPE, respectively. Using GaInAs/GaAs QW as a starting point to study the effect of nitrogen incorporation has several advantages, like e.g. easer identification of PR resonances of N-containing QWs. All PR spectra are dominated by GaAs band gap bulk-like signal above the energy of 1.4 eV. Below this energy the QW-related transitions are observed. The arrows in Fig.4.9 indicate transition energies obtained from the fitting procedure to the PR data using the FDGL fit, the most appropriate form of PR resonances in the case of confined transitions, like those in QWs, at room temperature [11]. The identification of all QW transitions was possible on the basis of calculations described above. The notation *nm*H(L) denotes the transition between *n*-th heavy-hole (light-hole) valence subband and *m*-th conduction subband. The resonance at the lowest energy is associated with the 11H transition which is a fundamental one in such QWs. Besides the 11H transition, PR spectra show an 11L transition (i.e. the lowest energy transition for light-holes) and transitions between excited QW states: 22H, 12H, 21H, and 32H. The transitions 12H and 21H are forbidden ones but due to the presence of a surface electric field in the structure [116, 117] or other imperfections of QW it is possible to observe such transitions in PR measurements. The magnitude of surface electric field in a semi-insulating structure decreases exponentially with the increase of distance to the surface. If a QW is close to the surface its potential can be changed and the symmetry of QW can be lost [116, 117]. Usually, the surface electric field is very weak and 100 nm cap is sufficient to separate QW from the surface electric field influence. However, in many cases this field makes the forbidden transitions observable. Usually in such cases, the Stark shift of QW transitions caused by the surface electric field can be neglected because we are in the limit of very low fields (F<1 kV/cm). In this regime of electric field the selection rules are changed only while energies of QW transitions shift very weakly (below the resolution of the experiment).

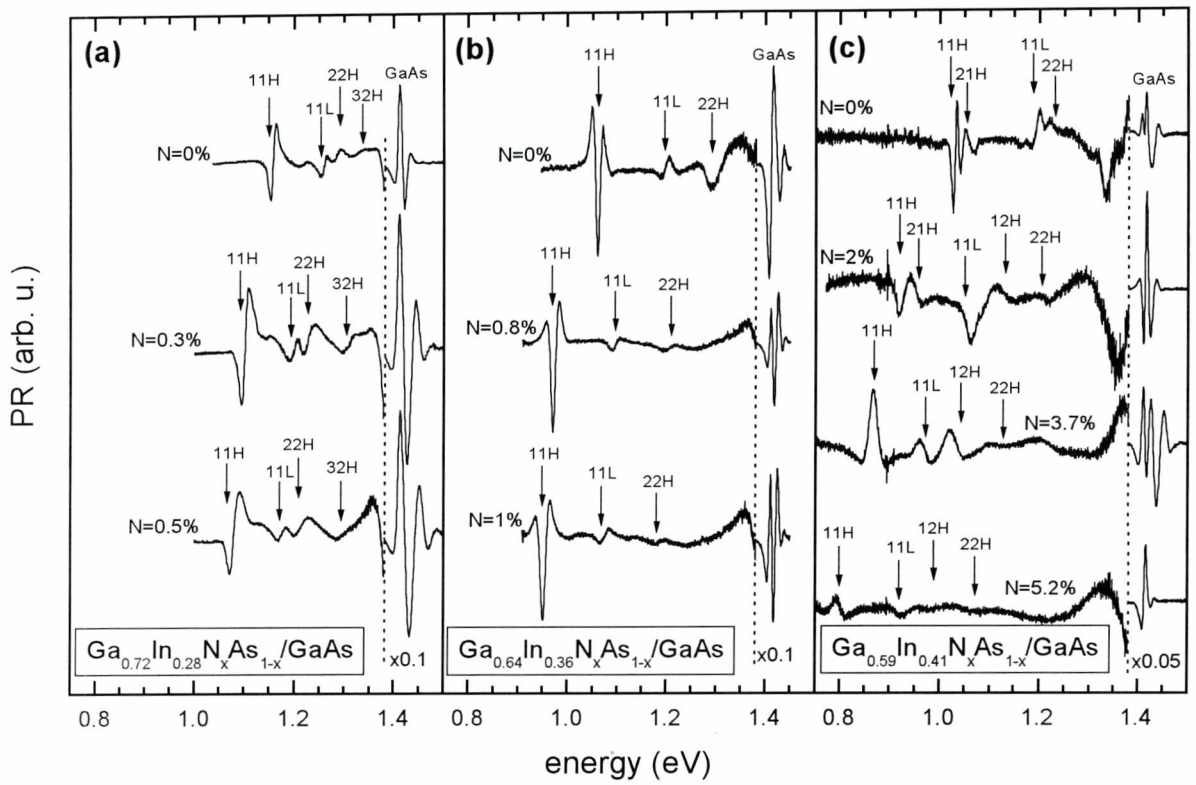

Figure 4.9. Room temperature PR spectra of $Ga_{0.72}In_{0.28}N_xAs_{x-1}$/GaAs (subset 'A') (a), $Ga_{0.64}In_{0.36}N_xAs_{x-1}$/GaAs (subset 'B') (b), $Ga_{0.59}In_{0.41}N_xAs_{x-1}$/GaAs (subset 'C') SQWs (c) grown by MBE. Samples were grown at WU in Germany. Samples were grown at WU in Germany.

In our structures, the existence of a surface electric-field is confirmed by the presence of GaAs-related Franz-Keldysh oscillations (FKO) [118]. The magnitude of the field changes from sample to sample. On the basis of FKO period, the surface electric field has been estimated to be: 14, 21, and 25 kV/cm for sample A1, A2, A3, respectively; and ~6 kV/cm for whole subset 'B'. Next 16 kV/cm for sample C3 and 13, 19, 26 kV/cm for samples D1, D2, and D3, respectively. The surface electric field was not estimated for samples C1, C2, and C4 due to the absence of FKOs in their spectra. The fact that nominally forbidden transitions are better visible for the structures with the surface electric field higher than 13 kV/cm indicates that the surface field changes the square-like profile of the well slightly. It is one of the reasons why the oscillator strength of nominally forbidden transitions is strong in some cases. Also, other factors like e.g. random alloy fluctuations, a valence band mixing effects hole wave-function mixing can influence the selection rules. Such factors seem to be especially important for the subset 'C', i.e. GaIn(N)As layers with the high concentration of In atoms.

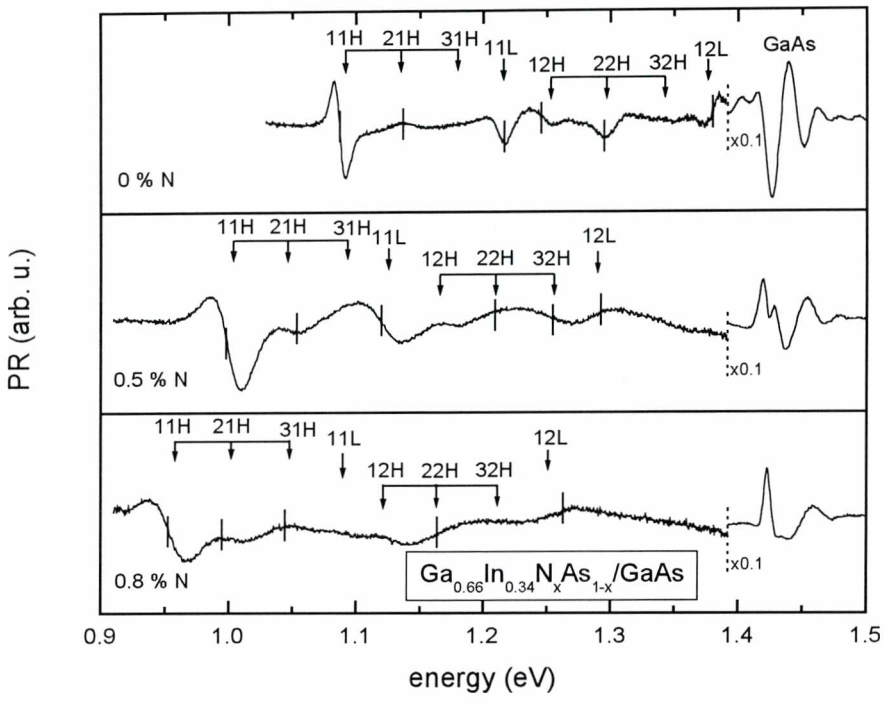

Figure 4.10. Room temperature PR spectra of $Ga_{0.66}In_{0.34}N_xAs_{x-1}$/GaAs (subset 'D') SQWs grown by MOVPE. Vertical arrows and dash indicate energies obtained from calculations and the fit by FDGL, respectively. Samples were grown at KTH in Sweden.

Regarding the behaviour of QW transitions after adding of nitrogen, it is seen that with the increase in nitrogen content, all the QW transitions shift towards lower energies. The analysis of the shift with the increase in nitrogen content seems to be the most interesting for the subset 'D', due to a strong PR signal and significant intensity of forbidden transitions. The arrows in Fig.4.10 indicate the transition energies obtained on the basis of calculations. The energies are in good agreement with energies obtained from the fit of the PR data by FDGL (compare arrows and vertical dash). The energy difference between heavy-hole levels remains almost constant after adding of nitrogen atoms. It results from a weak nitrogen-induced change in QW valence band and negligible changes in heavy-hole effective mass. The redshift of QW transitions comes mainly from the shift of electron levels and two factors influence its value. The first is an increase in QW depth and the second is an increase in electron effective mass. The impact of these two factors increases with the increase in nitrogen content. Such significant changes of conduction QW depth and electron effective mass cause that the energy difference between electron levels changes essentially after adding of nitrogen. For the nitrogen free SQW the indium content is so high that the band alignment for light-hole is of type II leading to indirect light-hole related transitions in real space. The energy difference between fundamental light- and

heavy-hole transitions does not change significantly after adding of nitrogen. This confirms the fact that the light-hole transitions remain indirect despite that nitrogen atoms reduce the strain in the QW layer and hence also the axial (shear) component of the strain responsible for the valence band splitting. These features evidently show that the incorporation of nitrogen atoms into GaInAs/GaAs QW influences mainly the conduction band while the valence band remains almost unchanged.

4.2.3 Electron effective mass and conduction band offset determination

According to Eq.13 an increase in the electron effective mass with the increase in nitrogen content takes place. In the case of the BAC electron effective mass, a satisfactory agreement with the experiment can be found only for one QWs with In = 34 % and N = 0.3 %, while the agreement drops dramatically for other QWs. In the case of high indium and nitrogen contents, the QW transitions have been obtained at higher energies than experimental values. Moreover, other authors [59] have reported a decrease of C_{NM} matrix element with the increase in indium content. Such behaviour of C_{NM} is intelligible and is rather expected within the BAC model. However, if the electron effective mass is taken after the BAC model with C_{NM} less than *2.7 eV* (e.g. *2.2 eV*), less harmony with experimental data is obtained. Another approach is to increase C_{NM} parameter. It has been found that it leads to a little better agreement with experimental data. The increase of C_{NM} parameter has been also considered by other authors [119], but this approach is rather controversial. Therefore, C_{NM} parameter has been fixed for each sample on the level of *2.7 eV* and the electron effective mass has been treated a free parameter.

Figure 4.11 shows the fitted m_e^* in GaInNAs/GaAs QWs for different indium and nitrogen contents. First, it has been found that m_e^* in GaInNAs is bigger than in GaInAs with the same indium concentration. Second, the m_e^* increases with the increase in nitrogen concentration. The values obtained by us are in good agreement with those found for bulk GaInNAs layers by Skierbiszewski et al. [101] and for GaInNAs/GaAs QWs by other authors [50, 53, 120-122]. Obtained m_e^* agrees with the BAC model only in the range of low indium and nitrogen concentrations. The variation of BAC parameters does not change the m_e^* value sufficiently (see BAC curves in Fig.4.11). Therefore, the electron effective mass cannot be taken after the BAC model if we want to calculate energy levels of GaInNAs/GaAs QW in the framework of the BAC approximation of GaInNAs band gap energy. In this approach it has been

found that in the range of investigated indium and nitrogen contents the influence of indium concentration on m_e^* can be neglected and m_e^* can be approximated by formula:

$$m_e^* = (0.072 + 0.011 \cdot x) \cdot m_0, \tag{6}$$

where x is the nitrogen concentration in %. The obtained formula gives the electron effective mass close to values obtained by BAC model for GaNAs compounds (see in Fig.4.11). In the case of GaInNAs compounds, an increase in In content leads to significant decrease of m_e^* within the BAC approach as seen in Fig.4.11.

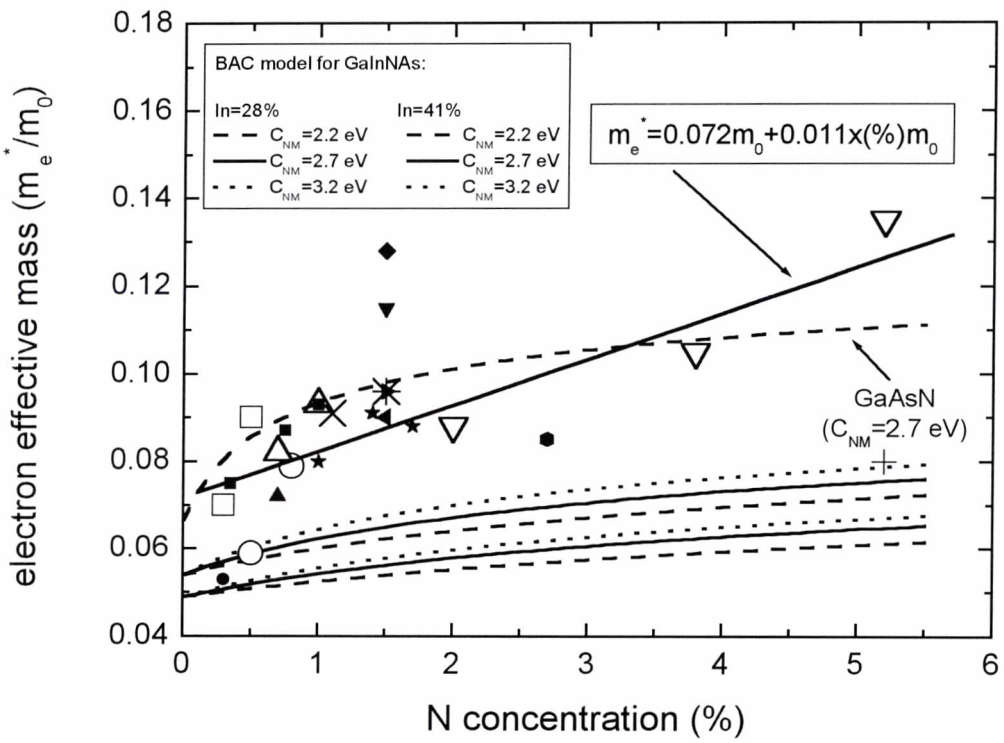

Figure 4.11. The electron effective mass as a function of N concentration obtained for GaInNAs/GaAs QWs. Open points represent experimental data obtained in this work: □ subset 'A' (28%In); ○ subset 'D' (34%In); △ subset 'B' (36%In); ▽ subset 'C' (41%In). Remaining points represent literature data: ● Ref.[53]; ■ Ref.[120]; ✳ Ref.[121]; ▼ 5%In, ▶ 9%In, ★ 14%In, ◆ 14.5%In, ◀ 20%In in $Ga_{1-y}In_yN_xAs_{1-x}$/GaAs MQW Ref. [50]; × 25%In, ⬢ 32%In, ▲ 34%In, + 38%In in $Ga_{1-y}In_yN_xAs_{1-x}$/GaAs QW Ref. [122].

Such strong change in m_e^* due to the incorporation of In atoms at the same N content is not observed. The m_e^* increase is a feature which is attributed to the presence of N atoms. An influence of In atoms on m_e^* is not excluded, however, BAC predictions are rather valid. Our results show that the incorporation 0.3-5.2 % of N atoms into GaInAs increases m_e^* by ~50-130

% in comparison to m_e^* of GaInAs, while the incorporation as much as 41 % of In atoms into GaAs decreases the m_e^* only 25 % in comparison to m_e^* of GaAs. Therefore, the influence of In content on m_e^* value can be neglected at the first approximation as in Eq.(6), especially that the scattering of the data is the order of 20 %.

Besides m_e^* parameter the Q_C is the second free parameter in our calculations. This parameter is crucial for the temperature characteristic of laser structures. It is important to have the type I structure with a deep confinement potential for electrons and suitably deep potential for holes. The conduction band offset can be determined on the basis of PR data because QW transitions, especially the excited ones (i.e. 22H, 21H, ...), are sensitive to variations of Q_C. In addition, the observation of partially forbidden transitions facilitates the verification of Q_C.

Figure 4.12 shows the Q_C parameter for the GaInNAs/GaAs SQWs with different indium and nitrogen concentrations obtained in this work (open points) and taken from literature (remaining points). In the case of QW investigated in this paper the indium content is relatively high (28%<In<41%) and in this range of indium content the Q_C for GaInAs/GaAs system is almost the same (i.e. Q_C=0.8 [53]). The incorporation of a small quantity of nitrogen atoms (N<5%) in InGaAs does not change Q_C drastically in comparison with InGaAs material with the same indium concentration. It has been obtained that with the increase in N concentration to 5% the Q_C increases up to 0.85. Hence, at the first approximation it can be assumed that Q_C for GaInNAs/GaAs system is the same as for GaInAs/GaAs one.

Note that such additional factors like (i) different nitrogen nearest-neighbour environments, (ii) N-related defects, are not included in the above considerations. It could lead to some dissonances between the experiment and calculations, because it has been found that these two factors have a significant influence on the band gap structure of Ga(In)NAs compounds. These aspects are discussed in the following subsections. Moreover, a small difference between real and determined nitrogen concentration in GaInNAs layer leads to essential changes in the GaInNAs band gap energy. Therefore, the simplest model has been used and BAC parameters have not been varied. Within this approach two essential results have been obtained. First, the m_e^* increases after adding of nitrogen atoms. Second, the Q_C in GaInNAs/GaAs system is almost the same as in GaInAs/GaAs one. These two features confirm the fact that nitrogen atoms modify mainly the conduction band.

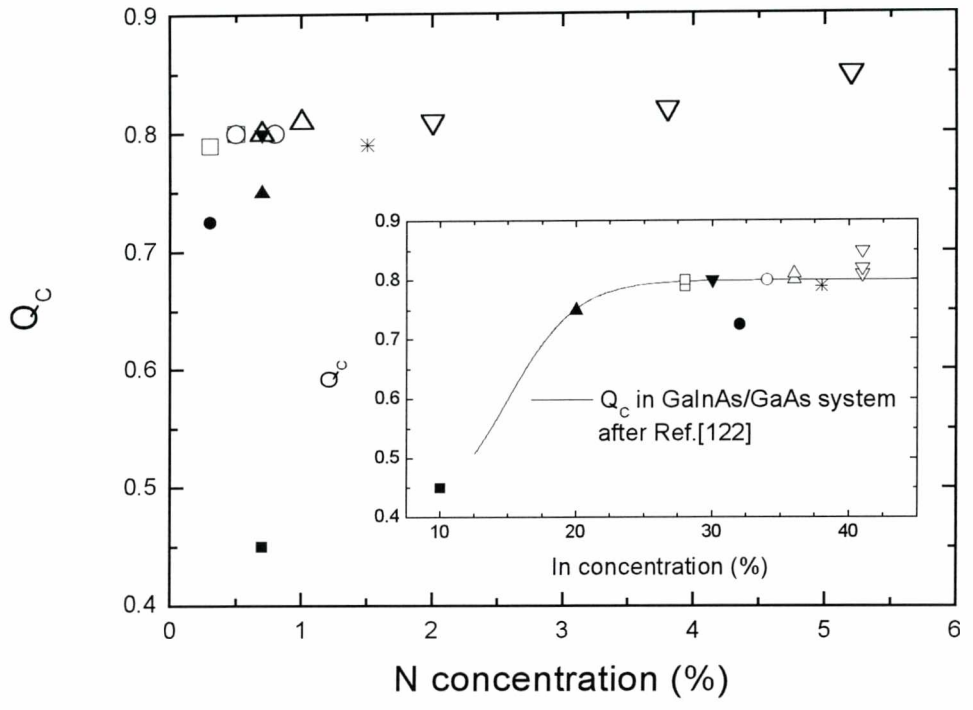

Figure 4.12. The conduction band offset in GaInNAs/GaAs structure versus N concentration and In concentration (inset). Open points represent experimental data obtained in this work: □ subset 'A' (28%In); ○ subset 'D' (34%In); △ subset 'B' (36%In); ▽ subset 'C' (41%In). Remaining points represent literature data: ● Ref.[53]; ∗ Ref.[121]; ■ 10%In, ▲ 20%In, ▼ 30 %In in $Ga_{1-y}In_yN_{0.007}As_{0.993}$/GaAs QW Ref. [50].

4.2.4 Broadening of photoreflectance resonances

The broadening of PR resonance is due to the electron-phonon interaction, alloy inhomogeneities and QW width fluctuations. Hence, an analysis of this parameter seems to be very useful while investigating the deterioration of optical quality due to the incorporation of nitrogen atoms in GaInAs compound.

Figure 4.13 shows the broadening parameter of the 11H transition for QWs analysed in the previous subsection. It has been observed that the broadening of PR resonance increases with the increase in nitrogen content for all subsets of QWs. The increase in the broadening parameter is mainly attributed to an increase in GaInNAs alloy inhomogeneities due to the incorporation of nitrogen atoms. It has been assumed that other factors, which also lead to a broadening of PR resonance, have similar contribution to the total PR broadening for each QW. The other factors origin from electron-phonon interactions and QW width fluctuations. At the fixed temperature

and the comparable roughness of QW interfaces it can be assumed that the contribution of the other factors to the increase of a broadening parameter is negligible.

The increase in inhomogeneities of GaInNAs with the increase of N atom concentration is due to the tendency of nitrogen atoms to clusterization (i.e. creation of nitrogen pairs or other clusters) [76, 77] and formation of N-related defect states (nitrogen interstitials, Ga vacancy complexes) [124]. Moreover, the band structure of GaInNAs compounds strongly depends on nitrogen nearest-neighbour environment as was shown in the Subsection 4.1.2. The mentioned phenomena lead to band gap fluctuations and to a tail of the density of states (DOS) as in Fig.4.4. On the basis of such a diagram it is easy to explain unusually broad PR resonance for QWs with smooth interfaces. Within an assumed model, the increase in broadening parameter indicates an increase in the magnitude of conduction band fluctuations and/or an increase of DOS tails. It is equivalent to the redistribution of nitrogen atoms between different nitrogen nearest-neighbour environments and/or the increase in the number of N-related defects.

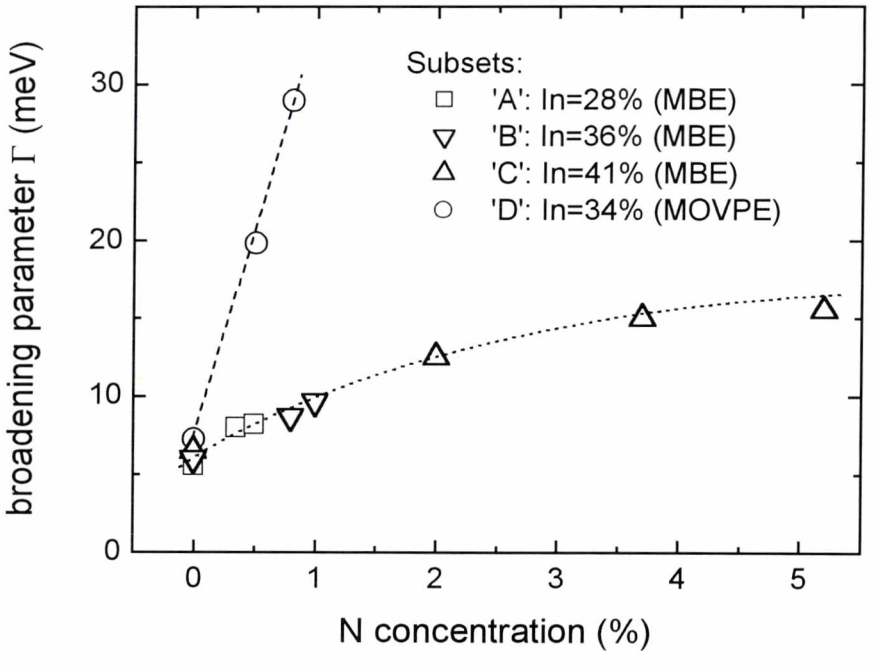

Figure 4.13. The broadening Γ of PR resonance related to 11H transition for the subset 'A', 'B', 'C', and 'D'.

In the case of MOVPE-grown QWs, the Γ parameter increases in comparison to MBE-ones by the factor of 1.2, 2.4, and 3.0 for QWs with 0 (reference QW), 0.5, and 0.7 % of nitrogen content, respectively. The bigger broadening obtained in the case of MOVPE structures could be understood because this epitaxial growth method is worse than the MBE, in general. But it has been concluded that the Γ increase has to have an additional origin, because these structures

posses rather good optical properties and the factor of Γ increase is significantly bigger for N containing QWs than for N free QWs (2.2 and 3.0 vs. 1.2). This phenomenon cannot be attributed to a poor structural quality of the QW structures, because the MOVPE process was refined, and all these QWs were in situ annealed for 10 minutes at 680 °C. This procedure has reduced points defect and improved optical properties significantly. Moreover, the good structural quality has been confirmed by structural investigations. Therefore, it has been concluded that an additional phenomenon is responsible for such a big value of the broadening. As was mentioned previously, the additional phenomenon is associated with the presence of different nitrogen nearest-neighbour environments. These different environments of nitrogen atoms appear due to annealing (this phenomenon is discussed in details in the Subsection 4.4). Within the assumed band gap diagram (see in Fig.4.4) the co-existence of different nitrogen nearest-neighbour environments leads to bigger fluctuations in conduction band. In the case of MBE-grown QWs different environments of N atoms can be neglected, because these structures were not annealed and the number of other than 4Ga environment probably is low. The other environments of N atoms are expected mainly for annealed QWs. In the case of MOVPE process, which is conducted at higher temperatures than MBE one, the number of the nitrogen environments other than 4Ga one cannot be neglected especially that these samples were annealed for 10 min at 680 °C.

4.3 Energy level structure of step-like GaInNAs/Ga(In)NAs/GaAs Quantum well structures

The step like GaInNAs/Ga(In)NAs/GaAs QW structures make it possible to achieve 1.3 and 1.55 μm emission at a lower nitrogen and/or indium content [27, 125-130]. So far, the optical properties of such step-like QWs have been mainly investigated in PL spectroscopy which probes only the ground state transition. Therefore, the energy level structure of the step-like QW system is unknown from the experimental point of view. Also, it is difficult to make theoretical predictions for such a system due to the lack of material parameters for the nitrogen diluted compounds, especially the band offset. Therefore, experimental investigations of the number of confined states in such 1.3 and 1.55 μm laser structures seem to be very interesting from both fundamental and application point of view. Figure 4.14 shows a comparison of the energy level structure for the three different QW structures. This figure demonstrates the main idea of step-like QW system and is useful to explain features observed in PR spectra.

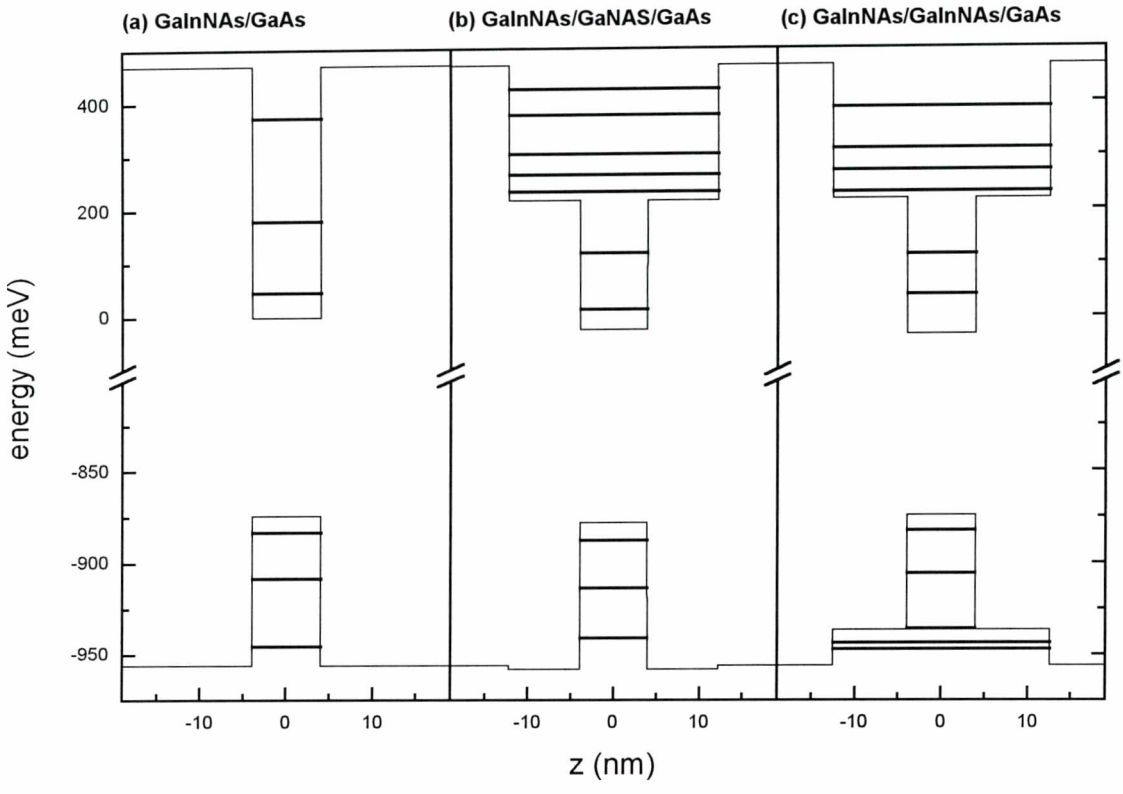

Figure 4.14. Energy level structures for three different QW systems obtained for some indium and nitrogen contents: (a) GaInNAs/GaAs, (b) GaInNAs/GaNAs/GaAs, and (c) GaInNAs/GaInNAs/GaAs.

4.3.1. The influence of GaNAs barrier on the energy level structure

Figure 4.15 shows PR spectra for step-like $Ga_{0.66}In_{0.34}N_xAs_{1-x}/GaN_{0.011}As_{0.989}/GaAs$ QW structures with nitrogen content $x=0.007$ (curve (ii)) and $x=0.008$ (curve (iv)). In addition, PR spectra of $Ga_{0.66}In_{0.34}N_xAs_{1-x}/GaAs$ SQWs, i.e. reference sample with the same nitrogen content ($x=0.007$ curve (i), and $x=0.008$ curve (iii)), are shown in Fig.4.15. All these structures were grown by MBE. In the case of reference SQWs, the 11H and 22H transitions are clearly visible. Also, the 11L transition, with light-hole state having bulk-like (3-D) properties, is noticeable. After the introduction of $GaN_{0.011}As_{0.989}$ step-like barrier the 11H transition shifts to red by 26 and 31 meV for the QW structure with nitrogen content of $x=0.007$ and $x=0.008$, respectively. The 22H transition shifts to red three times more than the 11H one mainly due to a significant shift of the second electron level. In addition, some resonances have appeared in PR spectrum above the 22H transition. These transitions are related to a higher than the second electron level. However, only the 33H transition has been identified because on the basis of calculations only

three confined states for heavy-holes have been obtained. The energy level structure of the valence QW does not change significantly due to almost flat valence band alignment for $GaN_{0.011}As_{0.989}$/GaAs system as it is seen in Fig.4.14(b). The essential changes in the hole-level structure appear after incorporating of GaInNAs step-like barrier (see Fig.4.14(c)). In this case new confined states appear for holes above the step-like GaInNAs barrier. Transitions related to these levels have been observed in PR spectrum of such a step-like QW structure.

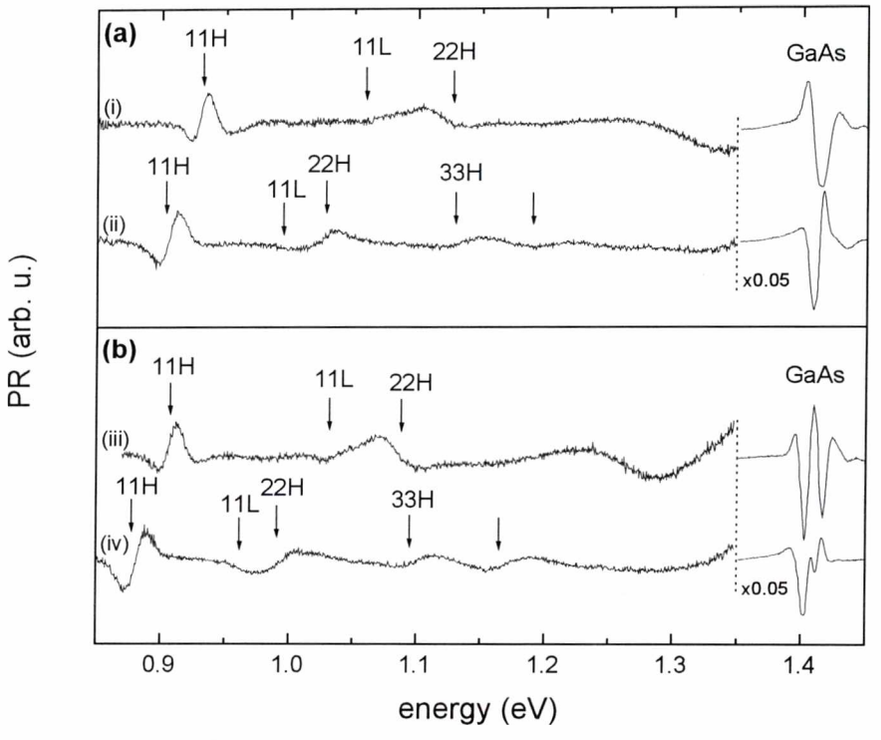

Figure 4.15. Room temperature PR spectra of step-like QW structures tailored at 1.3 μm. (a): $Ga_{0.64}In_{0.34}N_{0.007}As_{0.993}$(8nm)/GaAs SQW (reference sample) (i), $Ga_{0.66}In_{0.34}N_{0.007}As_{0.993}$(8nm)/$GaN_{0.011}As_{0.989}$(8nm)/GaAs QW structure (ii); (b): (iii) $Ga_{0.64}In_{0.34}N_{0.008}As_{0.992}$(8nm)/GaAs SQW (reference sample), (iv) $Ga_{0.66}In_{0.34}N_{0.008}As_{0.992}$(8nm)/$GaN_{0.011}As_{0.989}$(8nm)/GaAs QW structure. Samples were grown at LPN in France.

Figure 4.16 (a), (b) and (c) show PR spectrum for GaInNAs/GaAs (QW1), GaInNAs/GaNAs/GaAs (QW2) and GaInNAs/GaInNAs/GaAs (QW3) structures, respectively. In the case of QW1 structure the PR spectrum exhibits features typical for high nitrogen content GaInNAs/GaAs QWs, i.e. a weak PR signal and very broad PR resonances. These two features indicate that these structures are much worse than the previous 1.3 μm QW structures. Similar features are observed for QW2 structure, but in this case the PR signal is already about one magnitude stronger due to the lower nitrogen content. The other interesting feature is the lack of

PR resonance in the 1.1-1.35 eV range despite the fact that new electron levels have appeared after incorporating of GaNAs step-like barrier. Transitions related to the new electron levels are not observed because as was earlier mentioned no new confined states for holes have appeared after the introduction of GaNAs step-like barrier. Due to the selection rules the transitions between the hole subbands with index n=1,2 and the new electron subbands with index m=3,4,5,... are forbidden. In the case of QW3 structure, the GaInNAs step-like barrier causes that the QW profile changes, as it is seen in Fig.4.14, and new confined heavy-hole states with index n = 3,4,5,... appear. Hence, in PR spectrum *nm*H transitions with index higher than 3 can be observed. Such excited state transitions (EST) are visible in the PR spectrum of QW3 structure (see in Fig.4.16(c)). However, due to a small energy difference between the states confined above the step-like barrier the EST are not resolved and the PR signal looks similar to FKO.

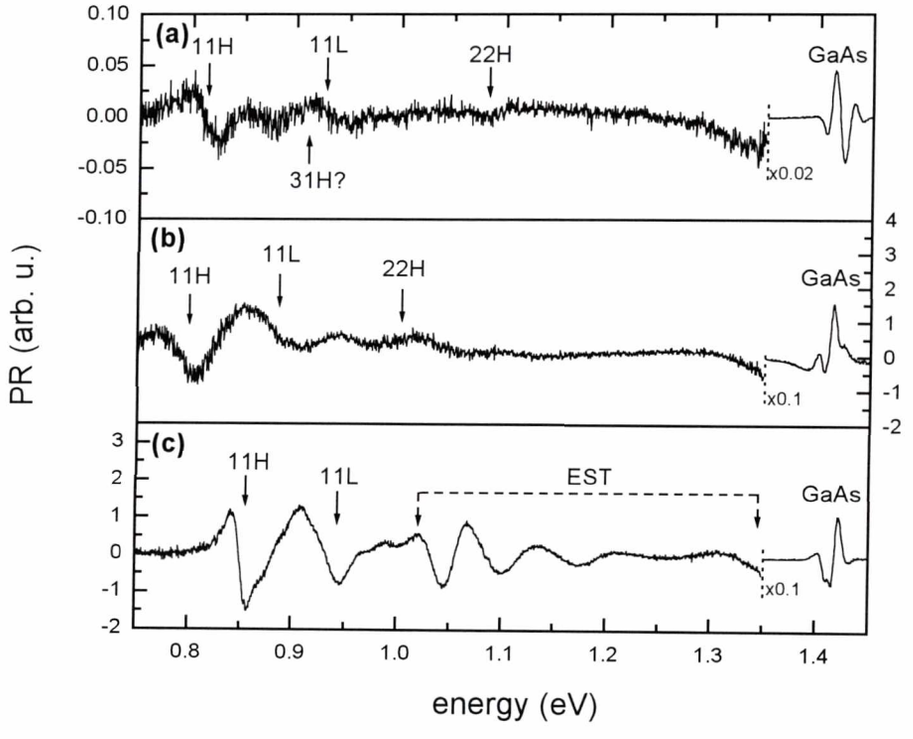

Figure 4.16. Room temperature PL and PR spectra of Sb containing Ga(In)NAsSb/GaAs QW structures. (a) sample with a GaInAs/GaAs SQW (reference QW) and a $Ga_{0.64}In_{0.36}N_{0.012}As_{0.973}Sb_{0.015}$(7nm)/$GaN_{0.02}As_{0.88}Sb_{0.1}$(5nm)/GaAs QW structure. (b) sample with a $Ga_{0.6}In_{0.4}N_{0.015}As_{0.97}Sb_{0.015}$(8nm)/$GaN_{0.024}As_{0.856}Sb_{0.12}$(5nm)/GaAs QW structure. Samples were grown at LPN in France.

4.3.2. Step-like GaInNAs/GaInNAs/GaAs double quantum well structures tailored at 1.55 μm

Three QW structures were selected to present in this subsection. The first is $Ga_{0.62}In_{0.38}N_{0.053}As_{0.947}$(8.2nm)/GaAs single QW (SQW) labelled as sample 'S-A'. This sample is the same as in previous section and is treated as a reference QW structure. The second and third are a step-like barrier GaInNAs/GaInNAs/GaAs double QW (DQW) structures which are composed of compressive strained GaInNAs QWs and tensile strained GaInNAs SLBs (samples 'S-B1' and 'S-B2'). The sequence of layers in the SLBQW structure is following GaAs/SLB(7.5nm)/QW(7.5nm)/SLB(15nm)/QW(7.5nm)/SLB(7.5nm)/GaAs. The content of GaInNAs barrier layers and GaInNAs QW layer is 3 % In and 2-2.5 % N, and 38 % In and 2-2.5 % N, respectively.

Figure 4.17 shows a comparison of PL spectra recorded at room temperature for the three QW structures. For this set of samples it has been observed that the intensity of PL is strongly correlated with the concentration of N atoms in the active region of the QW structure. In general, the intensity decreases with the increase in N concentration. Similar behaviour has been also observed for other sets of samples not shown there. In this subsection only samples designed at 1.55 μm are discussed.

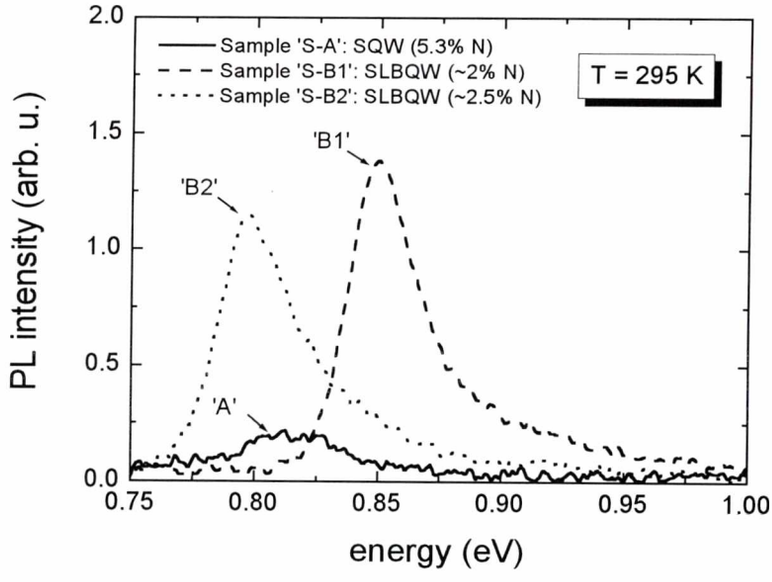

Figure 4.17. A comparison of room temperature PL spectra measured for the GaInNAs/GaAs SQW (solid line) and GaInNAs/GaInNAs/GaAs SLBQW structures (dashed line: sample 'S-B1'; dotted line: sample 'S-B2'). The excitation power is ~0.5 kW/cm^2. Samples were grown at WU in Germany.

In order to obtain an emission at 1.55 μm for a GaInNAs/GaAs SQW structure the concentration of N atoms has to be increased up to 5.3 % at high concentration of In atoms (38 %). It this case, despite the fact that electrons are confined in a very deep QW (~450 meV) and holes are confined in sufficient deep QW (~200 meV), the emission is very week. This feature is attributed to non-radiative recombination processes which are associated with the presence of N atoms. In order to reduce non-radiative channels of the recombination the concentration of N atoms has to be decreased in the active QW region. However, the decrease in N concentration significantly increases the band gap energy of GaInNAs. Therefore, if we want to keep emission at 1.55 μm we have to lower the QW barrier or to increase the QW thickness. The last approach leads to an increase in the number of confined states for both electrons and holes, and shifts the ground state emission very week. Moreover, the active region of a laser structure with such a broad QW is not efficient. Therefore, the first approach associated with lowering of QW barriers is more perspective. In samples shown in this subsection the effective barrier for the active QW region has been lowered by introducing compressive strained GaInNAs SLBs. In this way the emission at 1.55 μm has been achieved for QW structure with the 2-2.5 % concentration of N atoms, i.e. two times lower concentration than for the GaInNAs/GaAs SQW structure (sample 'S-A'). The intensity of PL for SLBQW structures is about 5-7 times higher than the intensity for the SQW structure (see sample 'S-A' in Fig.4.17). The increase of PL intensity has been attributed to the decrease of nitrogen concentration. On the other hand, the SLB leads to a sallower QW, thereby should lead to a weakness of PL intensity. PL results in Fig.4.17 show that for our samples the second factor is less important than the first factor associated with the non-radiative recombination related to the presence of N atoms. It indicates that lowering of N concentration by the introduction of GaInNAs SLBs is good approach to achieve better efficiency of GaInNAs-based lasers. Therefore in next step, it is interesting to find how deep is the active QW and how many states is confined in the QW. In order to determine the energy level structure for the SLBQWs PR spectroscopy supported by the calculations has been applied.

Figure 4.18 shows a comparison of PR spectra recorded at room temperature for the three QW structures. All PR spectra are dominated by GaAs band gap bulk-like signal above the energy of 1.4 eV. Below this energy the QW-related transitions are observed. The arrows in Fig.4.18 indicate transition energies obtained from the fitting procedure to the PR data using FDGL model.

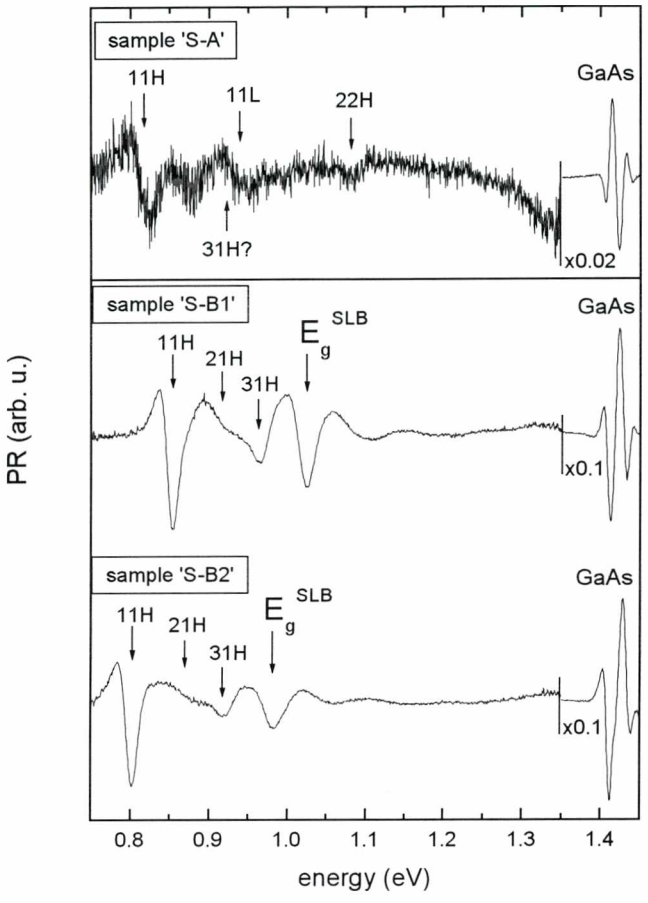

Figure 4.18. A comparison of room temperature PR spectra measured for the GaInNAs/GaAs SQW (sample 'S-A') and the step-like GaInNAs/GaInNAs/GaAs SLBQW structures (samples 'S-B1' and S-B2'). Samples were grown at WU in Germany.

The identification of all QW transitions was possible on the basis of calculations described in Subsection 4.3.1. The resonance at the lowest energy is connected with the 11H transition which is a fundamental one in such QWs. In the case of GaInNAs/GaAs SQW structure PR resonances related to 11H, 11L(31H?) and 22H are identified. A diagram of energy level structure for this SQW obtained on the basis the matching of the experiment with the calculations is shown in Fig.4.19. For this SQW structure two confined states for electrons and three confined states for heavy holes have been found. The light hole is unconfined for parameters assumed in the figure caption of Fig.4.19. PR features attributed for the 11L could be also attributed for the forbidden 31H transition. The light hole becomes to be confined in the QW with the increase in the valence band offset. A modification of BAC parameters after the other authors [59, 100], and a correction in the thickness and the content of the QW lead to some changes in energies of QW transitions. However, these changes are not drastic, and the

identification of QW transitions should be as in Fig.4.18, because experimental data show mainly the allowed transition. Therefore, it has been concluded that the energy level structure for this SQW is close to this presented in Fig.4.19.

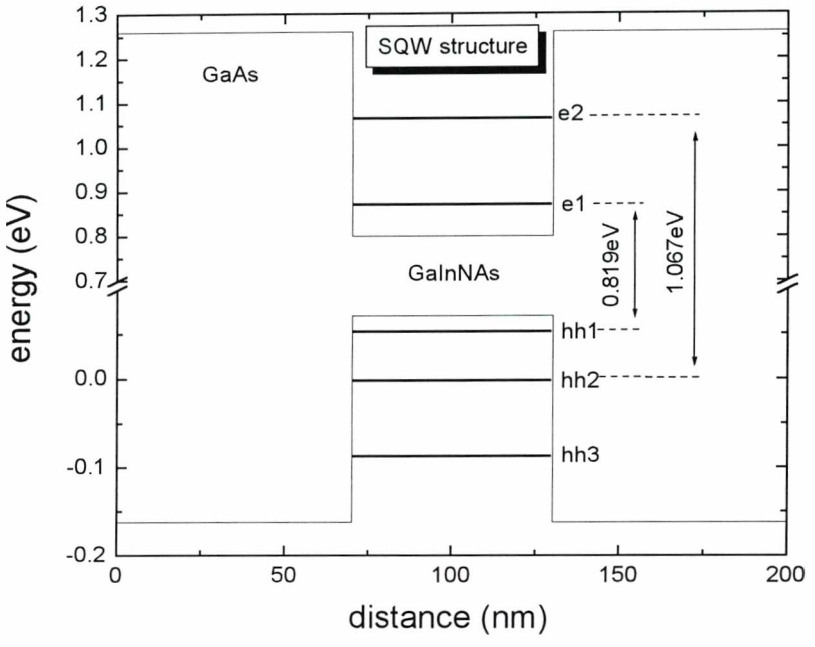

Figure 4.19. The energy level structure for GaInNAs/GaAs SQW obtained on the basis calculations. For the calculations it was assumed that the electron effective mass in GaInNAs layer is 0.09 m_0 and the conduction band offset is Q_C = 0.8. In order to determine the band gap energy for GaInNAs the BAC model with following parameters: C_{NM}=2.4 eV and E_N = 1.65 eV; was used.

Essential changes in the energy-level structure appear after incorporating compressive strained GaInNAs SLBs. The spectrum below GaAs band gap energy changes significantly. At the band gap energy of the SLB a resonance, which has been attributed to band gap-related absorption in the SLB, is observed. Such absorption is possible due to effectively high thickness of SLBs (the total thickness is 30 nm). Above the band gap energy of the SLB a single PR resonance is not observed. PR features observed between the band gap of SLB and GaAs are rather similar to Franz-Keldysh oscillation [9-12]. These features have been attributed to transitions between states confined above SLB. These states have almost continuum spectrum due to the high thickness of SLB. Therefore, the absorption between these states can be treated as the absorption in a bulk-like material. Below the band gap energy of SLB three PR resonances have been observed. These resonances have been attributed to transitions between heavy-hole subbands and the first electron subband. The strongest is the allowed 11H transition. Next two transition 21H and 31H are nominally forbidden ones, however, they can be observed due to

imperfections in this system [11, 116]. The observation of the set of QW transitions from different heavy-hole subband to the same electron subband facilitates to determine the energy level structure for this system. A diagram of energy level structure for the SLBQW (sample 'S-B1') obtained on the basis the matching of the experiment with the calculations is shown in Fig.4.20. Parameters taken to these calculations are shown in the figure caption. For such parameters it has been obtained that the light-hole is unconfined in the QW. However, a transition related to light hole is not precluded. Such a transition is possible in real system, but it should be an indirect transition in the real space. The energy level structure changes with the increase in N concentration from 2 to 2.5 %. In PR spectra only a redshift for the QW transitions without a change in the number of confined states is observed (compare samples 'S-B1' and 'S-B2' in Fig.4.18). This experimental observation is consistent with the calculations which have shown that after the increase in N concentration from 2 to 2.5 % the redshift of QW transitions takes place without change in the number of confined states.

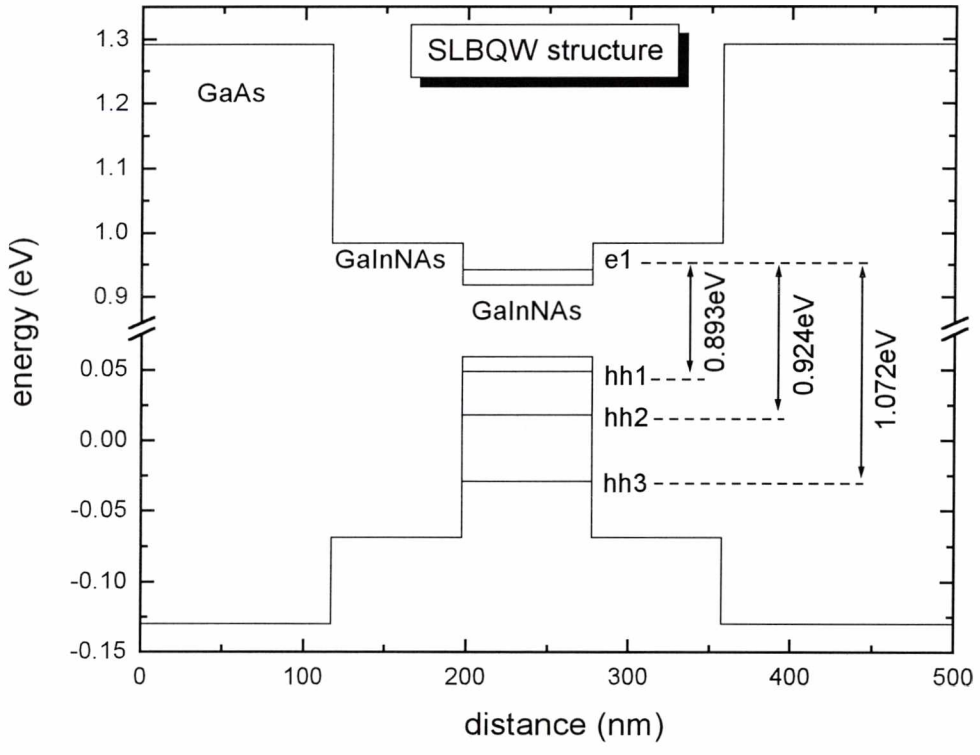

Figure 4.20. The energy level structure for GaInNAs/GaInNAs/GaAs SLBQW structure (sample 'S-B1') obtained on the basis of calculations. For the calculations it was assumed that N = 2 % in both SLB and QW, the electron effective mass in GaInNAs layer is 0.09 m_0 and the valence band offset is Q_C = 0.8. In order to determine the band gap energy for GaInNAs BAC model with following parameters: C_{NM}=2.4 eV and E_N = 1.65 eV was used.

4.4 Energy level structure of Sb containing Ga(In)NAs/GaAs QWs

The other approach in order to shift the laser emission of GaInNAs/GaAs system to 1.55 μm is to introduce Sb atoms to GaInNAs compound [131-134]. It makes it possible to obtain low band gap energy at relatively low nitrogen content. In this case the role of nitrogen atoms in GaInNAsSb compounds is the assurance of the deep confinement potential for electrons because for GaInAsSb/GaAs system the conduction band alignment is between type I and II, depending on the content. An example of PR and PL spectra for a Sb containing GaInNAs/GaAs system is presented in this subsection.

Figure 4.21 (a) shows PL and PR spectra of MBE grown sample with a GaInAs/GaAs SQW (reference QW) and a GaInNAsSb/GaNAsSb/GaAs QW structure. In the case of PL spectrum, it is seen that the integrated PL intensity is bigger for a Sb containing QW structure. If we neglect the non-radiative processes which are related to defects we should expect an increase in PL intensity for Sb containing QW structure due to an increase in the QW depth in comparison to the depth of reference QW. The increase in the broadening of PL emission for the Sb containing QW structure is mainly attributed to significant alloy fluctuations in GaInNAsSb compounds, because in general, it is expected that the five component compound possesses bigger inhomogeneities than a three component one.

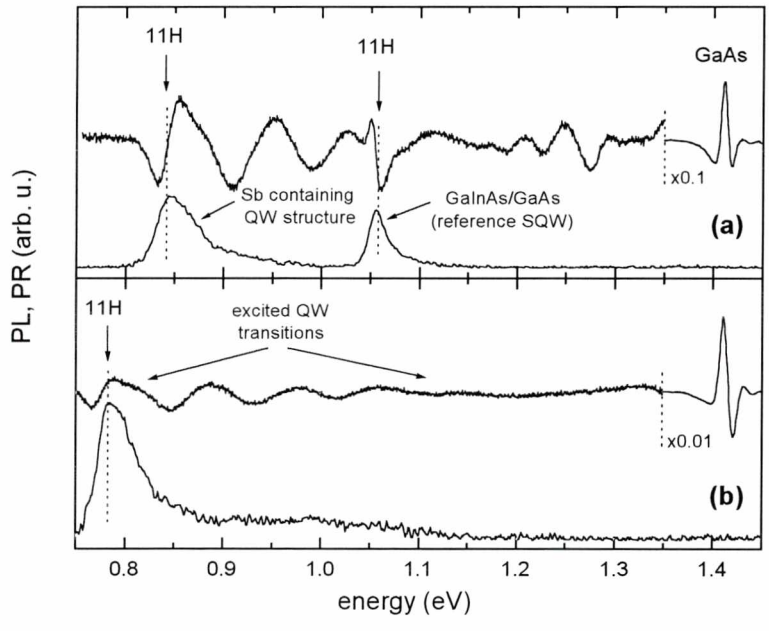

Figure 4.21. Room temperature PL and PR spectra of Sb containing Ga(In)NAsSb/GaAs QW structures. (a) sample with a GaInAs/GaAs SQW (reference QW) and a $Ga_{0.64}In_{0.36}N_{0.012}As_{0.973}Sb_{0.015}$(7nm)/$GaN_{0.02}As_{0.88}Sb_{0.1}$(5nm)/GaAs QW structure. (b) sample with a $Ga_{0.6}In_{0.4}N_{0.015}As_{0.97}Sb_{0.015}$(8nm)/$GaN_{0.024}As_{0.856}Sb_{0.12}$(5nm)/GaAs QW structure. Samples were grown at LPN in France.

PR spectrum of this sample is in good accordance with the PL one. The ground state transition at the same energy as in PL spectrum is observed. The broadening of PR resonance is bigger for Sb containing structure. Above the 11H transition some excited state transitions are observed. However, a further analysis of the excited state transitions is rather difficult due to a weak knowledge of the material parameters for Sb containing Ga(In)NAs compounds and the conduction band offset for Ga(In)NAsSb/GaAs system. In addition, PR resonances related to the excited QW transitions are not defined precisely because alloy inhomogeneities cause a significant broadening of PR resonances.

Figure 4.21 (b) shows PL and PR spectra of MBE grown sample with a Sb containing Ga(In)NAsSb/GaAs QW structure which is very similar to the previous one, but this sample is without a reference GaInAs/GaAs SQW. Hence, the analysis of excited QW transitions does not interfere with PR resonances related to other QW as in the previous sample. In this case in PL spectrum besides the 11H emission an emission between higher energy levels is observed. The PR spectrum is similar to the PR spectrum of previous Sb containing QW structure. The 11H transition observed in PR agrees with that observed in PL. In addition, the PR signal related to excited QW transitions is well correlated with the PL emission observed in this spectral region. The emission band observed between 0.9 and 1.1 eV is a tail-looking emission above the energy of the ground state, but its shape is not exponential one. Additionally, this disappears with the decrease of temperature (or excitation power at low temperature) what suggests that this band is attributed to a recombination between excited states. Such a recombination is visible because an occupation of excited states by carriers takes place at room temperature. Therefore, PR resonances between 0.85 and 1.2 eV have been attributed to the excited QW transitions. The PR resonances associated with the excited transitions are not resolved due to the high value of the broadening parameter. These resonances are not resolved either at low temperatures because phonon-related broadening is smaller than the broadening due to alloy inhomogeneities.

4.5 Post grown annealing of GaInNAs/GaAs quantum wells

So far, the effect of annealing on GaInAsN layers and QWs has been investigated mainly by photoluminescence [97, 11, 135], by transmission electron microscopy (TEM) [111], and by Fourier transform infrared (FTIR) absorption [87, 136]. The results from TEM show that the improvement of optical quality observed after annealing may be related to the homogenisation of

the In distribution in the quantum well [111]. Moreover, no indications of N clustering were found before or after annealing [137]. Additionally, a weak annealing-induced change in the QW profile has occurred due to some diffusion of atoms over in a rather short-range [111]. This effect is much smaller than that observed previously for InGaAsP/InP structures [138-140]. However, it cannot be neglected in the analysis of transition energies for post-growth modified GaInAsN/GaAs QWs.

As for bulk-like materials (see in Section 4.1), the Ga-N bond in GaInNAs/GaAs QW structures is strongly strained and during annealing, this local strain is reduced by the formation of In-N bonds. In consequence, the nitrogen atoms are found to be in various nearest neighbour configurations after annealing. This structural change should influence the QW transitions. Klar et al. [43] have investigated MOVPE-grown GaInAsN/GaAs quantum wells by PR and have observed that the fundamental QW transition can be split. This splitting is associated with the existence of (up to five) local band gaps arising from the nitrogen atoms having different nearest-neighbour configurations. It is expected that the annealing process causes both changes in these configurations [43] and atom diffusion across the QW interfaces [111, 141]. In this Section it is shown that the annealing-induced blue shift of QW transition, which is observed in absorption-type experiments, can be fully explained by these two effects. In the case of photoluminescence, effects associated with the exciton localization have to be included, in order to understand the blue shift of an emission peak.

4.5.1 Change in nitrogen nearest-neighbour environment vs. atom interdiffusion across quantum well interfaces

In order to explain the nature of annealing-induced blueshift of QW emission in the GaInNAs/GaAs QW system a set of SQWs annealed at different conditions has been investigated. SQW structures were grown on a 500μm thick (001)-oriented unintentionally doped GaAs substrate by solid source MBE. All our samples consisted of a 180nm thick GaAs buffer layer, a 70Å $Ga_{0.64}In_{0.36}As_{0.99}N_{0.01}$ well and a 100nm thick GaAs cap layer. The buffer and cap layer were grown at 590°C and the GaInNAs QW at approximately 440°C. The cap layer grown at 590°C in itself causes some in-situ annealing during growth. But the temperature is far too low and the duration too short, to fully anneal the GaInNAs-QW. Nevertheless, it should be noted that the as-grown samples do not represent the original configuration resulting from the low-temperature conditions used for the growth of the GaInNAs-layer. After growth, the

structures were then ex-situ annealed using there different procedures by RTA in a nitrogen cover-gas environment. For the purposes of this investigation samples were annealed at 650 °C for 120 s, at 700 °C for 90 s, and at 750 °C for 60 s.

Figure 4.22 shows PR spectra for the quantum wells investigated in the vicinity of the heavy hole ground state transition 11H recorded at 10 K together with curves approximating these spectra Eq.(4), and the modulus of particular PR resonances Eq.(9).

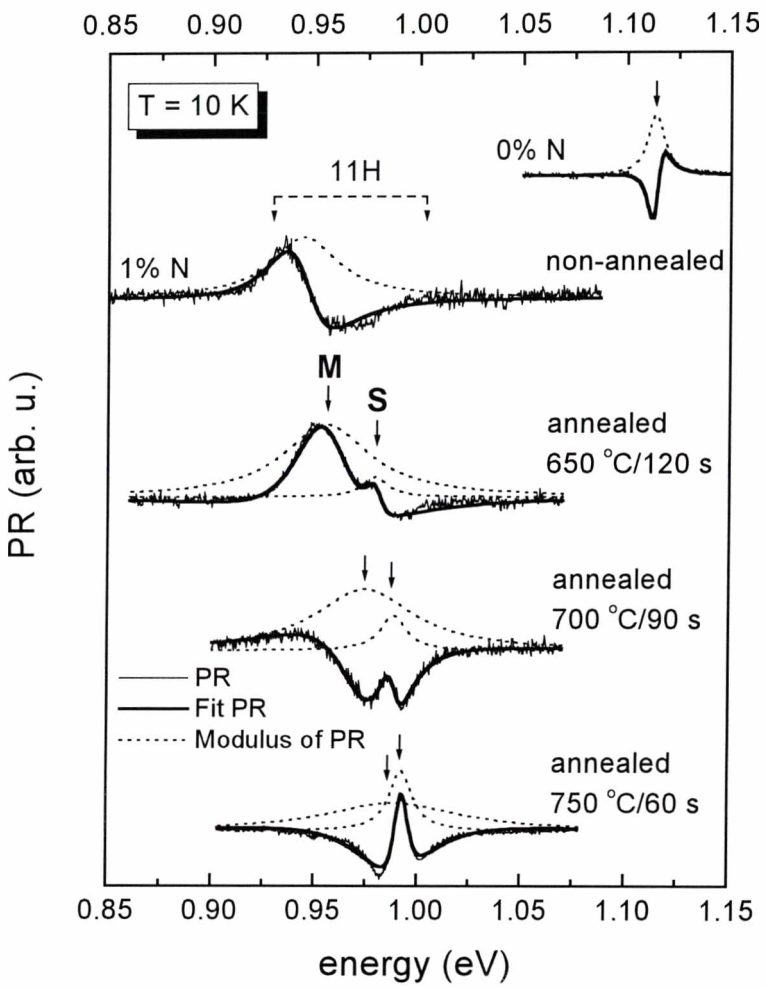

Figure 4.22. Low temperature PR spectra of as-grown and annealed $Ga_{0.64}In_{0.36}As_{0.99}N_{0.01}$/GaAs SQWs. Samples were grown at WU in Germany.

For the non-annealed SQW a rather broad signal is observed. It could be suggested that such a broad contour is connected with multiple QW-related excitonic transitions. However, it fits with a single PR resonance reasonably well and no more transitions can be distinguished in this case. The broadening parameter obtained equals 19 meV and is approximately four times greater than that obtained for the reference nitrogen free sample (see Fig. 4.22). In the case of the

annealed structures, a splitting of the fundamental transition is clearly visible; hence PR spectra have been fitted using two resonances. The transition at the lower energy (labeled M) has a broadening parameter comparable with the non-annealed SQW, while the second one (labelled S) has almost the same parameter as in the case of the reference structure (see Fig. 4.22). Such a pair of transitions cannot be explained by a superposition of heavy and light hole related features. The fundamental light hole transition was observed at a much higher energy, due to the axial component of the compressive strain and different QW confinement energy for heavy and light holes. Such a splitting of the 11H transition has previously been observed for MOVPE grown GaInAsN/GaAs QW, and has been attributed to the various nearest-neighbour configurations for the N atoms in the GaInAsN alloy. In accordance with the calculations of Klar et al. [43], the fundamental transition can be split into five. In the case of $Ga_{0.64}In_{0.36}As_{0.99}N_{0.01}$/GaAs QW the energy difference between the lowest energy (4Ga) and highest energy (4In) transition is about 50 meV and the difference between neighbouring transitions is approximately equal (10 meV in this case). The range of 50 meV is illustrated in Figure 4.22 by a dashed line between the arrows. It may be assumed that the broadening parameter for each of these five possible transitions is comparable and is likely to be slightly larger than for the reference SQW (due to some extra disorder caused by the fourth component of the alloy). Wherever the energy difference between consecutive transitions is similar to the broadening parameter, the individual PR resonances are usually not distinguishable (as for non-annealed sample). However, if one transition is amplified and has a significantly higher intensity (PR amplitude) than the others, then this resonance should be visible against the background of the other resonances. Such a case is observed in our annealed quantum wells. On the basis of its location this second resonance has been attributed to the 1Ga3In nitrogen configuration. This agrees very well with the calculations of Kim and Zunger using Monte Carlo simulations of a GaInAsN supercell [78]. They showed that the configuration of one gallium and three indium atoms around a nitrogen atom is the most favourable. During a process of fast growth of the quaternary layer the 4Ga configuration, with strongly strained Ga-N bonds, is most frequently obtained. The annealing procedure allows a (so called short range order) redistribution of atoms in the crystal lattice and the system tends to one with minimal energy, namely most favourable atom configuration (1Ga3In in this case). The final distribution should depend on the parameters of the RTA process. Klar et al. [43] observed that as the RTA temperature increases the higher energy transitions (related to more indium atoms) start to dominate in the PR spectrum. The second resonance for all the annealed structures is associated with the 1Ga3In nitrogen configuration, but then its energy should be independent of the annealing conditions. It is

observed that the 'S' feature intensity (PR amplitude) increases as increase in the annealing temperature increases (a higher RTA temperature favours the most probable configuration), whereas both the 'M' and 'S' PR transitions shift to higher energies when the annealing temperature increases. The latter can be attributed to the changes in the shape of the quantum well due to atom diffusion across the QW interface. The analysis of the morphology and composition of such QWs showed that a very thin intermediate layer can be created at the GaInAsN/GaAs interface [142], which can be smoothed out after annealing. Previous TEM measurements have confirmed that the interdiffusion of interfaces after annealing is very weak [111], but despite the fact that this effect is significantly weaker than in e.g. InGaAsP/InP structures, where it plays a crucial role [138-140], it cannot be neglected. Annealing causes the potential well to be smoothed (to a round well instead of a square well) and hence the energy level shift, which results in a blue shift of the ground state optical transition. In the case of a diffusion length of about 2 ML (approx. 0.5 nm) the transition energy of such a QW as ours can shift by even more than 10 meV [141]. Therefore, the total annealing-induced blue shift of the ground state transition is caused by two effects: changes in the nearest-neighbour configuration of nitrogen atoms and changes in the quantum well profile. However, as visible in Figure 4.22, the value of the energy shift is not the same for 'M' and 'S' features (the 'M' line shifts more rapidly as the annealing temperature increases). If we compare the values of this energy difference for each line between the samples annealed at 650 and 750 °C, we obtain 13 and 31 meV for the 'S' and 'M' transitions, respectively. The first shift is caused entirely by changes in the QW profile (assuming that this is related to the 1Ga3In configuration), whereas for the latter must be related to some additional effect. We have to remember that this 'M' feature is a multiresonance. Therefore, if the individual resonances are redistributed after annealing such that the higher energy ones became more intensive, then this results in an apparent shift of the whole 'M' feature.

This explanation of the annealing-induced blue shift of the QW transition was also confirmed by the PL experiment. Figure 4.23 shows low temperature PL spectra in the appropriate spectral range. One peak is observed for the non-annealed sample. This spectrum has been fitted using a single Gaussian curve. After annealing, a second peak appeared in the emission spectra. In this case, the PL spectra were fitted using two Gaussian curves. For all the samples investigated the PL peaks agree very well with the PR spectra, but they are slightly red-shifted. These Stokes shifts between the PL and PR signals are connected with the origin of the photoluminescence, which must be related to the bound exciton transitions. For the non-annealed $Ga_{0.64}In_{0.36}As_{0.99}N_{0.01}$/GaAs SQW the 14 meV Stokes shift is smaller than that reported by

Shirakata et al. [47] and Polimeni et al.[143], which indicates the high quality of the sample. However, this value is still quite large in comparison with the reference $Ga_{0.64}In_{0.36}As/GaAs$ SQW (less than 2 meV). The magnitude of this shift decreases after annealing to below 5 meV.

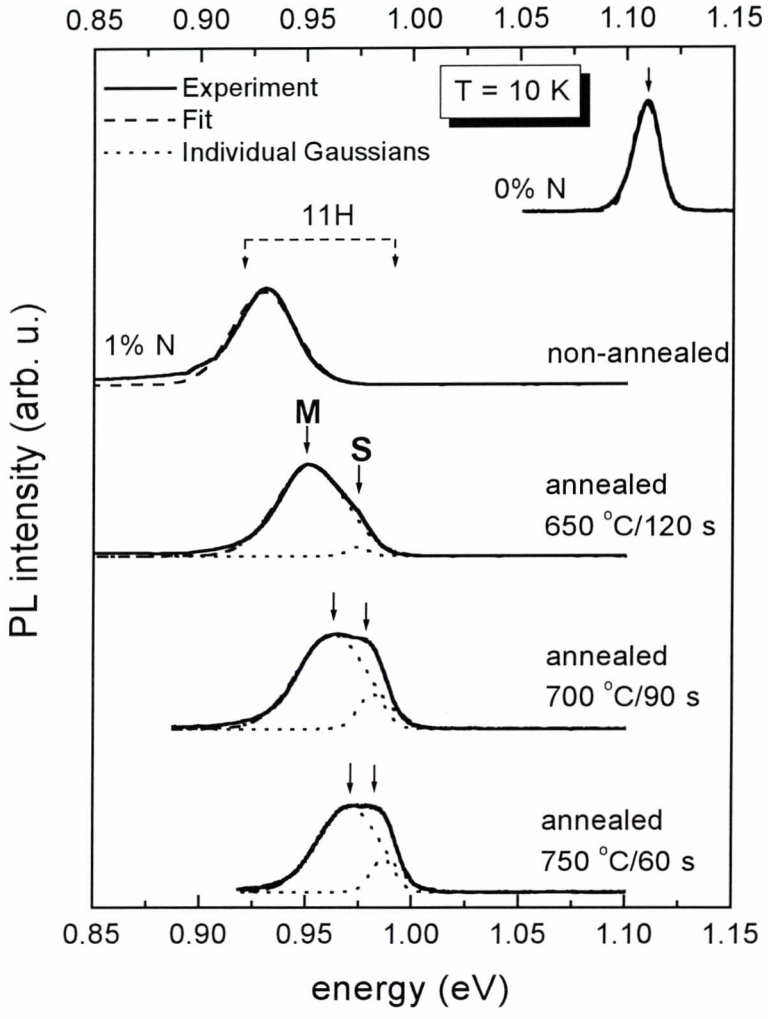

Figure 4.23. Low temperature PL spectra of $Ga_{0.64}In_{0.36}As_{0.99}N_{0.01}/GaAs$ SQW's and their decomposition into individual Gaussian curves. Samples were grown at WU in Germany.

Summarizing above findings, it has been shown that the RTA process induces an significant change in the character of the fundamental transition of a GaInAsN/GaAs quantum well. The observation of splitting of the ground state transition is associated with the existence of different configurations of the nitrogen atoms. The broad lower-energy feature is attributed to the superposition of several (up to four) transitions of comparable intensities. The second narrow resonance is associated with the favourable 1Ga3In configuration. The blue shift of the 'S' transition, as the annealing temperature increases is caused by a change in the QW profile due to the annealing-induced migration of atoms across QW interfaces, which is in agreement with

theoretical predictions made for GaInAsN/GaAs QW's [141], even though the diffusion length does not exceed a few monolayers. This has to be taken into consideration (beside the short range lattice reconfiguration effect) in the postgrowth processing of GaInAsN-based devices.

4.5.2 Influence of the growth temperature on the post-grown reconfiguration of nitrogen nearest-neighbour environment induced by annealing

Two sets of MQW structures were selected to present the influence of growth temperature on the magnitude of blueshif of QW transition due to the post-growth annealing. The MQWs samples were grown on *n*-type GaAs:Si (100) substrates by molecular beam epitaxy (MBE). Each sample consisted of a GaAs buffer layer, twenty 6.3-nm thick $Ga_{0.65}In_{0.35}As_{0918}N_{0.012}$ QWs separated by 22-nm thick GaAs barriers, and a GaAs cap layer, all nominally un-doped. The first set was grown at 410 °C and the second one at 470 °C. The samples were annealed *ex situ* at 650 and 750 °C for 60 seconds.

Figure 4.24 shows room-temperature PR spectra for the set of samples grown at 410 °C. Curves (a), (b) and (c) in Fig.4.24 show the PR spectra of as-grown, annealed at 650 and 750 °C GaInNAs/GaAs MQWs, respectively. A long-period oscillatory behaviour of the signal is seen in all samples throughout the energy range studied. This feature is associated with an interference effect which is related to the presence of n-doped GaAs substrate. However, the interference effect does not influence the PR line-shape associated with an interband transition [10]. In this case, the PR spectrum is a superposition of oscillating-like response and PR resonances associated with transitions in QW and GaAs buffer layer. PR features related to the interband absorption in QW and GaAs buffer layer are indicated by arrows in Fig.4.24, and they are distinguished despite the presence of oscillating-like structure. On the basis of the calculations like in Section 4.3, the three QW-related resonances have been attributed to the transition between first heavy-hole and first electron subbands (11H), first light-hole and first electron subbands (11L), and first heavy-hole and second electron subbands (12H).

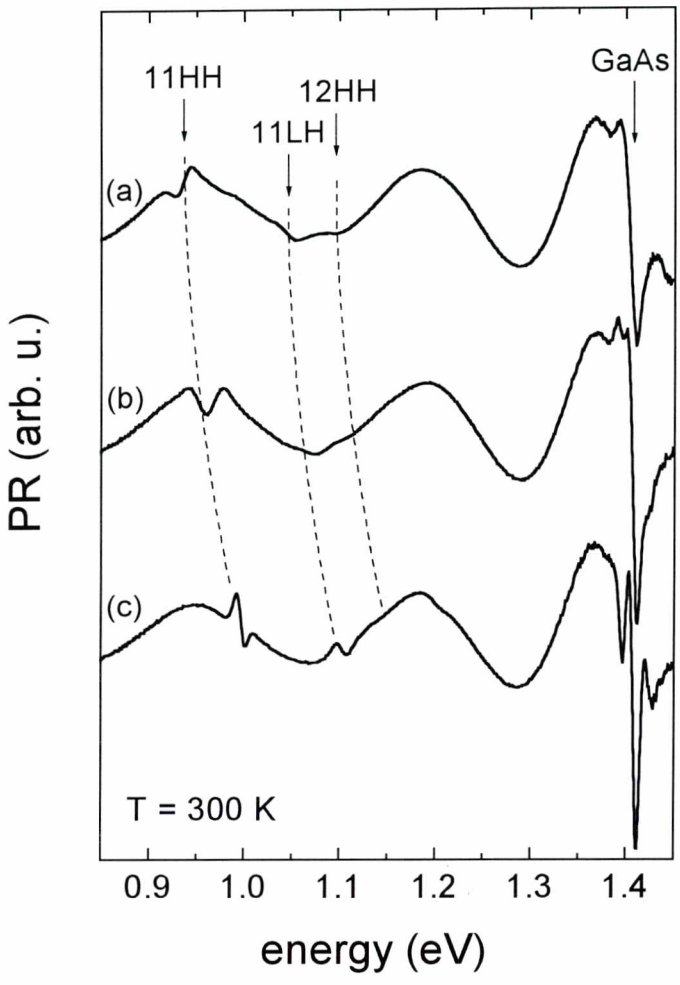

Figure 4.44. Room temperature PR spectra of as-grown (a), annealed at 650 (b), and 750 °C (c) GaInNAs/GaAs MQWs. Samples were grown at ORC in Finland.

To better analyze QW transitions, oscillating curves were calculated from the equation $\Delta R/R = \alpha \cdot \sin(\beta \cdot E + \varphi)$, where α, β, and φ are fitting parameters, mimicking the observed oscillations in the energy range of interest, 0.85 – 1.2 eV. The calculated curves were then subtracted from the experimental data to enhance QW-related PR resonances (Fig.4.25). Such processed spectra were analyzed by the use of the Kramers-Kronig analysis and the standard fitting procedure assuming Lorenzian and Gaussian line-shapes. The modulus of PR spectrum obtained by the use of KKA is shown together with the adequate PR spectrum in Fig.4.25. Energies of QW transitions taken from the KK modulus are shown in Fig.4.26. In addition, the broadening of 11H transition is shown in Fig.4.26. All these values are analyzed below.

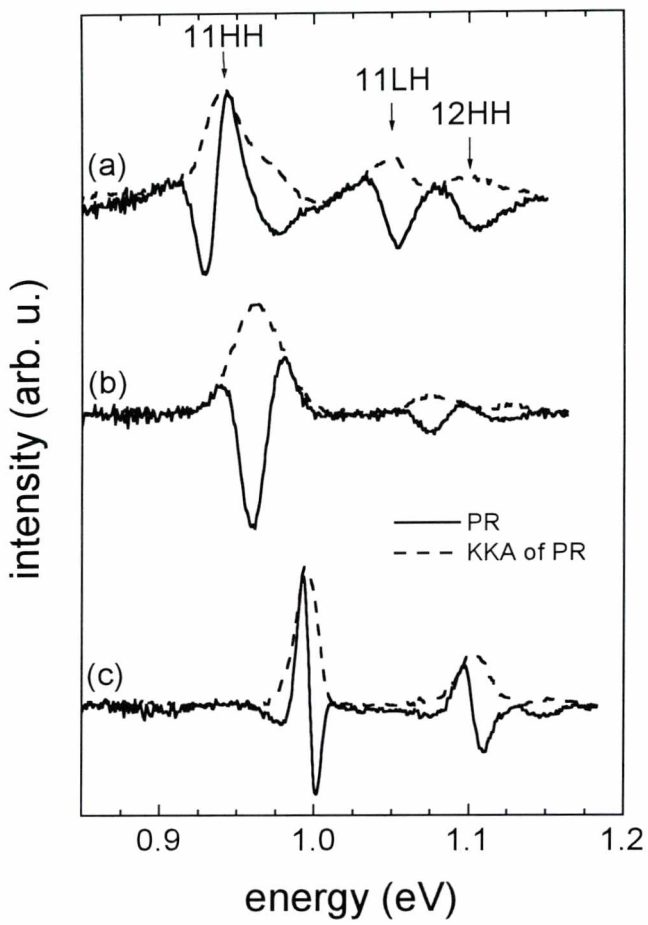

Figure 4.25. PR spectra of as-grown (a), annealed at 650 (b), and 750 °C (c) GaInNAs/GaAs MQWs after subtracting an oscillating background (solid line) and Kramers-Kronig modulus of PR signals (dashed line). Samples were grown at ORC in Finland.

The PR signals are different for different samples but vary systematically from one sample to another. For the as-grown sample, all three QW transitions possess complex character and they cannot be fitted by one Lorentzian or Gaussian PR resonance. Such PR line-shape is composed of few resonances which are associated with the presence of different nitrogen nearest-neighbour environments in this sample (N – In_4Ga_{4-m} ($0 \leq m \leq 4$) short-range-order clusters). The energy of PR resonance has been determined by KKA and is considered to be an 'effective' energy of the QW transition. In the GaInNAs/GaAs QW system the hole level in valence QW is accurately defined, while the electron level in conduction QW strongly depends on nitrogen nearest-neighbour environment. Such result has been obtained within thin binding calculations [43] and it is also intelligible in the framework of band anticrossing (BAC) model [32], based on the assumption that the nitrogen resonant level interacts only with the conduction

band. For as-grown MQWs the dominant part of 11H resonance is associated with a N – Ga_4 environment (4Ga for short). The remaining resonances, existing within the 11H transition, can be attributed to a trace of the second nitrogen environment, 1In3Ga, co-existing in the sample. Very similar behavior is observed for both 11L and 12H transitions. The formation of In-N bonds in GaInNAs can be seen in Raman spectra [84] as an appearance of In-N like LO_2 modes centred at the wave numbers of around 460 and 485 cm^{-1}. It has been found that In-N related modes exist already for the as grown sample (see in Fig.4.27). It means that '3GaIn' clusters already exist in the as-grown sample, hence PR resonances are complex.

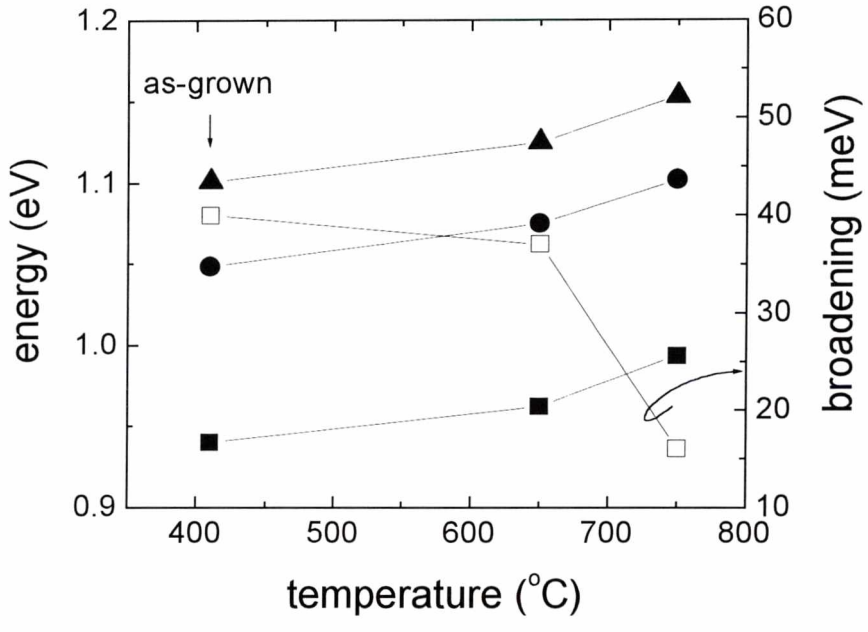

Figure 4.26. Energy of 11H (■), 11L (●), and 12H (▲) QW transitions obtained by the Kramers-Kronig analysis and broadening of the 1H transitions (□). Solid lines are a guide for eye.

After RTA at 650°C for 60 seconds, the effective energy of all three QW transitions shifts to blue, and the shape of PR lines changes significantly. However, the character of these transitions is still complex, despite the fact that the 11H transition or remaining transitions could be quite satisfactorily fitted by one Gaussian-like resonance which is the most appropriate line-shape for an QW transition at room temperature [11] (see solid line in Fig.4.28(a)). The good agreement of experimental data with the single resonance results from the fact that the energy separation between individual resonances is close to the broadening parameter of individual resonance. We obtain better agreement between the experimental data and the fit if we assume that the 11H-related transition is composed of two resonances which could be attributed to two

different nitrogen environments, probably 3Ga2In and 2Ga2In (see dashed line in Fig.4.28(a)). However, such fit is also not satisfactory because it was found that the energy separation between these two resonances is 14 meV, while their broadenings are 14 and 18 meV. In this case, a bigger energy separation (~20 meV) and a smaller broadening of PR resonance are expected. The energy separation increases and the broadening decreases if we assume that this transition is composed of three resonances. However, such fitting procedure could be controversial due to a high number of fitting parameters. The problem with fitting this spectrum is associated with the presence of more than two different clusters. It is possible that also 4Ga and Ga3In nitrogen environments exist in GaInNAs layer annealed at 650 °C and weak resonances associated with these nitrogen environments make contribution to the total PR line-shape. Therefore, in order to avoid this complication the Kramers-Kronig analysis has been used. This analysis makes it possible to determine the 'effective' energy of QW transition and helps to investigate the change in the PR line-shape.

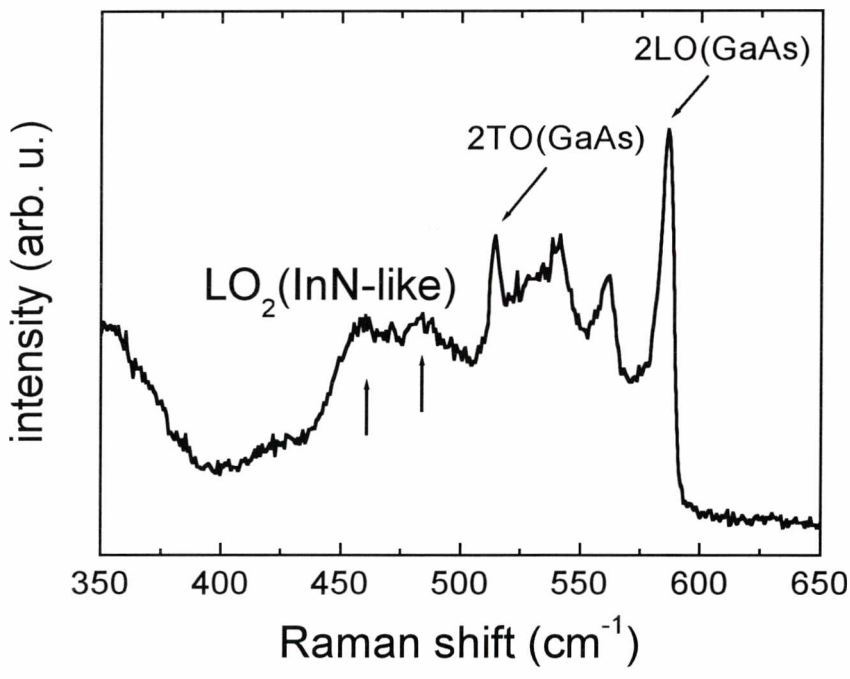

Figure 4.27. 77 K Raman spectra from as-grown GaInNAs/GaAs MQW. The vertical arrows indicate the presence of peaks assigned to In-N bonds. Samples were grown at ORC in Finland.

Essential differences in the PR line-shape and its width appear for MQWs annealed at 750°C for 60 seconds. In this case the 11H transition can be quite satisfactorily fitted by one

Gaussian-like resonance (see Fig. 4.28(b)). The broadening of the resonance is 6.4 meV. It means that in this sample one environment of nitrogen atom is dominant. Probably it is 3InGa environment which is the most favourable environment in terms of crystal energy [78]. It is noted that also 11L features behave very similar to the 11H one.

For GaInNAs/GaAs QWs, besides the change in nitrogen nearest neighbour environment, an atom interdiffusion across the QW interfaces also leads to a blue shift of QW transitions. However, for our MQWs the atom interdiffusion is rather small because any significant changes between XRD fringes of as-grown and annealed MQWs have been found (see in Fig.4.29). All diffraction patterns of each three samples are identical. The *Pendellösung* fringes confirm that the structures are of good structural quality. The similarity of the XRDs indicates that the shift of QW transitions cannot be attributed to any significant composition or thickness variations in the quantum wells. This is to say that Ga/In interdiffusion is minimal for the annealing at 650 and 750 °C, although some atomic-scale diffusion, undetectable by our XRD, cannot be completely ruled out. The interdiffusion process could significantly influence the energy of QW transitions if RTA was conducted at higher annealing temperature and for longer annealing time.

The coexistence of few band gaps is one of the most interesting features in this system. It has been observed that for spatial resolution of 0.5 mm the PR spectrum does not depend on the place on a sample. It means that the sample is homogeneous above 0.5 mm and eventual inhomogeneities are lower that 0.5 mm. In this system, due to the strong localization of electron wave function near the N centres, eventual spatial inhomogeneities of band gap energy would be close to few distances between nitrogen atoms. To our knowledge, such inhomogeneities have never been observed so far in an absorption-type experiment. However, it is assumed that the coexistence of few band gaps results from spatial inhomogeneities of the band gap in GaInNAs (spatial inhomogeneities in nitrogen nearest-neighbour environment, i.e. N – In_4Ga_{4-m} clusters). The relative density of state for each gap corresponds to the number of adequate clusters. The post-growth annealing leads to a redistribution of N atoms between the five possible environments. For the as-grown structure the environment is dominated by Ga atoms (N-Ga_4 cluster), whereas annealing provides enough energy for atoms to minimize strain and rearrange. It leads to an In-rich distribution of clusters, dominated by In-N bonds.

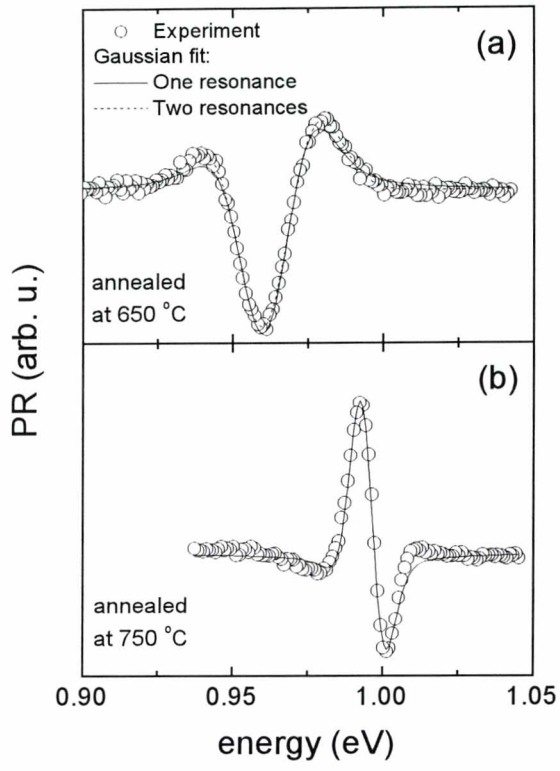

Figure 4.28. PR spectra of annealed at 650 (a), and 750 °C (b) GaInNAs/GaAs MQWs (open circles) and their fits by Gaussian-like lineshape (lines). Samples were grown at ORC in Finland.

The unique property that the band gap possesses distinct discrete values despite the alloy disorder is due to the large energy separations between the corresponding conduction band states and the strong electron localization near the N centres. Therefore in this system the band gap is a local property in the mezoscopic scale. Such a local behaviour of the band gap is one of the causes of the carrier localization effect at low temperatures, which is usually observed in GaInNAs layers and QWs. Due to the non-equilibrium growth of GaInNAs layers a disorder in nitrogen environment is rather usual. It is expected that the disorder depends on growth conditions and post-growth annealing. Generally, it is well known that the RTA causes an effective blue shift of GaInNAs band gap energy due to a decrease in the number of Ga-rich environment in favour of In-rich environments. However, the mechanism of the reconfiguration of nitrogen bonds is rather unclear, and only few papers consider this phenomenon. Klar et al. [43] have concluded that for GaInNAs/GaAs QWs grown by MOVPE the change in N environment is enhanced by As vacancies. He has proposed that N atom hops from Ga-rich to more favourable In-rich environments via As vacancies. In the next part of this subsection the

influence of growth temperature on the annealing induced change in nitrogen environment is presented.

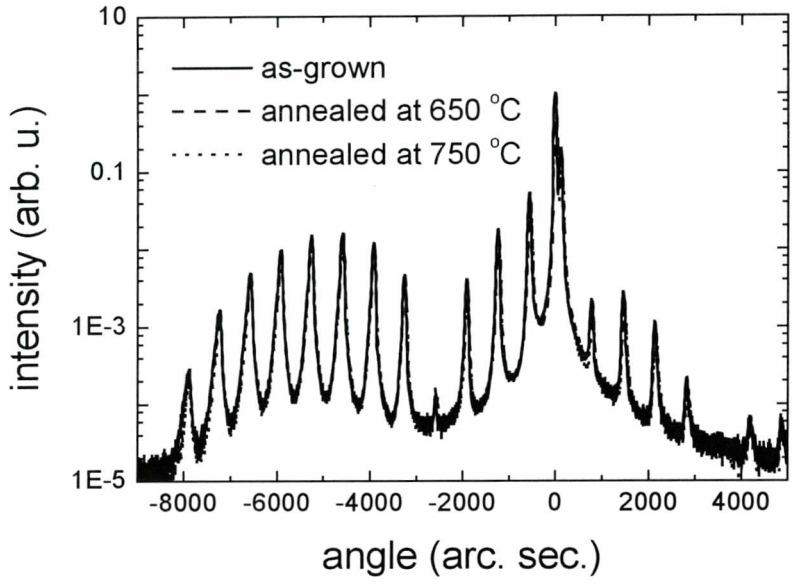

Figure 4.29. X-ray diffraction rocking curves from as-grown (solid line), annealed at 650 (dashed line), and 750 °C (dotted line) GaInNAs/GaAs MQWs. Samples were grown at ORC in Finland.

A comparison of the normalized modulus of PR spectrum for two sets of MQWs grown at different temperatures (410 and 470 C°) and annealed under the same conditions is shown in Fig.4.30. The vertical doted lines indicate expected band gap energies for different nitrogen nearest neighbour environments taken after Ref.[43]. For as-grown samples the two spectra are almost the same (see curves (a) in Fig.4.30), while for annealed samples they are significantly different (see curves (b) and (c) in Fig.4.30). It is clearly seen that the 'effective' blue shift is smaller for samples grown at 470 °C than for samples grown at 410 °C. It means that the magnitude of energy shift strongly depends on the initial structural configuration and number of point defects. In the case of as-grown MQWs the 4Ga is the dominant nitrogen environment and 3GaIn is the second environment which is present in the GaInNAs layer. The same distribution between magnitudes of 4Ga- and 3GaIn-related peaks indicates that for the two sets of MQWs the initial nitrogen environments are similar. The lower concentration of As vacancies in the GaInNAs layer grown at higher temperature is one of the possibilities which can explain the smaller blue shift. However, the real reason is rather more complicated and is difficult to settle. Probably, besides As vacancies other points defects, like e.g. Ga vacancies (promoted by limited

diffusion of cations onto the growing surface at low temperatures), could influence the process of N bonds reconfiguration.

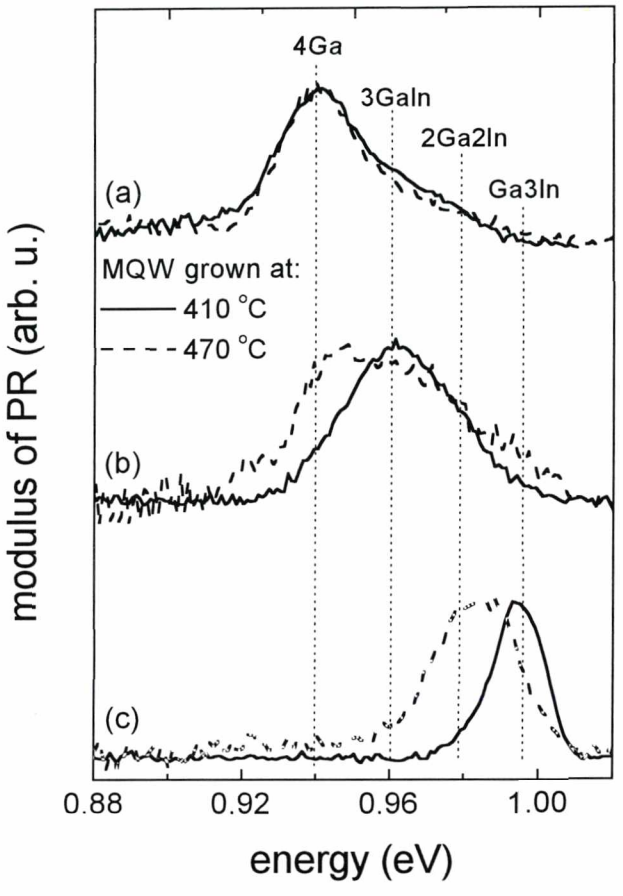

Figure 4.30. The normalized Kramers-Kronig modulus of PR spectrum in the vicinity of 11H transition. Solid and dashed lines correspond to MQWs grown at 410 °C and 470 °C, respectively. Curves (a), (b), and (c) correspond to as-grown, annealed at 650 °C, and 750 °C MQWs, respectively. Samples were grown at ORC in Finland.

4.6 Manifestation of the localization effect in photoreflectance spectroscopy

The effect of carrier localisation at low temperatures is typical of Ga(In)NAs compounds and their structures [46, 49, 52, 54, 56]. This effect influence both optical and electrical properties of Ga(In)NAs structures. In the case of optical properties detected in PL spectroscopy a emission band associated with recombination of localised excitons and carriers is observed instead free exciton and band-to-band recobmbination. PR technique probes optical properties, however, this technique is also sensitive to electrical properties because in order to obtain the PR signal the photo-generated electron-hole pairs have to separate and have to change the built-in

electric field. Therefore, it is expected that electron and hole traps will influence the mechanism of photomodulation of the band bending. In this section the influence of the carrier localisation on photomodulation mechanism is discussed. As have been shown the carrier localisation weakens the band bending photomodulation and leads to a decrease of PR signal [144, 145].

Figures 4.31 (a) and (b) show temperature dependences of photoreflectance spectra for $Ga_{0.95}In_{0.05}As_{0.98}N_{0.02}$ and $GaAs_{0.98}N_{0.02}$ layers, respectively. Each figure shows spectra of as-grown layers whereas corresponding photoluminescence spectra are shown in the insets. These samples have been discussed in the Section 4.1.

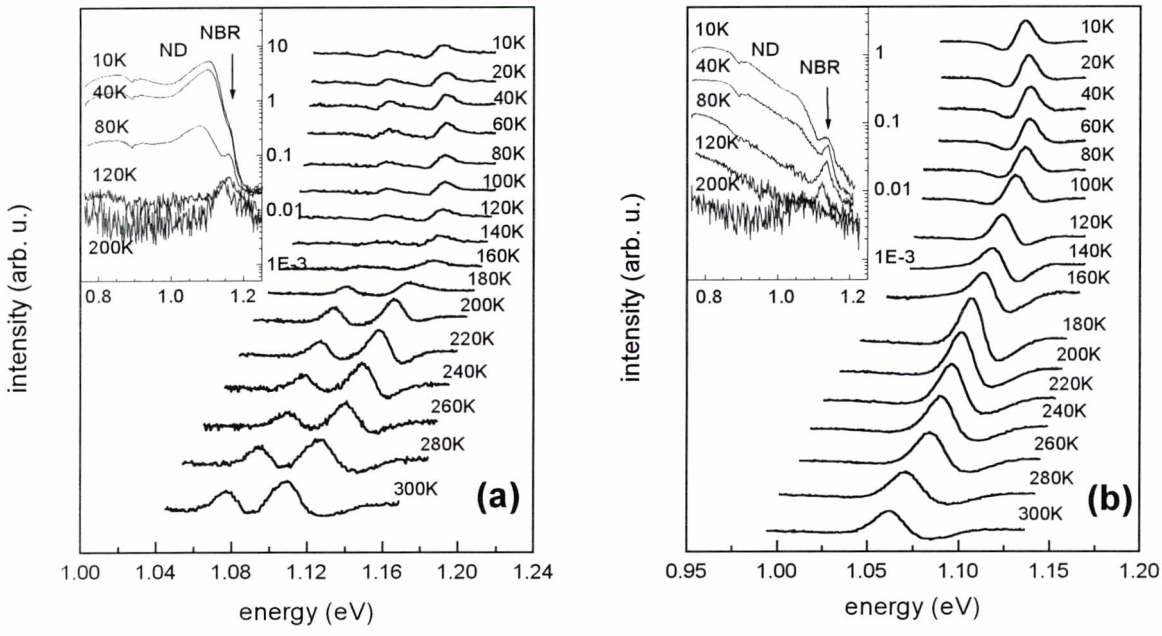

Figure 4.31. Temperature dependency of PR spectrum for $GaN_{0.02}As_{0.98}$ (a) and $Ga_{0.95}In_{0.05}N_{0.02}As_{0.98}$ (b) layers. The insets show PL spectra. Samples were grown at LPN in France.

For the GaInNAs layer, an increase of PR signal with the increase of temperature from 10 up to about 200 K is observed. The same property is also seen for ternary $GaAs_{0.98}N_{0.02}$ layers (see Fig. 4.32). In this case, the increase of PR signal is clearly visible in the whole temperature range from 10 to 300 K. The tendency of all these curves is independent of the pump power (in the range of 0.1 to 5 mW) and pump beam wavelengths (several lines with the photon energy always higher than GaAs band gap). It means that this temperature-induced change of PR signal is not related to the modulation conditions, but has a direct link with the material characteristics. This PR behaviour with temperature is not typical of a bulk-like semiconductor material as explained below. Usually, optical transitions observed in PR are described by critical point line shape model as Eq.(4). With an increase of temperature, the energy E_0 decreases accordingly to

Varshni formula [146] and the broadening parameter increases accordingly to Bose-Einstein like formula [147]. The phase angle in Eq.(4) does not have simple interpretation and is rarely analyzed. The amplitude is also usually neglected in the interpretation; however there are a few papers which very carefully investigated this parameter [148-152]. It has been shown that A can be related to material parameters and should be nearly temperature independent. Generally, the PR intensity (in the sense of peak to peak value) decreases with increasing temperatures but this is related to the temperature-induced changes of the broadening parameter rather than to amplitude variation. In the case of Fig.4.31 the evolution of PR features evidence that A varied with temperature. The modulation efficiency of the material decreased at low temperature. Rather than an A amplitude analysis (Eq.1), the integrated intensity of transitions obtained by a Kramers-Kronig analysis Eq.(8) is considered. The integral of Eq.(8) can be interpreted as the transition intensity and can be obtained without fitting procedure. The advantage of such analysis is that it by-passes the fitting procedure. In this approach we do not have to consider (even do not have to know) the PR line shape (Lorentzian or Gaussian, first or third derivate, etc.). This advantage becomes important to analyse the temperature dependence of the spectra, where the line shape can change from a Lorentzian-like to a Gaussian-like due to the changes of the dominant scattering processes. As in a common fitting procedure, in addition to the transition intensity, the Kramers-Kronig analysis provides the energy and broadening of the transition. Only the information concerning the phase angle is lost. A disadvantage of this method is the necessity to have well separated PR resonances [17] to determine correctly the integration limits for a particular transition.

It is seen in Eq.(9) that the integral of the modulus depends on both A and Γ. If one assumes that the modulation efficiency does not change significantly with the increase of temperature (A almost constant), the transition intensity should decrease with the increase of temperature due to the broadening parameter increase. Even, if the experimental line shape is not the same as in equation (1) the transition intensity will also decrease with temperature similar way due to the broadening. This property has been investigated for the GaNAs and GaInNAs layers.

Figure 4.32 shows the temperature dependence of transition intensity for the two samples. In the case of GaNAs layer the decrease takes place from 300 to 10 K for both heavy- and light-hole related features, whereas for the GaInNAs layer, a decrease in transition intensity is observed below 200 K. The feature has been connected with PL results, which are presented in the insets of Fig.4.31 and are discussed in Section 4.1. For the two samples an emission band associated with a recombination involving N-related defects (ND) is clearly visible. The band is

dominant in comparison to the near band recombination (NBR), and confirms the significant carrier localization in the layers.

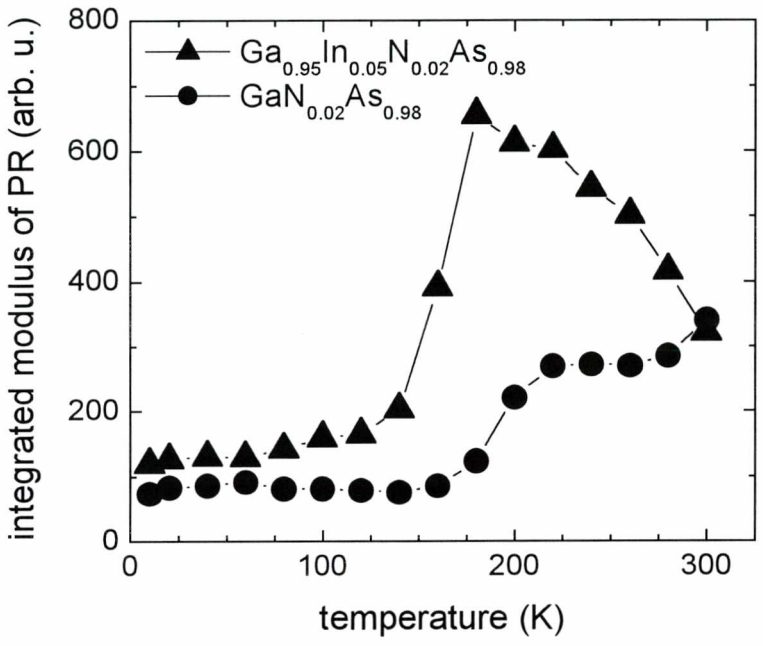

Figure 4.32. Integrated modulus of PR obtained from Kramers-Kronig analysis versus temperature. In the case of $GaN_{0.02}As_{0.98}$ layers the presented intensities are the sum of light-hole and heavy-hole transition intensities. Samples were grown at LPN in France.

Our conclusion is that this effect has to influence the efficiency of PR modulation. At low temperatures whereas the thermal energy is small, carriers induced by pump beam can be immediately localized on some potential fluctuations. The localized carriers cannot move and they do not contribute to the changes of the band bendings and hence to the modulation of a built-in electric field. With an increase in temperature the thermal energy increases and the localization energy can be exceeded, which is reflected in the possibility for carriers to move. Such behaviour induces an increase in the modulation efficiency, because moving carriers allow a change in the built-in electric field.

A decrease in photomodulation efficiency at low temperatures due to the carrier localization effect has been also observed for GaInNAs/GaAs QW structures [145]. It has been found that with the increase in nitrogen content the effect of carrier localization is enhanced and PR signal at low temperature decreases drastically. An example of this effect is shown in Fig.4.33. This figure shows the ratio of transition intensity at 300 and 10 K for the subset 'C' of SQWs. It is clearly visible that with the increase in nitrogen content the ratio rises due to the decrease of PR intensity at 10 K.

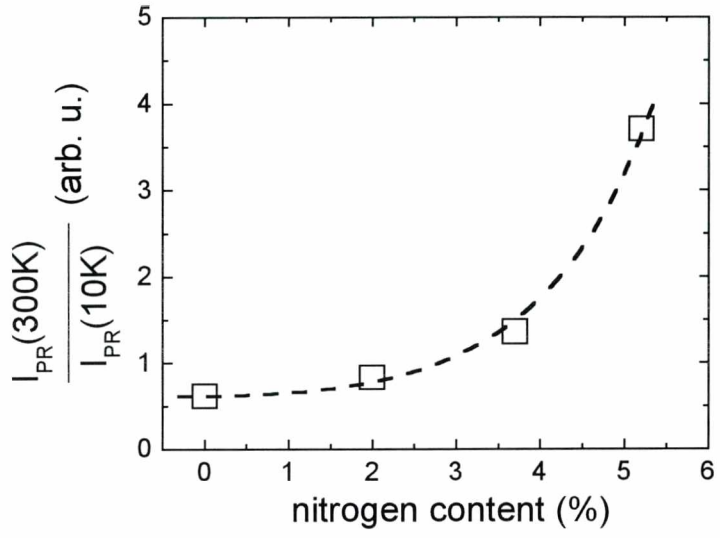

Figure 4.33. Ratio of room (300 K) and low temperature (10 K) PR amplitudes versus the nitrogen content for the series of $Ga_{0.59}In_{0.41}N_xAs_{1-x}$/GaAs SQWs. Samples were grown at WU in Germany.

The carrier localization effect is usually observed for nitrogen diluted GaAs and GaInAs layers and QWs [144, 145]. Hence, the low temperature PR measurements could be limited, especially for structures with high nitrogen content, because with the increase in nitrogen mole fraction the carrier localization effect is stronger and makes difficult the band bending photomodulation. It means that the electron-hole pairs induced by the pump beam are not capable of changing the built-in electric field, because they are immediately localized and cannot be separated in the structure. In this way the carrier localization phenomenon is responsible for difficulties in low temperature PR investigations of GaInNAs-based structures.

5. Summary and outlook

The long-wavelength emission on GaAs substrates has motivated the study of nitrogen diluted III-V compounds and their low dimensional structures. The aim of this thesis was to apply photoreflectance technique supported by photoluminescence technique to study the optical properties of GaAs-based materials promising for 1.3 and 1.55 μm laser application. The main tasks of this thesis were (i) to determine the energy level structure of Ga(In)NAs-based QW structures and (ii) to investigate the influence of post-growth annealing on optical properties of N containing III-V compounds and their QW structures.

Concerning the first task, it has been concluded that at the first approximation the incorporation of N atoms into GaInAs/GaAs QW influences mainly the electron QW, while the hole QW is similar to N-free QW system. It indicates that GaInNAs/GaAs QW structures tailored at 1.3 and 1.55 μm are promising from the point of view of the band gap alignments. It has been found that for investigated GaInNAs/GaAs QW structures the conduction band offset is $\Delta E_C \approx 0.8 \cdot \Delta E_g$. It assures strong confinement of electrons and sufficient confinement of holes into the QW region. Therefore, the expectation that GaInNAs/GaAs-based lasers will have better temperature characteristic (higher T_0) than InGaAsP/InP-based lasers is justified. The other issue is the deterioration of optical quality with the increase in nitrogen concentration. This issue is very important for laser structures. Therefore, the second task of this thesis was to investigate the influence of post-growth annealing on the optical quality of N-containing III-V compounds and their QW structures.

It has been shown that the post-growth annealing weakens the non-radiative- and defect-related recombination processes in favour of the band gap-related recombination. However, it simultaneously leads to a blueshift of band gap energy. The phenomenon of annealing-induced blueshift of band gap energy has been carefully investigated in photoreflectance spectroscopy and it has been found that this effect is associated with (i) the reduction of the tail of DOS and (i) the change of nitrogen nearest-neighbour environments from Ga-rich to In-rich environment. In the case of QW structures, the effect of the atom interdiffusion across QW interfaces has been considered and it has been concluded that this effect is negligible for GaInNAs/GaAs QWs in contrast to InGaAsP/InP QWs.

For all of the topics the author has studied a number of extensions which are not show in this thesis. The extensions are partially presented in the papers published by the author with the co-workers, see in the section entitled *List of publications*. Concerning the outlook of this work,

the research on long wavelength optoelectronic devices has seen a lot of progress in the last few years. Indeed, by now GaInNAs active regions have been implemented successfully in 1.3 μm VCSEL's by variety of research groups; initially only with MBE-techniques, but recently also with MOVPE. At this moment a lot of attention is focused on 1.55 μm lasers. In this case, the deterioration of optical quality with the increase in nitrogen concentration is the main difficulty in achieving high efficient GaInNAs-based lasers emitting at 1.55 μm. Therefore, in order to avoid this problem N concentration is reduced to 1-2 % and Sb atoms are incorporated into GaInNAs compound. In addition, step-like Ga(In)NAs barriers are introduced into the QW structure. It is expected that in this way 1.55 μm VCSEL's grown on GaAs substrate will be achieved. Despite the huge progress in the fabrication of GaInNAs-based lasers, a lot of fundamental properties of N-containing III-V compounds are not fully understood. Therefore, this topic will be very attractive for the next few years. Results presented in this thesis show that photoreflectance spectroscopy supported by photoluminescence spectroscopy is a powerful tool to investigate the optical properties of this system. Therefore, such investigations are intensively continued by the author.

6. References

[1] K.-H. Schlerth, *'III-V semiconductor lasers: application in telecommunication systems – suitability for spectroscopy'*, Infrared Physics and Technology **37**, 129 (1996).

[2] J.S. Harris Jr, *'GaInNAs long-wavelength lasers: progress and challenges'*, Semicond. Sci. Technol. **17**, 880 (2002).

[3] See for example papers in Semicond. Sci. Technol. **17**, (2002).

[4] O.B. Shchekin and D.G. Deppe, *'1.3 μm InAs quantum dot laser with T_0=161 K from 0 to 80 °C'*, Appl. Phys. Lett. **80**, 3277 (2002).

[5] M. Kondow, K. Uomi, A. Niwa, T. Kitatani, S. Watahiki, and Y. Yazawa, *'GaInNAs: A novel material for long-wavelength-range laser diodes with excellent high-temperature performance'*, Jpn. J. Appl. Phys. **35**, 1273 (1996).

[6] M. Weyers, M. Sato, and H. Ando, *'Red shift of photoluminescence and absorption in dilute GaAsN alloy layers'*, Jpn. J. Appl. Phys. **31**, L853 (1992).

[7] J.F. Geisz and D.J. Friedman, *'III-V-N semiconductor for solar photovoltaic applications'*, Semicond. Sci. Technol. **17**, 769 (2002) and there in.

[8] P.M. Asbeck, R.J. Welty, C.W. Tu, H.P. Xin, and R.E. Welser, '*Heterojunction bipolar transistors implemented with GaInNAs materials*', .Semicond. Sci. Technol. **17**, 898 (2002) and there in.

[9] M. Cardona in *'Modulation Spectroscopy'* Academic Press, New York, 1969.

[10] F.H. Pollak, in: *Handbook on Semiconductors*, edited by T. S. Moss, vol. 2, (Elsevier Science, Amsterdam, 1994), pp. 527-635.

[11] O.J. Glembocki and B.V. Shanabrook, *'Photoreflectance spectroscopy of microstructures'* in D.G. Seiler, C.L. Littler. (Eds.), *'Semiconductors and Semimetals'* Vol.36, Academic Press, New York, 1992, p.221.

[12] J. Misiewicz, P. Sitarek, G. Sek, R. Kudrawiec, *'Semiconductor heterostructures and device structures investigated by photoreflectance spectroscopy'*, Materials Science **21**, 264 (2003).

[13] P.J. Klar, C.M. Townsley, D. Wolverson, J.J. Davies, D.E. Ashenford, and B. Lunn, *'Photomodulated reflectivity of $Zn_{1-x}Mn_xTe/ZnTe$ multiple-quantum wells with below-bandgap excitation'*, Semicond. Sci. Technol. **10**, 1568 (1995).

[14] D.E. Aspnes, '*Third-derivative modulation spectroscopy with low-field electroreflectance*', Surf. Sci. **37**, 418 (1973).

[15] D.E. Aspnes, '*Band nonparabolicities, broadening, and internal field distributions: The spectroscopy of Franz-Keldysh oscillations*', Phys. Rev B **10**, 4228 (1974).

[16] T.J.C. Hosea, *'Estimating critical-point parameters from Kramers-Kronig transformations of modulated reflectance spectra'*, phys. stat. sol. (b) **182**, K43 (1994).

[17] T.J.C. Hosea, *'Estimating critical-point parameters of modulated reflectance spectra'*, phys. stat. sol. (b) **189**, 531 (1995).

[18] K. Jezierski, P. Markiewicz, J. Misiewicz, M. Panek, B. Sciana, T. Korbutowicz, and M. Tłaczała, *'Application of Kramers-Kronig analysis to the photoreflectance spectra of heavily doped GaAs/SI-GaAs structures'*, J. Appl. Phys. **77**, 4139 (1995).

[19] G.D. Gilliland, '*Photoluminescence Spectroscopy of crystalline semiconductors*', Mat. Scien. Eng. R **18**, 99 (1997).

[20] M. Colocci, M. Gurioli, and A. Vinatteri, *'Thermal ionization of excitons in GaAs/AlGaAs quantum well structures'*, J. Appl. Phys. **68**, 2809 (1990).

[21] H.W. Yoon, D.R. Wake, and J.P.Wolfe, *'Effect of exciton-carrier thermodynamics on the GaAs quantum well photoluminescence'*, Phys. Rev. B **54**, 2763 (1996).

[22] V. Donchev, Tzv. Ivanov, I. Ivanov, M. Angelov, K. Germanova, *'High-temperature excitons in GaAs quantum wells embedded in AlAs/GaAs superlattices'*, Vacuum **58**, 478 (2000).

[23] R. Kudrawiec, L. Bryja, J. Misiewicz, A. Forchel, *'Temperature evolution of photoluminescence from an $In_{0.22}Ga_{0.78}Sb/GaSb$ single quantum well'*, Mat. Sci. Eng. B **110**, 42 (2004).

[24] J.E. Fouquet, A. E. Siegman, *'Room-temperature photoluminescence times in a $GaAs/Al_xGa_{1-x}/As$ molecular beam epitaxy multiple quantum well structure'*, Appl. Phys. Lett. **46**, 280 (1985).

[25] R. Kudrawiec, private communication to be published.

[26] P. Sitarek, '*Application of photoreflectance spectroscopy to investigation of semiconductor heterostructures*', Ph. D. thesis, Institute of Physics, Wroclaw University of Technology, Poland (1999) in polish.

[27] M. Fischer, D. Gollub, M. Reinhardt, M. Kamp, and A. Forchel, *'GaInNAs for GaAs based lasers for the 1.3 to 1.5 mu m range'*, J. Cryst. Growth **251**, 353 (2003).

[28] J. Derluyn, *'Development of a low temperature MOCVD process for GaInNAs materials'*, Ph. D. thesis, INTEC-Ghent University, Belgium (2002).

[30] E.-M. Pavelescu, Ph. D. thesis, Tampere University of Technology, Finland, in preparation (2004).

[31] L. Malikova, F.H. Pollak, and R. Bhat, *'Composition and temperature dependence of the direct band gap of $GaAs_{1-x}N_x$'*, J. Electron. Mater. **27**, 484 (1998).

[32] W. Shan, W. Walukiewicz, J.W. Agger III, E. E. Haller, J.G. Geisz, D.J. Friedman, J.M. Olson, and S.R. Kurtz, *'Band anticrossing in GaInNAs alloys'*, Phys. Rev. Lett. **82**, 1221 (1999).

[33] J.D. Perkins, A. Mascarenhas, Y. Zhang, J.F. Geisz, D.J. Friedman, J.M. Olson, and S.R. Kurtz, *'Nitrogen-activated transitions, level repulsion, and band gap reduction in $GaAs_{1-x}N_x$ with $x<0.03$'*, Phys. Rev. Lett. **82**, 3312 (1999).

[34] Y. Zhang, A. Mascarenhas, H.P. Xin, and C.W. Tu, *'Valence-band splitting and shear deformation potential of dilute $GaAs_{1-x}N_x$ alloys'*, Phys. Rev. B **61**, 4433 (2000).

[35] W.K. Hung, M.Y. Chern, Y.F. Chen, Z.L. Yang, and Y.S. Huang, *'Optical properties of $GaAs_{1-x}N_x$ on GaAs'*, Phys. Rev. B **62**, 13028 (2000).

[36] W. Shan, K.M. Yu, W. Walukiewicz, J.W. Ager III, E.E. Haller, M.C. Ridgway, *'Reduction of band-gap energy in GaNAs and AlGaNAs synthesized by N^+ implantation'*, Appl. Phys. Lett. **75**, 1410 (1999).

[37] H. Gruning, L. Chen, Th. Hartmann, P.J. Klar, W. Heimbrodt, F. Hohsdorf, J. Koch, and W. Stolz, *'Optical spectroscopic studies of N-related bands in Ga(N,As)'*, phys. status solidi (b) **215**, 39 (1999).

[38] J.D. Perkins, A. Mascarenhas, J.F. Geisz, and D.J. Friedman, *'Conduction-band-resonant nitrogen-induced levels in $GaAs_{1-x}N/sub_x$ with $x<0.03$'*, Phys. Rev. B **64**, 121301(R) (2001).

[39] P.J. Klar, H. Gruning, H. Heimbrodt, J. Koch, F. Hohnsdorf, W. Stolz, P.M.A. Vincente, and J. Camassel, *'From M isoelectronic impurities to N-induced bands in the GaN_xAs_{1-x} alloy'*, Appl. Phys. Lett. **76**, 3439 (2000).

[40] P.J. Klar, H. Gruning, W. Gungerich, H. Heimbrodt, J. Koch, T. Torunski, W. Stolz, P. Polimeni, and M. Capizzi, *'Global changes of the band structure and the crystal lattice of Ga(N,As) due to hydrogenation'*, Phys. Rev. B **67**, 121206(R) (2003).

[41] M.M. Fahmi, A. Khan, J.A. Griffin, G.L. Harris, L.H. Robins, A.G. Birdwell, Y-S. Kang, D.J. Smith, T. Steiner, and S.N. Mohammad, *'Nitrogen-activated bowing of dilute $In_yGa_{1-y}As_{1-x}N_x$ based on photoreflectance studies'*, J. Appl. Phys. **94**, 7576 (2003).

[42] A. Khan, N. Nelson, J.A. Griffin, D.J. Smith, T. Steiner, and S.N. Mohammad, '*Nitrogen activated bowing parameter of $GaAs_{1-x}N_x$ ($x \leq 1\%$) obtained from photoreflectance spectra*', Solid-State Electron. **48**, 291 (2004).

[43] P.J. Klar, H. Grüning, J. Koch, S. Schäfer, K. Volz, W. Stolz, W. Heimbrodt, A. M. Kamal Saadi, A. Lindsay, and E.P. O'Reilly, '*(Ga, In)(N, As)-fine structure of the band gap due to nearest-neighbor configurations of the isovalent nitrogen*', Phys. Rev. B **64**, 121203(R) (2001).

[44] R. Kudrawiec, E.-M. Pavelescu, J. Wagner, G. Sęk, J. Misiewicz, J. Konttinen, and M. Pessa, *'The photoreflectance evidence of multiple band gaps in dilute GaInNAs layers lattice–matched to GaAs'*, J. Appl. Phys. in press (2004).

[45] G. Sek, K. Ryczko, J. Misiewicz, M. Fischer, M. Reinhardt, and A. Forchel, *'Photoreflectance spectroscopy of InGaAsN/GaAs quantum wells grown by MBE'*, Thin Solid Films **380**, 240 (2000).

[46] L. Grenouillet, C. Bru-Chevallier, G. Guillot, P. Gilet, P. Duvaut, C. Vannuffel, A. Million, and A. Chenevas-Paule, *'Evidence of strong carrier localization below 100 K in a GaInNAs/GaAs single quantum well'*, Appl. Phys. Lett. **76**, 2241 (2000).

[47] S. Shirakata, M. Kondow, and T. Kitatani, *'Photoluminescence and photoreflectance of GaInNAs single quantum wells'*, Appl. Phys. Lett. **79**, 54 (2001).

[48] S.A. Choulis, B.A. Weinstein, T.J.C. Hosea, M. Kamal-Saadi, E.P. O'Reilly, A.R. Adams, and W. Stolz, *'Effects of confinement on the coupling between nitrogen and band states in $InGaAs_{1-x}N_x/GaAs$'*, phys. stat. sol. (b) **223**, 151 (2001).

[49] A. Polimeni, M. Capizzi, M. Geddo, M. Fisher, M. Reinhard, A. Forchel, *'Effect of nitrogen on the temperature dependence of the energy gap in $In_xGa_{1-x}As_{1-y}N_y/GaAs$ single quantum wells'*, Phys. Rev. B **63**, 195320 (2001).

[50] J.B. Heroux, X. Yand, and W.I. Wang, *'Photoreflectance spectroscopy of strained (In)GaAsN/GaAs multiple quantum wells'*, J. Appl. Phys. **92**, 4361 (2002).

[51] J.B. Heroux, X. Yand, and W.I. Wang, *'Optical characterization of strained InGaAsN/GaAs multiple quantum wells'*, J. Vac. Sci. Technol. B **20**(3), 1154 (2002).

[52] P. Sitarek, K. Ryczko, G. Sek, J. Misiewicz, M. Fisher, M. Reinhardt, A. Forchel, *'Optical investigations of InGaAsN/GaAs single quantum well structures'*, Solid-State Electronics **47**, 489 (2003).

[53] S.A. Choulis, T.J.C. Hosea, S. Tomic, M. Kamal-Saadi, A.R. Adams, E.P. O'Reilly, B.A. Weinstein, and P.J. Klar, '*Electronic structure of $In_yGa_{1-y}As_{1-x}N_x/GaAs$ multiple quantum wells in the dilute-N regime from pressure and k·p studies*', Phys. Rev. B **66**, 165321 (2002).

[54] J. Misiewicz, R. Kudrawiec, K. Ryczko, G. Sęk, A. Forchel, J.C. Harmand, and M. Hammar, ''Photoreflectance investigation of the energy level structure in GaInNAs-based quantum wells'', J. Phys. Cond. Mat. in press (2004).

[55] M. Geddo, R. Pezzuto, M. Capizzi, A. Polimeni, D. Gollub, M. Fisher, and A. Forchel, '*Photoreflectance investigations of hydrogenated (InGa)(AsN)/GaAs heterostructures*', Eur. Phys. J. B **30**, 39 (2002).

[56] R. Kudrawiec, G. Sek, K. Ryczko, J. Misiewicz, P. Sundgren, C. Asplund, and M. Hammar, '*'The nature of optical transitions in $Ga_{0.64}In_{0.36}As_{1-x}N_x/GaAs$ single quantum wells with low nitrogen content ($x \leq 0.008$)'*, Solid State Commun. **127**, 613 (2003).

[57] J. Misiewicz, P. Sitarek, K. Ryczko, R. Kudrawiec, M. Fische, M. Reinhardt, and A. Forchel, '*Influence of nitrogen on carrier localization in InGaAsN/GaAs single quantum wells*', Microelectronics Journal **34**, 737 (2003).

[58] J. Misiewicz, G. Sek, R. Kudrawiec, K. Ryczko, D. Gollub, J.P. Reithmaier, and A. Forchel, '*Photomodulation spectroscopy applied to low-dimensional semiconductor structures*', Microelectronics Journal **34**, 351 (2003).

[59] M. Hetterich, A. Grau, A.Yu. Egorov, and H. Reichert, '*Influence of indium on the electronic states in GaInNAs/GaAs quantum well structures*', J. Appl. Phys. **94**, 1810 (2003).

[60] S.A. Choulis, S. Tomic, E.P. O'Reilly, and T.J.C. Hosea, '*Determining the band-structure of an InGaNAs/GaAs semiconductor laser structure using non-destructive photomodulated reflectance measurements and k·p studies*', Solid State Commun. **125**, 155 (2003).

[61] S. Shirakata, M. Kondow, and T. Kitatani, '*Optical properties of GaInNAs/GaAs prepared by molecular beam epitaxy*', J. Physics and Chemistry of Solids **64**, 1533 (2003).

[62] J. Derluyn, I. Moerman, M.R. Leys, G. Patriarche, G. Sek, R. Kudrawiec, W. Rudno-Rudzinski, K. Ryczko, and J. Misiewicz, *''Control of nitrogen incorporation in Ga(In)NAs grown by metalorganic vapor phase epitaxy''*, J. Appl. Phys. **94**, 2752 (2003).

[63] R. Kudrawiec, G. Sek, J. Misiewicz, D. Gollub, and A. Forchel, '*Explanation of annealing-induced blueshift of the optical transitions in GaInAsN/GaAs quantum wells*', Appl. Phys. Lett. **83**, 2772 (2003).

[64] M. Geddo, G. Guizzetti, M. Capizzi, A. Polimeni, D. Gollub, and A. Forchel, '*Photoreflectance evidence of the N-induced increase of the exciton binding energy in an $In_xGa_{1-x}As_{1-y}N_y$ alloy*', Appl. Phys. Lett. **83**, 470 (2003).

[65] P.J. Klar, '*Recent developments in metastable dilute-N III-V semiconductors*', Progress in Solid State Chemistry **31**, 301 (2003).

[66] I. Vurgaftman and J.R. Meyer, *'Band parameters for nitrogen-containing semiconductors'*, J. Appl. Phys. **94**, 3675 (2003).

[67] W.J. Fan, S.F. Yoon, T.K. Ng, S.Z. Wang, W.K. Loke, R.Liu, and A. Wee, *'Comparison of nitrogen compositions in the as-grown GaN_xAs_{1-x} on GaAs measured by high-resolution x-ray diffraction and secondary-ion mass spectroscopy'*, Appl. Phys. Lett. **80**, 4136 (2002).

[68] C. Skierbiszewski, P. Perlin, P. Wisniewski, W. Knap, T. Suski, W. Walukiewicz, W. Shan, K.M. Yu, J.W. Ager, E.E. Haller, J.F. Geisz, and J.M. Olson, *'Large, nitrogen-induced increase of the electron effective mass in $In_yGa_{1-y}N_xAs_{1-x}$'* Appl. Phys. Lett. 76, 2409 (2000).

[69] M.-A. Pinault and E. Tournie, '*On the origin of carrier localization in $Ga_{1-x}In_xN_yAs_{1-y}/GaAs$ quantum wells*', Appl. Phys. Lett. 78, 1562 (2001).

[70] S.R. Kurtz, A.A. Allerman, C.H. Seager, R.M. Sieg, and E.D. Jones, '*Minority carrier diffusion, defects, and localization in InGaAsN, with 2% nitrogen*' Appl. Phys. Lett. **77**, 400 (2000).

[71] A. M. Mintairov, T. H. Kosel, J. L. Merz, P. A. Blagnov, A. S. Vlasov, V. M. Ustinov, and R. E. Cook '*Near-Field Magnetophotoluminescence Spectroscopy of Composition Fluctuations in InGaAsN*', Phys. Rev. Lett. **87**, 277401 (2001).

[73] E. Tournie, M.-A. Pinault, and A. Guzman, '*Mechanisms affecting the photoluminescence spectra of GaInNAs after post-growth annealing*', Appl. Phys. Lett. **80**, 4148 (2002).

[74] J.-M. Chauveau, A. Trampert, K. H. Ploog, and E. Tournie, '*Nanoscale analysis of the In and N spatial redistributions upon annealing of GaInNAs quantum wells*', Appl. Phys. Lett. **84**, 2503 (2004).

[75] H.F. Liu, C.S. Peng, E.-M. Pavelescu, T. Jouhti, S. Karirinne, J. Kontitinen, and M. Pessa, '*Annealing effects on optical and structural properties of 1.3-μm GaInNAs/GaAs quantum-well samples capped with dielectric layers*', Appl. Phys. Lett. **84**, 418 (2004).

[76] P.R.C. Kent, L. Bellaiche, and A. Zunger, '*Pseudopotential theory of dilute III-V nitrides*', Semicond. Sci. Technol. **17,** 851 (2002) and there in.

[77] P.R.C. Kent and A. Zunger, *'Evolution of III-V nitride alloy electronic structure: the localized to delocalised transition'*, Phys. Rev. Lett. **86**, 2613 (2001).

[78] K. Kim and A. Zunger, '*Spatial Correlations in GaInAsN Alloys and their Effects on Band-Gap Enhancement and Electron Localization*', Phys. Rev. Lett. **86**, 2609 (2001).

[79] P.R.C. Kent and A. Zunger, '*Nitrogen pairs, triplets, and clusters in GaAs and GaP*', Appl. Phys. Lett. **79**, 2339 (2001).

[80] P.R.C. Kent and A. Zunger, '*Theory of electronic structure evolution in GaAsN and GaPN alloys*', Phys. Rev. B **64**, 115208 (2001).

[81] T. Matsuoka, T. Sasaki, and A. Katsui, '*Growth and properties of a wide-gap semiconductor InGaN*', Optoelectron. Devices Technol. **5**, 53 (1990).

[82] H.Ch. Alt, A.Yu. Egorov, H. Riechert, B. Wideemann, J.D. Meyer, R.W. Michelmann, and K. Bethge, '*Local vibrational mode absorption of nitrogen in GaAsN and InGaAsN layers grown by molecular beam epitaxy*', Physica B **302-303**, 282 (2001).

[83] H.Ch. Alt, A.Yu. Egorov, H. Riechert, J.D. Meyer, and B. Wideemann, '*Incorporation of nitrogen in GaAsN and InGaAsN alloys investigated by FTIR and NRA*', Physica B **308-310**, 877 (2001).

[84] J. Wagner, T. Geppert, K. Kohler, P. Ganser, and N. Herres, '*N-induced vibrational modes in GaAsN and GaInAsN studied by resonant Raman scattering*', J. Appl. Phys. **90**, 5027 (2001).

[85] J. Wagner, T. Geppert, K. Kohler, P. Ganser, M. Maier, '*Bonding of nitrogen in dilute GaInAsN and AlGaAsN studied by Raman spectroscopy*', Solid-State Electronics **47**, 461 (2003).

[86] T. Kitatani, M. Kondow, and M. Kudo, '*Transition of infrared absorption peaks in thermally annealed GaInNAs*', Jpn. J. Appl. Phys. **40**, L750 (2001).

[87] S. Kurtz, J. Webb, L. Gedvilas, D. Friedman, J. Geisz, J. Olson, R. King, D. Joslin, and N. Karam, '*Structural changes during annealing of GaInAsN*', Appl. Phys. Lett. **78**, 748 (2001).

[88] T. Makimoto, H. Saito, N. Kobayashi, '*Excitonic luminescence and absorption in dilute GaAsN alloy*', Appl. Phys. Lett. **70**, 2984 (1997).

[89] I.A. Buyanova, W.M. Chen, C.W. Tu, '*Recombination processes in N-containing III-V ternary alloys*', Solid-State Electronics **47**, 467 (2003) and there in.

[90] I.A. Buyanova, W.M. Chen, and C.W. Tu, '*Magneto-optical and light-emission properties of III-As-N semiconductors*', Semicond. Sci. Technol. **17**, 815 (2002) and there in.

[91] X. Yang, J.B. Heroux, M.J. Jurkovic, and W.I. Wang, '*Photoluminescence of as-grown and thermally annealed InGaAsN/GaAs quantum well grown by molecular beam epitaxy*', J. Vac. Sci. Technol. B **17**(3), 1144 (1999).

[92] H. Saito, T. Makimoto, and N. Kobayashi, '*MOVPE growth of strained InGaAsN/GaAs quantum wells*', J. Cryst. Growth **195**, 416 (1998).

[93] E. Tournie, M.-A. Pinault, S. Vezian, J. Massies, and O. Tottereau, '*Long wavelength GaInNAs/GaAs quantum-well heterostructures grown by solid-source molecular-beam epitaxy*', Appl. Phys. Lett. 77, 2189 (2000).

[94] H. Dumont, L. Auvray, Y. Monteil, F. Saidi, F. Hassen, and H. Maaref, '*Radiative N-localized recombination and confinement in GaAsN/GaAs epilayers and quantum well structures*', Optical Materials **24**, 303 (2003).

[96] E.V.K. Rao, A. Ougazzaden, Y. Le Bellego, and M. Juhel, *'Optical properties of low band gap* $GaAs_{(1-x)}N_x$ *layers: influence of post-growth treatments'*, Appl. Phys. Lett. **72**, 1409 (1998).

[97] S. Shirakata, M. Kondow, and T. Kitatani, *'Temperature-dependent photoluminescence of high-quality GaInNAs single quantum wells'*, Appl. Phys. Lett. **80**, 2087 (2002).

[98] A. Al-Yacoub and L. Bellaiche, '*Quantum mechanical effects in (Ga,In)(As,N) alloys*', Phys. Rev. B **62**, 10847 (2000).

[99] I. Gorczyca, C. Skierbiszewski, T. Suski, N.E. Christensen, and A. Svane, '*Presure and composition depedence of the electronic structure of* $GaAs_{1-x}N_x$', Phys. Rev. B **66**, 081106(R) (2002).

[100] A. Lindsay, and E.P. O'Reilly, '*Theory of enhanced bandgap non-parabolicity in GaN_xAs_{1-x} and related alloys*', Solid State Commun. **112**, 443 (1999).

[101] C. Skierbiszewski, '*Experimental studies of the conduction-band structure of GaInNAs alloys*', Semicond. Sci. Technol. **17**, 803 (2002).

[102] Kazuyuki Uno, Masako Yamada, Toshiyuki Takizawa, and Ichiro Tanaka, '*Thermal Annealing Effect in GaInNAs Thin Films Estimated by Fluorescence X-Ray Absorption Fine Structure Spectroscopy*', Jpn. J. Appl. Phys., Part 1 **43**, 1944 (2004).

[103] R. Kudrawiec, J. Misiewicz, L.H. Li, and J.C. Harmand, *'Experimental investigation of the C_{MN} matrix element in the band anticrossing model for GaAsN and GaInAsN layers'*, Solid State Commun. **129**, 353 (2004).

[104] R. Kudrawiec, G. Sek, J. Misiewicz, L.H. Li, and J.C. Harmand, *'Investigation of recombination processes involving defect-related states in (Ga,In)(As,Sb,N) compounds'*, Eur. Phys. J. B, in press (2004).

[105] L. Grenouillet, C. Bru-Chevallier, G. Guillot, P. Gilet, P. Ballet, P. Duvaut, G. Rolland, and A. Million, '*Evidence of strong carrier localization below 100 K in a GaInNAs/GaAs single quantum well*', *J. Appl. Phys.* **91**, 5902 (2002).

[106] J.C. Harmand, G. Ungaro, L. Largeau, and G. Le Roux, '*Comparison of nitrogen incorporation in molecular-beam epitaxy of GaAsN, GaInAsN, and GaAsSbN*', Appl. Phys. Lett. **77**, 2482 (2000).

[107] R.J. Kaplar, D. Kwon, S.A. Ringel, A.A. Allerman, S.R. Krutz, E.D. Jones, and R.M. Sieg, '*Deep levels p- and n-type InGaAsN for high-efficiency multi-junction III-V solar cells*', Solar Energy Materials & Solar Cells **69**, 85 (2001).

[108] P. Krisprin, S.G. Spruytte, J.H. Harris, and K.H. Ploog, '*Electron traps in Ga(As,N) layers grown by molecular-beam epitaxy*', Appl. Phys. Lett. **80**, 2120 (2002).

[109] P. Krisprin, V.Gambin, J.H. Harris, and K.H. Ploog, '*Ga(As,N) layers in the dilute N limit studied by depth-resolved capacitance spectroscopy*', Appl. Phys. Lett. **81**, 3987 (2002).

[110] V. Lordi, V. Gambin, S. Friederich, T. Funk, T. Takizawa, K. Uno, and J.S. Harris, '*Nearest-neighbour configuration in (GaIn)(NAs) probed by X-ray absorption spectroscopy*', Phys. Rev. Lett. **90**, 145505 (2003).

[111] M. Albrecht, V. Grillo, T. Remmele, H. P. Strunk, A. Yu. Egorov, Gh. Dumitras, H. Riechert, A. Kaschner, R. Rietz, and A. Hoffmann, '*Effect of annealing on the In and N distribution in InGaAsN quantum wells*', Appl. Phys. Lett. **81**, 2719 (2002).

[112] S. Jiang, S.C. Shen, S.M. Wang, and T.G. Andersson, '*Photomodulated reflectance spectra of $In_{0.2}Ga_{0.8}As/GaAs$ single quantum wells*', Appl. Phys. Lett. **66**, 1948 (1995).

[113] Y.C. Wang, W.C. Hwang, Z.P. Yang, G.S. Chang, and J.S. Hwang, '*Studies of lattice-matched InGaAs/InAlAs single quantum well by photoreflectance spectroscopy and wet chemical etching*', Solid State Commun. **111**, 223 (1999).

[114] D.J. Hall, T.J.C. Hosea, and C.C. Button, '*Analysis of strained InGaAs/InGaAsP single quantum wells using room temperature photoreflectance*', Semicond. Sci. Technol. **13**, 302 (1998).

[115] G. Bastard '*Wave mechanics applied to semiconductor heterostructures*' (Paris: Les Editions de Physique, 1992).

[116] R. Kudrawiec, G. Sek, P. Sitarek, K. Ryczko, J. Misiewicz, T. Wang, and A. Forchel, '*Three beam photoreflectance as a powerful method to investigate semiconductor heterostructures*', Thin Solid Films **450**, 71 (2004).

[117] G. Sek, K. Ryczko, J. Misiewicz, M. Bayer, T. Wang, and A. Forchel, '*Influence of built-in electric field on forbidden transitions in $In_xGa_{1-x}As/GaAs$ double quantum well by three-beam photoreflectance*', Acta Physica Polonica A **100**, 417 (2001).

[118] H. Shen and M. Dutta, '*Franz-Keldysh oscillations in modulation spectroscopy*', J. Appl. Phys. **78**, 2151 (1995).

[119] H. D. Sun, M.D. Dawson, M. Othman, J.C.L. Yong, J.M. Rorison, P. Gilet, L. Grenouillet, and A. Million, '*Optical transitions in GaInNAs/GaAs multi-quantum wells with varying N content investigated by photoluminescence excitation spectroscopy*', Appl. Phys. Lett. **82**, 376 (2003).

[120] M. Hetterich, M.D. Dawson, A.Yu. Egorov, D. Bernklau, and H. Riechert, '*Electronic states and band alignment in GaInNAs/GaAs quantum-well structures with low nitrogen content*', Appl. Phys. Lett. **76**, 1030 (2000).

[121] Z. Pan, L.H. Li, Y.W. Lin, B.Q. Sun, D.S. Jiang, and W.K. Ge, '*Conduction band offset and electron effective mass in GaInNAs/GaAs quantum-well structures with low nitrogen concentration*', Appl. Phys. Lett. **78**, 2217 (2001).

[122] G. Baldassarri Höger von Högersthal, P. Polimeni, M. Masia, M. Bissiri, M. Capizi, D. Gollub, M. Fischer, and A. Forchel, '*Magnetophotoluminescence studies of (InGa)(AsN)/GaAs heterostructures*', Phys. Rev. B **67**, 233304 (2003)

[123] M.J. Joyce, M.J. Johnson, M. Gal, and B.F. Usher, '*Concentration-dependent band offset in $In_xGa_{1-x}As/GaAs$ strained quantum wells*', Phys. Rev. B **38**, 10978 (1988).

[124] W. Li, M. Pessa, T. Ahlgren, and J. Decker, '*Origin of improved luminescence efficiency after annealing of Ga(In)NAs materials grown by molecular-beam epitaxy*', Appl. Phys. Lett. **79**, 1094 (2001).

[125] L.F. Bian, D.S. Jiang, S.L. Lu, J.S. Huang, K. Chang, L.H. Li, and J.C. Harmand, '*The effect of inserting strain-compensated GaNAs layers on the luminescence properties of GaInNAs/GaAs quantum well*', J. Cryst. Growth **250**, (2003) 339.

[126] J.A. Gupta, P.J. Barrios, G.C. Aers, R.L. Williams, and Z.R. Wasilewski, '*Properties of 1.3 μm InGaNAs laser material grown by MBE using a N_2Ar RF plasma*', Solid-State Electronics **47**, 399 (2003).

[127] L.H. Li, G. Patriarche, A. Lemaitre, L. Largeau, L. Travers, and J.C. Harmand, '*Comparison of GaInNAs/GaAs and GaInNAs/GaNAs/GaAs quantum wells emitting over 1.3 mu m wavelength*', J. Cryst. Growth **251**, 403 (2003).

[128] E.–M. Pavelescu, C.S. Peng, T. Jouhti, J. Konttinen, W. Li, M. Pessa, M. Dumitrescu, and S. Spanulescu, '*Effects of insertion of strain-mediating layers on luminescence properties of 1.3-μm GaInNAs/GaNAs/GaAs quantum-well structures*', Appl. Phys. Lett. **80**, 3054 (2002).

[129] E.-M. Pavelescu, T. Jouhti, C.S. Peng, W. Li, J. Konttinen, M. Dumitrescu, P. Laukkanen, and M. Pessa, '*Enhanced optical performances of strain-compensated 1.3- mu m GaInNAs/GaNAs/GaAs quantum-well structures*', J. Cryst. Growth **241**, 31 (2002).

[130] H.Y. Liu, M. Hopkinson, P. Navaretti, M. Gutierrez, J.S. Ng, and J.P.R. David, *'Improved optical properties of 1.55 μm GaInNAs/GaAs sultiple-quantum wells with Ga(In)NAs barrier and space layer'*, Appl. Phys. Lett. **83**, 4951 (2003).

[131] G. Ungaro, G. Le Roux, R. Teisser, and J.C. Harmand, '*GaAsSbN: a new low-bandgap material for GaAs substrates*', Electron. Lett. **35**, 1246 (1999).

[132] L.H. Li, V. Sallet, G. Patriarche, L. Largeau, S. Bouchoule, L. Travers, and J.C. Harmand, '*Investigations on GaInNAsSb quinary alloy for 1.5 μm laser emission on GaAs*', Appl. Phys. Lett. **83**, 1298 (2003).

[133] S. Bank, W. Ha, V. Gambin, M. Wistey, H. Yuen, L. Goddard, S. Kim, and J.S. Harris Jr, '*1.5 μm GaInNAs(Sb) lasers grown on GaAs by MBE*', J. Cryst. Growth **251**, 367 (2003).

[134] K. Volz, V. Gambin, W. Ha, M.A. Wistey, H. Yuen, S. Bank, J.S. Harris, '*The role of Sb in the MBE growth of (GaIn)(NAsSb)*', J. Cryst. Growth **251**, 360 (2003).

[135] Z. Pan, T. Miyamoto, D. Schlenker, F. Koyama, and K. Iga, '*Quality improvement of GaInNAs/GaAs quantum well growth by metalorganic chemical vapor deposition using tertiarybutylarsine*', Jpn. J. Appl. Phys. Part 1 **38**, 1012 (1999).

[136] S.R. Kurtz, J.F. Klem, A.A. Allerman, R.M. Sieg, C.H. Seager, and E.D. Jones, '*Minority carrier diffusion and defects in InGaAsN grown by molecular beam epitaxy*', Appl. Phys. Lett. **80**, 1379 (2002).

[137] H. A. McKay, R.M. Feenstra, T. Schmidtng, U. W. Pohl, and J.F. Geisz, '*Distribution of nitrogen atoms in dilute GaAsN and InGaAsN alloys studied by scattering tunnelling microscopy*', J. Vac. Sci. Technol. B **19**, 1644 (2001).

[138] E. H. Li, Ed., *Semiconductor Quantum well Intermixing - Material Properties and Optoelectronic Applications* (Gordon & Breach, Amsterdam, 2000).

[139] R. Kudrawiec, G. Sęk, W. Rudno-Rudziński, J. Misiewicz, J. Wójcik, B. J. Robinson, D. A. Thompson, P. Mascher, '*Investigation of the non-square InGaAsP/InP quantum wells in the electric field by photoreflectance*', Acta Phys. Pol. A **102**, 649 (2002).

[140] R. Kudrawiec, G. Sęk, W. Rudno-Rudziński, J. Misiewicz, J. Wójcik, B. J. Robinson, D. A. Thompson, P. Mascher, '*Photoreflectance study of the interdiffusion effects in the InGaAsP-based quantum well laser structures*', Physica E **17**, 602 (2003).

[141] M.C.Y. Chan, Ch. Surya, and P.K. Wai, '*The effects of interdiffusion on the subbands in $Ga_xIn_{1-x}N_{0.04}As_{0.96}$/GaAs quantum well for 1.3 and 1.55 μm operation wavelengths*', J. Appl. Phys. **90**, 197 (2001).

[142] G. Patriarche, L. Largeau, and J.-C. Harmand, D. Gollub, '*Morphology and composition of highly strained InGaAs and InGaAsN layers grown on GaAs substrate*', Appl. Phys. Lett. **84**, 203 (2004).

[143] A. Polimeni, M. Capizzi, M. Geddo, M. Fisher, M. Reinhardt, and A. Forchel, '*Effect of temperature on the optical properties of (InGa)(AsN)/GaAs single quantum wells*', Appl. Phys. Lett. **77**, 2870 (2000).

[144] R. Kudrawiec, G. Sęk, J. Misiewicz, L.H. Li, and J.C. Harmand, *'Influence of carrier localization on modulation mechanism in photoreflectance of GaAsN and GaInAsN'*, Appl. Phys. Lett. **83**, 1379 (2003).

[145] R. Kudrawiec, J. Misiewicz, M. Fischer, and A. Forchel, *'Optical properties of GaInNAs/GaAs quantum wells: character of optical transitions and carrier localisation effect'*, phys. stat. solidi (a) **201**, 364 (2004).

[146] Y. P. Varshni, Physica **34**, 149 (1967).

[147] L. Vina, S. Logothetidis, and M. Cardona, '*Temperature dependence of the dielectric function of germanium*', Phys. Rev. B **30**, 1979 (1984).

[148] A. Kaneta, and S. Adachi, '*Photoreflectance study of hexagonal CdSe*', J. Phys. D **32**, 2337 (1999).

[149] A. Kaneta, and S. Adachi, '*Photoreflectance study in the E_1 and $E_1 + \Delta_1$ transition regions of ZnTe*', J. Phys. D **33**, 901 (2000).

[150] A. Kaneta, and S. Adachi, 'Photoreflectance *study in the E_1 and $E_1 + \Delta_1$ transition regions of CdTe*', J. Appl. Phys. **87**, 7360 (2000).

[151] H. Moriya, A. Kaneta, and S. Adachi, '*Photoreflectance study of crystalline silicon*', Mat. Scien. Eng. B **76**, 232 (2000).

[152] T. Mishima, M. Miura, S. Ozaki, S. Adachi, '*Photoreflectance study in the E_0 and $E_0 + \Delta_0$ transition regions of GaP*', J. Appl. Phys. **91**, 4904 (2002).